UNIVERSITAT DE BARCELONA

The role of the zebrafish *tbx5* paralogues during eye, pectoral fin and heart development

Aina Pi Roig

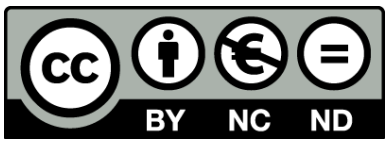

UNIVERSITAT DE BARCELONA

FACULTAT DE BIOLOGIA

DEPARTAMENT DE GENÈTICA, MICROBIOLOGIA I ESTADÍSTICA

PROGRAMA DE DOCTORAT EN GENÈTICA

Aina Pi Roig

The role of the zebrafish *tbx5* paralogues during eye, pectoral fin and heart development.

Tesis Doctoral 2018

UNIVERSITAT DE BARCELONA

FACULTAT DE BIOLOGIA

DEPARTAMENT DE GENÈTICA, MICROBIOLOGIA I ESTADÍSTICA

PROGRAMA DE DOCTORAT EN GENÈTICA

Tesis Doctoral presentada per

Aina Pi Roig

amb el títol

The role of the zebrafish *tbx5* paralogues during eye, pectoral fin and heart development.

Per a optar al títol de Doctora per la Universitat de Barcelona

Tesis Doctoral realitzada en el Departament de Genètica, Microbiologia i Estadística
sota la direcció del Doctor Jordi Garcia Fernàndez i co-dirigida
per la Doctora Carolina Minguillón Gil.

Director,	Co-directora,	Autora,
Dr. Jordi Garcia-Fernàndez	Dra. Carolina Minguillón	Aina Pi Roig

Barcelona, Gener 2018

Cover images are a tbx5aBAC:GFP embryo at 48hpf that express GFP in the developing retina, pectoral fin and heart.

Acknowledgements

Aquesta tesi ha estat un llarg camí, ple d'emocions i moments que han marcat la meva vida. Tants, que la veritat és que no sé ben bé com començar i agrair a totes aquelles persones que han estat al meu costat durant aquests anys de tesis.

Primer de tot m'agradaria agrair als meus directors de tesi per animar-me a seguir aquest camí i haver compartit tants moments de ciència i haver-me portat fins on sóc. També a tothom amb qui hem compartit lab, pels grans moments, consells i amistats. Malauradament, el que té la ciència, molts esteu repartits pel món, però és impossible oblidar-se de ningú i ara que acabo queden moltes visites pendents a fer! :)

A les amigues de Sant Cugat per tants anys d'amistat i suport! Als biotecs, per tots els moments genials que m'heu fet passar des del primer dia en què ens vam conèixer, i a totes les amistats que al llarg d'aquests anys m'heu escoltat i arrencat un somriure quan ho he necessitat!

Finalment, a la tota la meva extensa família, amb qui mai hi pot haver un moment d'avorriment! Però especialment als pares i la Senda, per creure en mi i pel seu suport incondicional!

Aquesta tesis és en gran part gràcies a tots vosaltres, per haver-me recolzat i encomanat el vostre entusiasme per seguir endavant amb aquest projecte! A tots vosaltres, moltíssimes gràcies! :)

Abstract

Tbx5 is a transcription factor expressed in the developing eyes, heart and upper limbs. Mutations in human TBX5 cause Holt-Oram syndrome (HOS), a condition characterised by heart and upper limb malformations. In zebrafish, a novel *tbx5* gene (*tbx5b*), which emerged from the teleost specific genome duplication, is co-expressed with its paralogue (*tbx5a*).

To understand *tbx5* paralogues function and relationship in the different tissues where they are expressed (*i.e.* eye, heart and pectoral fin) in zebrafish, downregulation by morpholino oligonucleotides (MO) injection has been performed. The results reveal that *tbx5* genes are essential for the development of these organs, where they have different requirements and relationships to ensure proper dorsoventral (DV) retina axis organization, the establishment of cardiac laterality and the induction and sustained outgrowth of the pectoral fin.

In the retina, *tbx5* genes role is redundant and both paralogues knock-down causes a reduction of the dorsal retina identity, concomitant with an expansion of the ventral retina markers expression, that results in defective DV patterning and subsequent thinner retinotectal projections. In contrast, *tbx5a* and *tbx5b* have gene-specific functions during pectoral fin development: *tbx5a* is required for the initiation of pectoral fin outgrowth, whereas *tbx5b* is later responsible for the sustained outgrowth of the pectoral fin. In the case of heart morphogenesis, both paralogues cooperate in the same pathway. In addition, our results uncover a novel role for *tbx5* paralogues in the establishment of heart asymmetry in zebrafish embryos in both asymmetric events (*i.e.* cardiac jogging and looping) and an earlier role for *tbx5a* during the directional migration and of the cardiac precursors in the midline. Further analysis of the role of *tbx5a* during the establishment of left-right (LR) asymmetry shows that the expres-

sion of left-side markers from the Nodal signalling pathway expressed in the lateral plate mesoderm (LPM) is also randomized.

Laterality defects during zebrafish development in *tbx5a* morphant are also found in neural and visceral laterality, suggesting an early role of *tbx5a* in LR establishment. Strikingly, *tbx5a* knock-down in the DFCs/KV (dorsal forerunner cells / Kupffer's vesicle) lineage, the organ responsible for LR asymmetry generation, also results in cardiac jogging randomization.

Furthermore, our results show an early *tbx5a* expression during gastrulation and an altered expression pattern for *charon* and a reduction on *bmp4* expression levels around the KV at 10SS. In addition, a reduction on Bmp signalling levels in *tbx5a* DFC-specific morphants is detected, which is consistent with the identification of a putative binding site for Tbx5 that is conserved in high vertebrates for *bmp2b* and *bmp4*. Finally, the analysis of *tbx5a* morphants also show that they have a reduced KV.

Overall, we propose a model in which *tbx5* is required during zebrafish early development to achieve a proper KV size that will ensure a robust directional flow within the KV and Bmp signalling in the KV itself and its surroundings. These signalling cues ensure the correct activation of the Nodal signalling pathway and are subsequently transmitted to the LPM to guide organ primordia to their final position along the LR axis.

Resum

Tbx5 és un factor de transcripció expressat durant el desenvolupament dels ulls, el cor i les extremitats superiors. Mutacions en TBX5 humà causen el síndrome de Holt-Oram, caracteritzat per malformacions al cor i en l'extremitat superior. En peix zebra, un nou gen tbx5 (*tbx5b*) va emergir de la duplicació específica del genoma dels teleostis i és co-expressat amb el seu paràleg (*tbx5a*).

Per entendre la funció i la relació dels paràlegs de *tbx5* en els diferents teixits on s'expressen (*i.e.* ull, cor i aleta pectoral) en peix zebra, es va utilitzar la injecció de morfolinos per a reduir els nivells de *tbx5*. Els resultats revelen que els gens *tbx5* són essencials pel desenvolupament d'aquests òrgans, on hi tenen diferents requeriments i relacions per tal d'assegurar una correcta organització dorso-ventral (DV) a la retina, l'establiment de la lateralitat cardíaca i la inducció i creixement sostingut de l'aleta pectoral.

En la retina, el rol dels gens *tbx5* és redundant i el *knock-down* d'ambdós paràlegs causa una reducció de la identitat dorsal en la retina, concomitant amb una expansió de l'expressió dels marcadors ventrals, que resulta en projeccions retinotectals més fines. En canvi, *tbx5a* i *tbx5b* tenen funcions específiques en l'aleta pectoral: *tbx5a* és necessari per la iniciació del desenvolupament de l'aleta pectoral, mentre que *tbx5b* és responsable de mantenir un creixement sostingut de l'estructura. En el cas de la morfogènesi del cor, ambdós paràlegs cooperen en la mateixa via. A més, els nostres resultats revelen un nou rol per als paràlegs *tbx5* en l'establiment de la lateralitat del cor en els embrions de peix zebra en ambdós esdeveniments assimètrics (*jogging* i *looping)* i un rol encara més primerenc per a *tbx5a* durant la migració i fusió dels precursors cardíacs a la línea mitja. Els anàlisis del rol de *tbx5a* durant l'establiment de l'assimetria esquerra-dreta (LR) mostren que l'expressió dels marcadors del costat

esquerra de la via de senyalització de Nodal s'expressen de manera aleatòria en la placa mesodèrmica lateral (LPM) en els morfants per *tbx5a*.

Els defectes de lateralitat també afecten la lateralitat neural i visceral, suggerint un rol primerenc de *tbx5a* durant el desenvolupament. Sorprenentment, la reducció de l'expressió de *tbx5a* mitjançant la injecció de morfolino contra *tbx5a,* afectant només el llinatge cel·lular que dóna lloc l'òrgan responsable de generar l'assimetria LR (KV: Kupffer's Vesicle), també provoca aleatorietat en l'esdeveniment del *jogging*.

Els nostres resultats mostren una expressió temprana de *tbx5a* durant la gastrulació. A més, els embrions morfants per *tbx5a* presenten un patró d'expressió aberrant per *charon* i una reducció dels nivells d'expressió de *bmp4* al voltant de la KV a l'estadi de 10SS. La reducció en el nivell de senyalització de Bmps en els morfants per *tbx5a* en què només s'afecta la KV concorda amb presència d'un possible lloc d'unió per a Tbx5 en *bmp2b* i *bmp4*, conservat en vertebrats superiors. Finalment, anàlisis en la KV mostren que els morfants per *tbx5a* tenen una KV reduïda.

Com a model general, proposem que *tbx5* és necessari durant el desenvolupament temprà del peix zebra per tal d'assolir una mida adequada de la KV que asseguri un flux direccional robust en la KV i una correcta senyalització de Bmps a la KV i al seu voltant. Aquesta senyalització assegura una activació correcta de la via de Nodal i la següent transmissió d'aquesta senyalització a la LPM per tal de guiar els primordis dels òrgans cap a la seva posició final al llarg de l'eix LR.

Table of Contents

List of Abbreviations

AER	Apical Ectodermal Ridge
AP	Antero-Posterior
AVC	Atrioventricular Canal
BMP	Bone Morphogenetic Protein
BMPR	BMP Receptor
CRISPR	Clustered Regularly Interspaced Short Palindromic Repeats
DFC	Dorsal Forerunner Cell
DV	Dorso-Ventral
ECM	Extracellular Matrix
EGF	Epidermal Growth Factor
FGF	Fibroblast Growth Factor
FISH	Fluorescent ISH
GDF	Growth Differentiation Factor
GFP	Green Fluorescent Protein
GRP	Gastrocoel Roof Plate
HOS	Holt-Oram Syndrome
Hpf	hours postfertilization
hst	heartstring
ISH	In Situ Hybridisation
KV	Kupffer's Vesicle
HOS	Holt-Oram Syndrome
LPM	Lateral Plate Mesoderm
LR	Left-Right
LRO	Left-Right Organizer
MO	Morpholino Oligonucleotide
NLS	Nuclear Localization Signal

NT	Naso-Temporal
Ntl	No tail
OC	Optic Cup
OV	Optic Vesicle
PD	Proximo-Distal
qPCR	quantitative Polymerase Chain Reaction
RA	Retinoic Acid
RGC	Retinal Ganglion Cells
RPE	Retinal Pigmented Epithelium
RT-PCR	Reverse Transcripton PCR
Shh	Sonic Hedgehog
spaw	southspaw
SS	Somite stage
TGF	Transforming Growth Factor
YSL	Yolk Syncytial Layer

Introduction

1. Origin, evolution and relevance of the Tbx2 subfamily of genes

1.1. T-box genes: main features

The founding member of the T-box gene family was discovered in mice in 1927[1,2]. It was named *Brachyury* (Greek: brakhu´s, short; oura´, tail) or *T*, since its mutation causes short-tailed mice in heterozygous animals. Mutations in this gene affect embryonic development since it is required for the formation of posterior mesoderm and axial development[3,4]. Further research demonstrated that *Brachyury* is evolutionary conserved[1,4] and that it belongs to a multigene family that encodes DNA-binding transcription factors: the T-box[2,5–7]. T-box genes are remarkably conserved along metazoans and they have also been recently identified in several non-metazoan lineages: Ichtyosporea, Filasterea and early-branching fungi (Neocallimastigomycota, Chytridiomycota, and Mucoromycotina)[8]. Based on HUGO (Human Genome Organization) nomenclature, there are 18 members of the T-box gene family (including the T-box 23 pseudogene) that are organized into 5 subfamilies, although the number of subfamilies and their specific members vary in the different animal groups along evolution (Figure 1). Notable conservation of T-box members exists between lineages that have been evolving since the last common ancestor of metazoans. Nevertheless, high diversification can be noticed at the onset of metazoan evolution[2] (Figure 1).

T-box genes are expressed throughout development in dynamic patterns showing both gene-unique and overlapping expression domains[6]. As developmental transcription factors, T-box genes exert numerous functions and roles in early-fate decisions and during differentiation and organogenesis and hence, they are fundamental to ensure correct embryonic development. Moreover, mutations in several members of this family result in syndromic conditions and birth defects in humans (e.g. Tbx1: DiGeorge Syndrome[9,10], Tbx19: Isolated Acth Deficiency[11,12]). In addition, although they have been primarily reported to have an early role during embryogenesis, several studies

have uncovered functions for these genes in certain cancers and in adult stem cells populations[6,13,14].

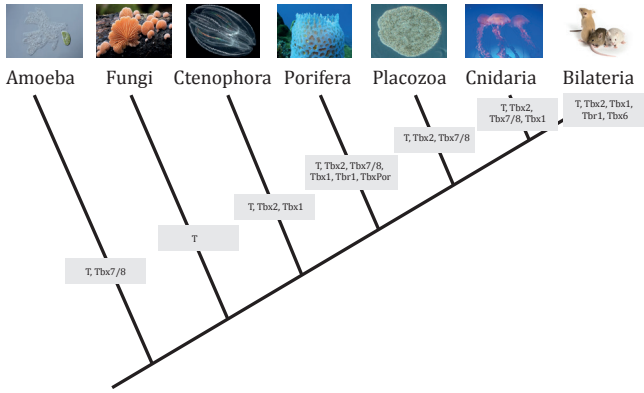

Figure 1 | *T-box genes subfamilies*. *Of note, Brachyury or T, the most ancient member, is present in unicellular organisms as it is Tbx7/8, a class not present in Bilateria. Sponges have a diverse set of T-box genes including several that have not been retained in Bilateria, whereas Tbx6 subfamily genes apparently arose in Bilateria. Adapted from Papaioannou et al., 2014[2].*

T-box proteins possess a conserved structure characterised by the presence of a DNA binding domain, from which the name of the family arises: T-domain (at the protein-level) or T-box (at the gene-level) and a transcriptional effector domain[2,7,15,16]. The T-domain spans 180-200 amino acids and is conserved in all members of the family[2,15,17]. This regulatory module allows for the specific recognition and binding to DNA sequences (Figure 2). Specificity of T-box proteins for their target sites lies mainly within the T-domain, although specificity does not appear to reflect binding affinity[7,16]. Indeed, a study suggests that functional specificity between different T-box classes is likely achieved by interaction with alternative cofactors, as opposed to differences in binding specificity[8]. In addition to the T-domain, T-box proteins also contain a transcriptional effector domain located at the C-terminal side. It has been shown that T-box proteins can function as transcriptional activators and repressors[3,4,17,18] and some of them (e.g. T and Tbx4) appear to have both activities depending on the biological context[4,19]. Despite the position of these motifs along the protein may vary among the

different factors of the family, their relative order is conserved in all the members of the family and their orthologs[5,20]. Additionally, in many members of the family a NLS (Nuclear Localization Signal) - essential for their subcellular localization - has been identified [e.g. Tbx1, Tbx3, Tbx5, Tbx6[21], Xbra[12] (Figure 2)].

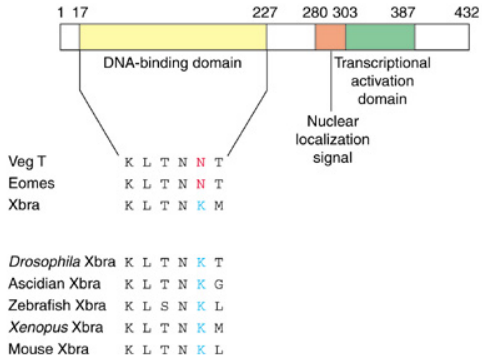

Figure 2 | *The structure of T-box proteins.* *T-box proteins contain a DNA binding domain (T-domain) at the N-terminal and a transcriptional activator and/or repressor domain at the C-terminal. An example of the conservation of a specific residue in position 149 in Xbra, which is always a lysine (K, blue) in different species but not in other T-box proteins (N, red) is shown. Adapter from Wilson and Conlon, 2002[7].*

The prediction of the function of T-box genes function is quite complicated due to their functional variety[6]. T-box proteins can homodimerize, heterodimerize or cooperatively bind other transcription factors depending on the biological context[6]. In addition, as previously mentioned, T-box proteins can function as activators or repressors, and some of them can function as both depending on the promoter context. There are also cases of promoter competition between T-box members in which one T-box protein is able to compete off another at a particular promoter [e.g. Ntl (no tail) and Tbx6 can compete to regulate T-site-dependent transcription of the target gene *myoD* (myogenic differentiation) in adaxial cells in zebrafish[22]]. Finally, the study of the regulatory landscape of T-box proteins has been largely addressed by the generation of dominant negative proteins (e.g. truncated proteins containing only the T-domain) which gene-

rates results that are difficult to interpret, since the action of the truncated proteins may influence other T-box genes and targets[2,6,15,23]. Hence, although the effects of the engineered protein should be specific, in some occasions the dominant negative protein results in different or more severe phenotypes than those in the null mutants[24], indicating interference with other protein/s. Therefore, to interpret and extract conclusions from these experiments becomes complicated and still several aspects on the T-box regulatory landscape and function remain to be elucidated.

Mutations in T-box genes result in developmental defects in several organisms, which include dominant or semidominant human developmental syndromes. Remarkably, since T-box proteins are highly sensitive to dosage, both an excess and a lack of protein equally result in a phenotype[6]. The complexity of the expression pattern of T-box genes has impeded mutational analysis to address all their putative roles. One of the most relevant limitation is the early lethality that prevents investigation of later developmental roles. New conditional or hypomorphic alleles, among other engineering strategies, are required to better understand the role of these genes during development. Thus, although some developmental requirements for T-box genes have been demonstrated only few downstream target genes affecting these functions have been described[6,15].

1.2. T-box subfamilies: Origin and classification

Since the discovery of the first T-box gene identified, *Brachyury*, further research has characterised all the members of this family of transcription factors and, nowadays, T-box genes have acquired a great importance in the developmental biology field. T-box members can be phylogenetically classified in five subfamilies based on the homology of the T-domain: T, Tbx1, Tbx2, Tbx6 and Tbr1[2,13] (Figure 3).

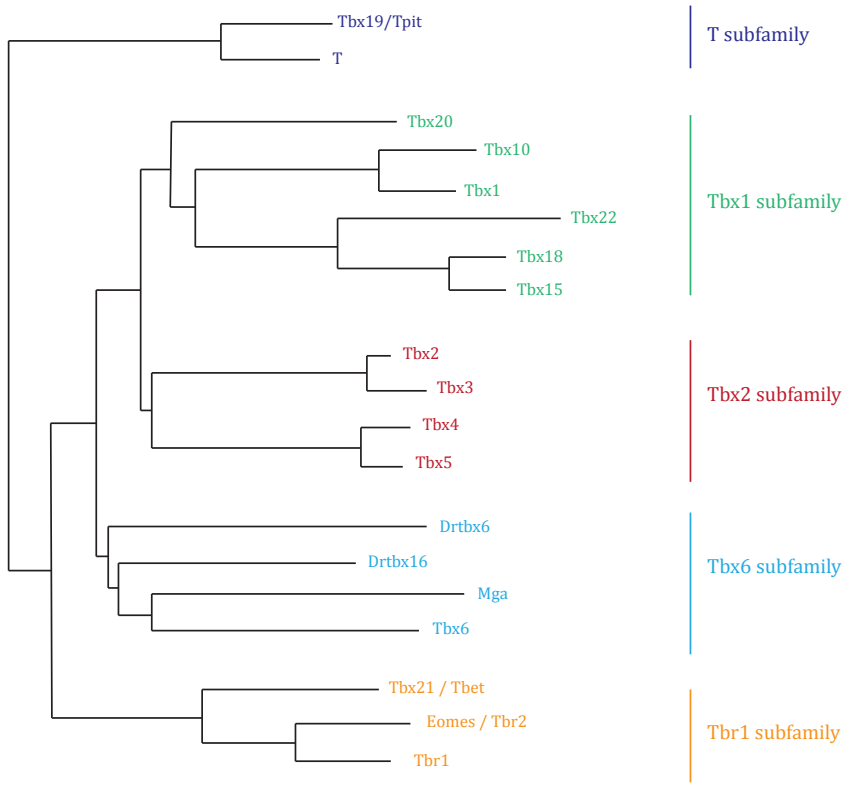

Figure 3 | *Schematic representation of the T-box gene subfamilies in vertebrates.* *The depicted genes are present in mammals except the zebrafish genes drtbx6 and drtbx16, which do not have mammalian orthologs. Adapted from Naiche et al., 2005*[6].

T-box genes are found dispersed throughout the vertebrate genome with the exception of the paralogous pairs that form the Tbx2 subfamily: *Tbx2* and *Tbx3*, which are linked to *Tbx4* and *Tbx5*, respectively. The Tbx2 subfamily of T-box genes are of special interest due to their implication in the evolution of vertebrate paired appendages, the eyes and the heart and, like Hox genes, for the longevity of their chromosomal linkage[25]. The physical linkage of these gene pairs (*Tbx2* clustered with *Tbx4* and *Tbx3* located with *Tbx5*) is preserved prior to the divergence of protostomes and deuterostomes[25], suggesting its importance for the development of metazoan animals. Despite the exact reason why the linkage between these genes is constrained remains unknown, it is

likely that they share regulatory elements required for their expression in common expression domains[26].

The current genomic arrangement of the Tbx2 subfamily has its origin in the tandem duplication of a single ancestral gene (*Tbx2/3/4/5*) prior to the divergence of the vertebrate and invertebrate lineages giving rise to *Tbx2/3* and *Tbx4/5*[5,27]. This tandem-duplication event was followed by a duplication of the derived pair (*Tbx2/3* and *Tbx4/5*)[5], possibly during the genome duplication events that occurred close to the root of the vertebrate lineage giving rise to *Tbx2*, *Tbx3*, *Tbx4* and *Tbx5*[28]. Additionally, duplicate members are found in teleosts due to the whole genome duplication event that their genome suffered 320-350mya[29,30]. From this evolutionary event, there are some clade-specific paralogues, having 7 members for the Tbx2 subfamily: *tbx2a*, *tbx2b*, *tbx3a*, *tbx3b*, *tbx4*, *tbx5a* and *tbx5b*[31] (Figure 4).

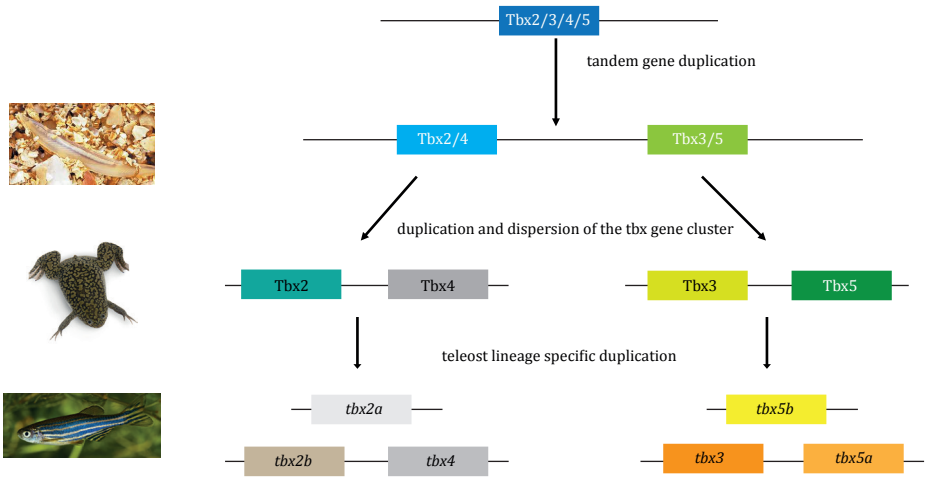

Figure 4 | *Origin of the Tbx2 subfamily of genes by tandem duplication and cluster dispersion.* *Teleosts lineage underwent an additional whole genome duplication from which they still preserve two copies for tbx2, tbx3 and tbx5 genes. tbx3a and tbx3b appear under the name of tbx3 since both lie in the same chromosome together with tbx5a.*

1.3. Expression and function of the Tbx2 subfamily genes

Tbx2 subfamily members have been extensively studied given their fundamental functions during multiple biological processes: they are expressed in vital organs for the proper development of the embryo, in which, despite having overlapping expression patterns they also exert unique developmental functions[6]. With the exception of *Tbx2*, mutations in the other 3 subfamily members are responsible for genetic birth defects and syndromes in human: *TBX3*: Ulnar-Mammary Syndrome[32], *TBX4*: Small Patella Syndrome[33] and *TBX5*: Holt-Oram Syndrome[15].

TBX2 has been described to be expressed in multiple organs and tissues in humans. These structures include the ovaries, placenta, heart, kidney, lung, breast, prostate, testis, thymus and polymorphonucleocytes[21,34]. Despite it has not yet been associated to any human genetic syndrome, TBX2 has been reported to be involved in multiple developmental events that include the patterning and morphogenesis of several tissues, like the heart or the hypothalamus in the brain, coordinate cell fate and organs including the limb, kidney, lung, mammary gland and craniofacial structure. It is also overexpressed in some cancers (e.g. melanoma, pancreatic, bladder, carcinoma, breast and liver) and can suppress senescence[15].

TBX3 is expressed in the upper limbs, heart, liver, bladder, placenta, uterus, mammary glands and pituitary, adrenal and tyroid glands in human[35,36]. It acts as a transcriptional repressor and is thought to play a role in the anterior/posterior axis of the tetrapod forelimb[36]. Haploinsufficiency of *TBX3* causes Ulnar-Mammary Syndrome (UMS, OMIM#181450), firstly described in 1975 by McKusick[38]. UMS is an autosomal dominant condition characterized by limb defects, mammary and apocrine gland hypoplasia and genital anomalies[39]. This developmental disorder has incomplete penetrance. Some organs are more affected than others in UMS, probably because they require

higher amounts of TBX3 or that other genes of the T-box family compensate for the lack of TBX3 in other tissues[40].

TBX4 is broadly expressed in the allantois, lower limbs, lung and proctodeum[41]. Indeed, it has been described to be critical for the formation of the umbilicus and the initiation of the hindlimb[41,42]. Mutations in this gene result in Small Patella Syndrome (SPS; OMIM#147891) or Scott-Taor Syndrome, a rare autosomal dominant disorder firstly described by Scott and Taor in 1979[43]. SPS is characterised by patellar aplasia or hypoplasia and by anomalies of the pelvis and feet, including disrupted ossification of the ischia and inferior pubic rami[33].

Tbx5 has been characterized in most vertebrate lineages and is widely expressed during the development of various embryonic structures, including the heart, the eyes and the anterior set of paired appendages[44]. Mutations in human *TBX5* cause Holt-Oram syndrome (HOS; OMIM#142900), an autosomical dominant condition that was firstly described in 1960[45]. HOS is characterized by upper limb and shoulder girdle defects, associated with a congenital heart lesion[46] (Figure 5 A, A'). A vast variety in the severity of the abnormalities presented exists, ranging from subtle digital malformations to focomelia in the skeletal tissues or from simple or multiple atrial or ventricular septation defects to much more severe aberrant heart conditions[47]. Nevertheless, the typical phenotype is a triphalangeal thumb with a secundum atrial septal defect (ASD)[46]. In HOS, the consensus is that this condition is caused by haploinsufficiency rather than pathogenic mutations, located throughout the coding sequence[47,48]. Indeed, genetic alterations linked to *TBX5* coding or splice regulatory sequences underlie approximately 70% of patients[49,50]. These mutations create dominant-negative forms of the protein or severely truncated proteins that are thought to act as null alleles[47,49,51,52] and mutations within the T-domain that diminish DNA binding ability and binding with interaction partners[53,54]. Although HOS classically affects both cardiac

and upper limb fields, several cases have been reported to affect more severely either the heart[47,48,55] or the upper limb[48,55], suggesting that tissue-specific roles for different domains of the protein exist[56]. Despite the mechanisms of these biased defects remain to be fully understood, some models argue for the existence of distinct binding motifs that allow the recognition of specific binding partners[56–60]. Finally, it is worth mentioning that the expression pattern of *Tbx5* is largely conserved in vertebrates (Figure 5 B) and hence, studies to elucidate the role of *Tbx5* have been pursued in the main vertebrate model organisms including mouse, chick, *Xenopus* and zebrafish. Despite the mouse model for *Tbx5* loss-of-function is the best characterized and conforms a platform to study cardiac and upper limb defects[61,62], each model system has its particular benefits.

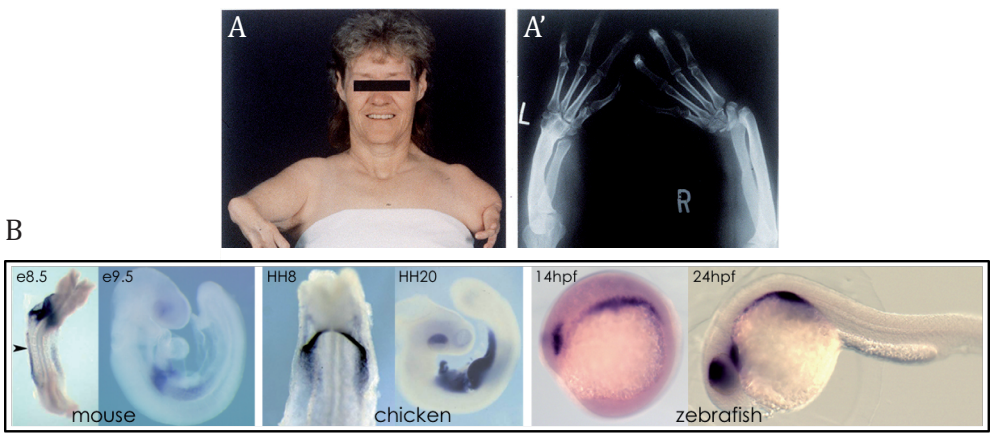

Figure 5 | *Mutations in human TBX5 cause HOS and the expression of Tbx5 is conserved among vertebrates.* *HOS is characterized by cardiac lesions and upper limb defects (A-A'; adapted from eMedMD,). Tbx5 is expressed in the eye, heart and forelimbs in mouse, chicken and zebrafish during embryonic development (B; adapted from CMG* lab). Black arrowhead points to the prospective forelimb in mouse.*

** Carolina Minguillón Gil laboratory*

2. The study of the Tbx2 subfamily genes in zebrafish

2.1. The zebrafish as a model system

Danio rerio (zebrafish) is a teleost that has become a powerful animal model for the study of developmental processes in vertebrates (Figure 6 A). The use of zebrafish as a laboratory animal model is of distinctive interest due to a series of advantages, including external fertilisation and a relatively synchronized *ex-utero* development with a high number of embryos per lay (200-300 eggs) (Figure 6 B). In addition, their optical transparency and the completion of rapid morphogenesis of primary organs within the first 48hpf (hours postfertilization)[68] enables to use live imaging to track early morphogenetic events and follow key events during organogenesis (Figure 6 C, C').

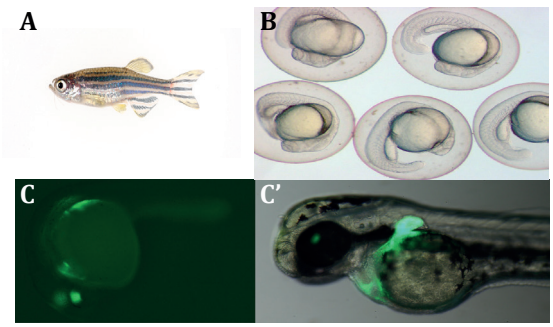

Figure 6 | *Zebrafish have multiple advantages as model organisms.* *Adult female (A). Synchronized ex-utero developing zebrafish embryos (B). Transgenic embryo drives EGFP expression to the retina, heart and pectoral fin at 24hpf (C) and 48hpf (C'). Images from CMG lab.*

Furthermore, the availability of a well annotated genome together with an increasing pool of new technologies for genome editing that go beyond the existence of mutants and the reverse genetics approaches to direct gene targeting, such as TALEN (Transcription Activator-Like Effector Nucleases) and CRISPR (Clustered Regularly Interspaced Short Palindromic Repeats), make them a suitable model for several morphogenetic studies. Techniques for large-scale genome mutagenesis and gene mapping,

transgenesis, protein knock-down or overexpression, cell transplantation and chimaeric embryo analysis and chemical screens have exponentially increased the value of the zebrafish as an animal model for a broad range of experimental studies[69]. In addition, morpholino oligonucleotides (MO) injection for blocking sites on RNA, is a versatile knock-down tool available to target a wide range of RNA for outcomes such as blocking translation, modifying splicing of pre-mRNA, inhibiting miRNA maturation and activity, as well as less common biological targets and diagnostic applications[70]. Specific MO knock-down often is the best approach to identify the function of the target gene, since it avoids genetic compensation that can occur in the mutant or phenotypic rescue by maternally provided mRNA[71].

A drawback for the use of zebrafish as a model resides on the fact that their genome contains an extra copy for many of its genes, which may make it more difficult to elucidate the role of some genes during development, since the phenotype obtained by interfering with one gene might be (totally or partially) rescued by its paralogue depending on the developmental context. Nonetheless, the same fact can also be beneficial in other cases, where a sub-functionalisation event between paralogue genes may allow for the better dissection of the different functions of the gene in different spatiotemporal contexts.

2.2. Expression and function of the Tbx2 subfamily genes in zebrafish

The seven members of the Tbx2 subfamily present in zebrafish (*i.e. tbx2a*, *tbx2b*, *tbx3a*, *tbx3b*, *tbx4*, *tbx5a* and *tbx5b*) are expressed in multiple tissues and organs during development and have been linked to several morphogenetic events.

tbx2a is required to specify the endodermal pouches during development of the pharyngeal arches[72], is also responsible for heart chamber size[73,74] and is related to

pronephros segmentation together with its paralogue *tbx2b*[75]. It has also been described to be expressed in several other structures, such as the developing retina, otic placode, pectoral fin and some neural structures (e.g. diencephalon, hypothalamus)[75]. Its paralogue, *tbx2b*, has been related to hepatocyte differentiation[76], photoreceptor fate determination[76], pineal and parapineal development and specification of the correct number of pineal cells and their asymmetric migration[78,79], heart chamber size[70] and pronephros segmentation[75] together with *tbx2a*. Finally, *tbx2b* has also been described to be essential for neural differentiation along the dorsoventral axis of the zebrafish retina[80].

tbx3a, expressed in the developing pectoral fin bud, the heart tube[69] and the notochord[81], has been shown to be involved in heart morphogenesis[69]. Its paralogue *tbx3b*, is also expressed in the heart and together with *tbx2a* has been shown to be necessary to repress the chamber genetic programme in the non-chamber myocardium as well as being required for the control of cell proliferation in the atrioventricular canal (AVC)[69].

tbx4 is expressed in the pelvic fin[82] and in several neural structures, such as the presumptive neural retina and the diencephalic neurons[83,84]. *tbx4* has been shown to have a fundamental role during the development of the pelvic fin, since mutations in this gene result in the failure of pelvic fin development[82].

tbx5 paralogues (*i.e. tbx5a* and *tbx5b*) are mainly expressed in the pectoral fin, heart and retina[44] (Figure 7 A-D'). Nonetheless, while the onset of *tbx5a* expression is already described at 6-7SS[85] (somite stage) in the eye field, the earliest signal of *tbx5b* is not detected until 14hpf in the developing eye (Figure 7 A, A'). At this developmental time-point both genes are co-expressed in this territory, but only *tbx5a* is expressed in the lateral plate mesoderm (LPM) (Figure 7 A'). *tbx5b* expression in the LPM is de-

tected from 17hpf onwards and (Figure 7 B). Nevertheless, *tbx5a* is expressed in a broader AP (antero-posterior) domain than *tbx5b* (compare Figure 7 B with 7 B'). *tbx5a*-expressing LPM cells are suggested to contain two distinct populations: the anterior population will eventually give rise to the early cardiac field, whereas the most posterior one will contribute to the pectoral fin bud mesenchyme[85,86]. It is evidenced in Figure 7 B that *tbx5b* is expressed in the anterior subset of cells, also positive for *tbx5a* expression, that will give rise to the embryonic heart. At 18hpf, the two populations of LPM cells are clearly distinguished, since the rostral population has begun its anterior migration (as bilateral heart tubes) and the caudal one migrates posteriorly to form the pectoral fin buds (compare Figure 7 E with 7 F, G). At this stage, differences between *tbx5* paralogues become more evident: *tbx5b* expression is only detected in the rostral population, while *tbx5a* signal is detected in both populations (compare Figure 7 C with 7 C'). It is particularly striking that *tbx5b* expression is not detected in the pectoral fin cell precursors, but it is co-expressed with its paralogue in the other territories. Later, around 20hpf, both genes continue to be co-expressed in the developing eyes and in the heart cone (Figure 7 D, D'), whilst the cell population committed to become the pectoral fins only show *tbx5a* expression (Figure 7 D').

Zebrafish embryos with compromised *tbx5a* function show a complete absence of pectoral fins (Figure 7 H, I), whereas heart development is disturbed at significantly later developmental stages as it can be observed at 3dpf in the *tbx5a hst* (*heartstring*) mutant[87] (Figure 7 J, K) and eye development remains to be thoroughly analysed. Regarding *tbx5b*, it had been shown that its knock-down resulted in a reduction in pectoral fin size (Figure 7 H', I') and defective cardiac looping (Figure 7 J', K'). Nonetheless, retinal phenotype was not studied in *tbx5b* morphants[88].

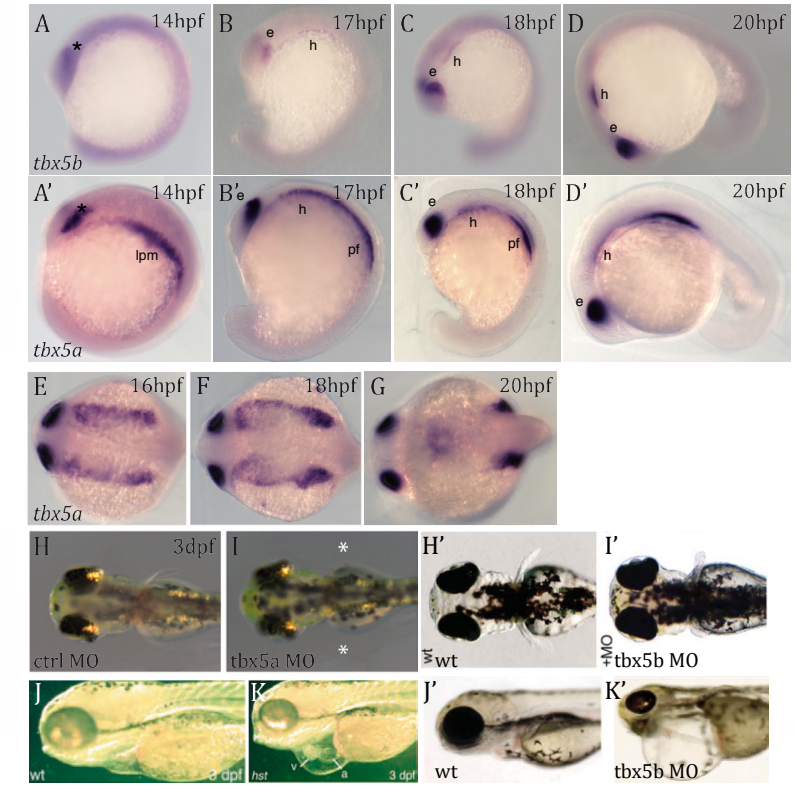

Figure 7 |*Expression pattern of tbx5 genes during zebrafish development and tbx5 knock-down phenotypes.* *tbx5a is co-expressed with tbx5b in the retina, heart and pectoral fins. Lateral views with anterior to the left at 14hpf (A-A'), 17hpf (B-B'), 18hpf (C-C') and 20hpf (D-D'). Dorsal views with anterior to the top for tbx5a expression at 16hpf (E), 18hpf (F) and 20hpf (G). tbx5a MO knock-down results in the lack of fin buds (I) and tbx5b morphants have smaller fins (I') at 3dpf compared to control/wild-type pectoral fins that are already elongated (H, H'). tbx5a hst mutants and tbx5b morphants show pericardial edema together with an unlooped, stretched heart (K-K') compared to the normal heart in wildtypes (J-J') at 3dpf. Dorsal views with anterior to the left (H, I) and lateral views with anterior to the left (J, K). A-D' adapted from Albalat et al., 2010[44], E-I CMG lab, J,K, adapted from Garrity et al., 2002[87], H', I', J', K' adapted from Parrie et al., 2013[88]. Black asterisks in A-A' label the eye field. White asterisks label the area where pectoral fins should have emerged in tbx5a MO knock-down in I. e: eye field, h: heart, lpm: lateral plate mesoderm, pf: pectoral fin.*

3. Retinal Development

3.1. General features

Eye formation is a complex developmental process that requires the coordination of a series of morphogenetic events and the regulated expression of several genes. Therefore, this process has served as a paradigm for organogenesis. After three major, stereotyped events take place –namely evagination, invagination and rotation– the final shape of the eye is acquired[89,90]. This process begins with the specification of the eye territory at early gastrulation and concludes at the pharyngula stage at the onset of neuronal differentiation[89,90]. In zebrafish, lateral evagination (Figure 8 A) of the ventral diencephalon at approximately 11hpf gives rise to the optic vesicle (OV)[91]. Subsequent interactions and contacts established between the surface ectoderm and the OV result in a concerted invagination (Figure 8 B) at 16hpf, that leads to the formation of a bilayered structure, the optic cup (OC), where the inner layer corresponds to the retina and the outer layer is the retinal pigmented epithelium (RPE) and the lens[89,91]. Finally, a 90º clockwise rotation by 22hpf, brings the dorsal retina to its final position[91] (Figure 8 C). Some studies consider an intermediate step between OV evagination and the formation of the OC, in which the OV elongates, and a furrow constricts the connection between the eye and the brain, forming the optic stalk[92].

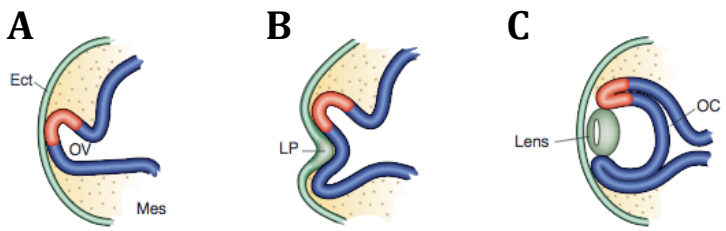

Figure 8 | *Schematic representation of the main events of vertebrate eye development.* *Evagination (A), invagination (B) and rotation (C). The surface ectoderm (Ect) is depicted in green, the presumptive and dorsal retina in red and the presumptive bilayered OC in purple. Mes: Mesoderm. Adapted from Weaver and Hogan[95].*

At the molecular level, it has been shown that the homeodomain transcription factor Rx/RAX (*rx3*/*chokh* in zebrafish) mediates some of these cellular behaviours during the evagination step[89], since in *rx3* mutants OV evagination is disrupted in a cell-autonomous manner[93,94]. Furthermore, downregulation of the cell adhesion molecule Nlcam, a potential direct target of *rx3* in zebrafish, is required to enable the outward migration of retinal progenitor cells in the eye field to contribute to the evaginating OV[95]. Rx promotes non-canonical Wnt signalling, that controls morphogenetic movements of ocular cells[96] and is essential for the expression of other key regulators, such as *pax6*, *lhx2*, *six3* to control, directly or indirectly, specification of retina progenitor cells in the optic vesicle[89].

During the evagination of the OV, the neural retina and RPE domains are specified[89]. Remarkably, the LIM homeobox transcription factor *lhx2*, is the earliest known patterning gene required in the early optic vesicle for specification into both neural retina and RPE and to regulate optic cup formation[97]. Then, the homeobox gene *vsx2* and the bHLH (basic helix-loop-helix) transcription factor *mitf*, are the first genes that show domain-specific expression for the retina and RPE, respectively[98–103].Following OV evagination, its distal side and lens ectoderm invaginate, forming the OC in a process that is dependent upon tissue-tissue interactions[89]. In addition, pre-placodal lens specification is critical for invagination of the distal optic vesicle[89]. Interestingly, disruption of the function of the homeobox transcription factors *Six3* or *Pax6* or the HMG (High Mobility Group) transcription factor *Sox2* during the pre-placodal stage, results in failure of thickening of the lens placode and lens formation, and disrupted invagination that leads to arrest at the OV stage[89,104–110]. In contrast, overexpression of *Six3* results in the formation of ectopic lenses[111,112]. In addition, a role for Bmps in lens induction and Fgf signalling in the lens placode have been shown to be required for the correct OV invagination[89,113–116]. Retinoic Acid (RA) has also been demonstrated to be necessary for OC morphogenesis, providing an essential signal to the neural retina required for morphogenetic movements that lead to ventral invagination of the OC[73,117].

While the morphogenetic movements take place to enable the proper folding of the presumptive eye, patterning along the different retina axes also takes place and once established, the different identities in the retina are maintained to ensure subsequent correct retinotectal projections and visual function. At 24hpf, not only pan-eye genes that specifically define the eye field in earlier stages remain expressed [e.g. *rx3* or *pax6* (Figure 9 A)], but also genes involved in eye patterning along the dorso-ventral (DV) [e.g. *tbx2b*, *tbx5a* (Figure 9 B), *tcf4* (Figure 9 C) or *vax2* (Figure 9 D)], naso-temporal (NT) (e.g. *vax2*) and proximo-distal (PD) (e.g. *pax2a*) axes and topographical guidance clues for the correct organization of the projections to the optic tectum, such as *efn-b2a* or *ephB2* (Figure 9 E, F), among other signalling molecules and their respective receptors.

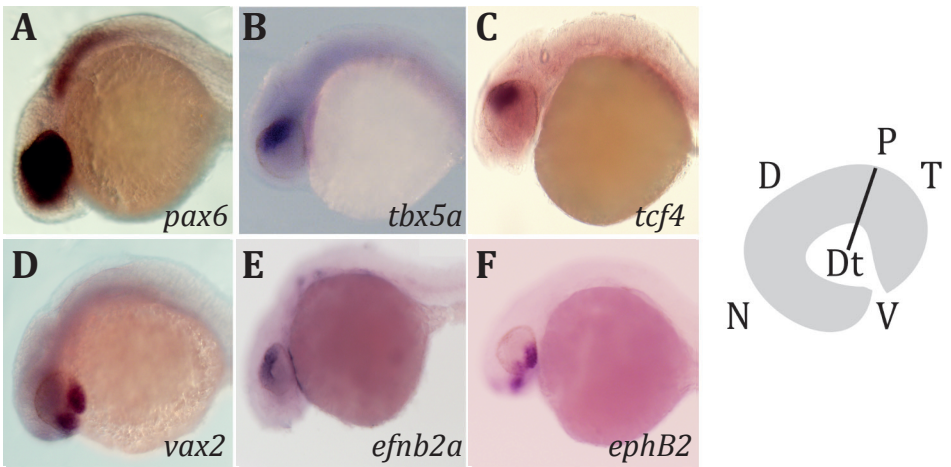

Figure 9 | *Eye field and retinal DV domain at 24hpf.* *Pax6 (A) labels all the retinal territory, whereas tbx5a (B) and tcf4 (C) are markers for dorsal identity and vax2 (D) for ventral identity. efnb2a (E) and ephB2 (F) also highlight the dorsal and ventral territory, respectively. Images are lateral views with anterior to the left. Scheme of the retinal axes on the right side of the panel. D: dorsal, V: ventral, N: nasal, T: temporal, P: proximal, Dt: distal. The black line represents the proximodistal axis.*

3.2. DV patterning of the vertebrate retina

A key step during eye development is the establishment of the DV polarity of the retina, which begins immediately after evagination of the retinal precursors, as evidenced by the expression of specific genes in discrete retinal domains (e.g. *tbx5* expression in the presumptive dorsal retina or *vax2* in the presumptive ventral domain and optic stalk from 12hpf[119]). More specifically, during DV patterning two phases can be distinguished: an initiation and a maintenance phase[114]. Although some authors describe that both Sonic Hedgehog (Shh) and RA are responsible to specify ventral identity[119–122] others have shown that RA is not required for the DV patterning the retina[118,124]. Moreover, the expression of *pax2a*[125], *tbx5*[1] and *vax2*[126] in the retina prior to the onset of RA signalling[127] supports this dispensability of RA. Hence, Shh signalling from the ventral midline is responsible to trigger the initiation of ventral identity[128]. Similarly, there is some controversy with regard to the factors required to induce dorsal identity, although some signalling cascades have been identified for the maintenance of dorsal retina identity [e.g. Wnts and BMPs (Bone Morphogenetic Proteins)[128–131]]. Current models for vertebrate retina DV patterning include a gradient of Bmp signalling, resulting from *Bmp2* and *Bmp4* expression in the dorsal retina and surrounding tissues[129,130] and the expression of Bmp inhibitors in the ventral side. In zebrafish, *gdf6a* (Growth Differentiation Factor 6a), a BMP ligand, was shown to be necessary to induce dorsal fate in the retina and activate dorsal marker gene expression (*bmp4*, *tbx5a*, *tbx2b*, and *efnb2*) while repressing the expression of the ventral fate determinant *vax2*[132]. In other animal models (e.g. mouse), *Tbx5* was found to be regulated by *Tbx2*, which in turn would be under the control of *Bmp4*[119]. This contrasts with the observations made in zebrafish, where no discernible retinal phenotype was detected after *bmp4* MO knock-down[114] and instead *gdf6a* is responsible of dorsal retinal patterning initiation independent of *bmp4*. Few years later, another publication reported that *bmp2b* acts upstream *gdf6a*[133] regulating its expression.

3.3. The role of the Tbx2 subfamily genes in the DV patterning of the retina

The members of the Tbx2 subfamily have been described to be related to dorsal retina identity, specially *Tbx2* and *Tbx5*, and as such, are frequently used as markers of dorsal retina characteristics[21,114,119,133–136]. *Tbx2* is dynamically expressed in the presumptive retina and its loss of function causes a reduction of retinal volume due to increased apoptosis and a delay of ventral OV invagination leading to the formation of small and abnormally shaped OC in mice[119]. In addition, it is also essential for the maintenance, but not for the induction of expression of other dorsal determinants such as *Tbx5*[119]. In zebrafish, whereas there is no functional data implicating *tbx2a* in eye development, *tbx2b* has been related to the cellular mechanisms regulating dorsal neuronal differentiation. *tbx2b* is first expressed throughout the retinal neuroepithelium at 15hpf (Figure 10 A). By 24hpf, *tbx2b* distribution is markedly asymmetric with higher levels dorsally than ventrally (Figure 10 B). This asymmetry proceeds through 30hpf (Figure 10 C, D) and 48hpf (Figure 10 E). At 48hpf, expression is largely confined to the proliferative marginal zones at the retinal periphery, although fainter expression can also be observed in the RGC (retinal ganglion cells) layer (Figure 10, arrow)[80].

With regard to *tbx5* paralogues, *tbx5a* expression starts at around 12hpf in the posterior halves of the retina. This expression is intensified and after eye rotation it gets finally confined to the dorsal retina (Figure 10 A'-C'), where it is restricted to a narrow sector of neuroepithelium that appears to be in contact with the lens and is directly opposed to the choroid fissure, surrounding the posterior groove. By 36hpf, this expression domain is reduced to a few columnar cells of the neuroepithelium adjacent and dorsal to the lens, and finally expression is lost by 48hpf, prior to the differentiation of the RGCs in the dorsal retina[85]. Although *tbx5b* expression is initiated in the posterior retina slightly later in development, around 14hpf, its expression in the posterior retina and it evolves in the same manner as *tbx5a*[44] (Figure 7 A-D).

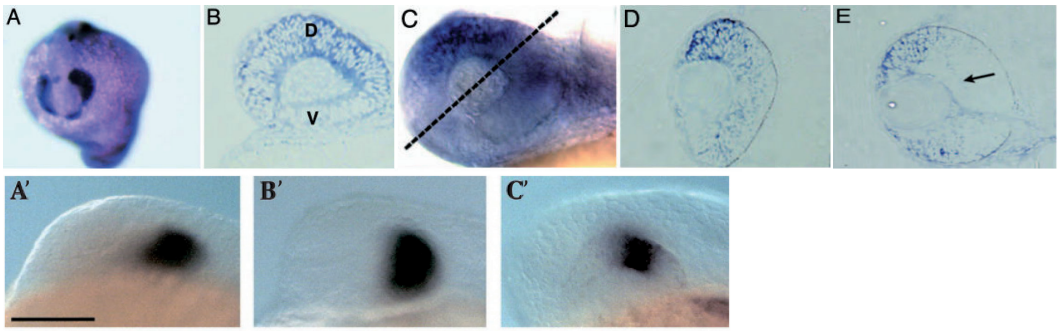

Figure 10 | *tbx2b and tbx5a expression during retinal development.* *tbx2b expression at 15hpf (A). Sagital section through a 24hpf eye with highest levels in the dorsal retina (B). tbx2b expression at 30hpf is prominent in the dorsal retina (C-D). Section at the plane is indicated by dashed line. At 48 hpf, strong tbx2b expression is observed in the dorsal retinal periphery, and fainter expression is observed in the ventral periphery and throughout the ganglion cell layer (arrow) (E). tbx5a expression is restricted to the posterior halves of the eyes at 15SS (A), 20SS (B) and becomes restricted to a dorsal sector of the neural retina from 30hpf (C) to 36hpf, before it is lost prior to the organisation of the retinal epithelium into distinct layers A-E: Adapted from Gross and Dowling, 2005[80], A'-C': Lateral views with anterior to the top, adapted from Begemann and Ingham, 2000[85].*

3.4. Retinotectal projections

Correct axon pathfinding requires proper patterning of the tissues that will harbour the axonal tract, and the precise localisation of axon guidance cues along these tracts at the time of axon outgrowth[137]. RGC projections exit the eye and project across the ventral diencephalon to reach the optic tract, where they project to their primary central targets: the optic tectum in non-mammalian vertebrates[138].

Fundamental aspects of retinotectal development are conserved across vertebrates, including the initial molecular guidance of axons through gradients of ephrins and Eph receptors, and arbour refinement through neural activity[139]. Eph and ephrin families of axon guidance molecules provide positional information required for retinotectal map formation. Interactions between Eph receptor tyrosine kinases and ephrin ligands re-

sult in changes in cell adhesion and cytoskeletal rearrangements, eliciting repulsive or attractive responses. Finally, accurately ordered projections within the optic tectum reflect their position within the retina[136]. Defined *ephrinB* and *ephB* expression domains along DV axis are essential for proper topographical map construction in the tectum[136] (Figure 11). In chick and mice has been shown that *Efnb2* expression in the dorsal retina is induced by *Tbx5* and *Tbx2* when *Bmp4* and *Bmp2* are overexpressed, while in the ventral retina *Vax2* is repressed[128,139]. Impaired expression of any of these molecules leads to abnormal retinotectal mapping[140–142].

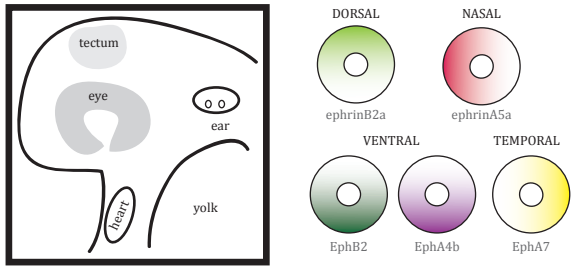

Figure 11 | ***Schematic representation of the distributions of gradients of Eph receptors and ephrin ligands in the zebrafish retina****. Adapted from Kita et al., 2015[139].*

In addition to the axon guidance cue family of ephrin/Eph, Semaphorin3D, Slit/Robo and Netrins have also a roles in axon pathfinding in zebrafish[139]. Furthermore, Shh signalling pathway has been described to be indirectly required for intraretinal axon pathfinding through patterning the optic stalk and correct expression of downstream guidance molecules, the *cxcl12a* chemokine, at the optic disc that directs RGC axons out of the eye[137]. Shh signalling acts non-cell-autonomously for intraretinal axon pathfinding in zebrafish and inhibition of Shh signalling during optic vesicle patterning is sufficient to induce intraretinal axon pathfinding errors later during development[137]. Also, interference in RA signalling, blocking RA receptors (RAR) provoke axons projecting ipsilaterally and aberrant around the eye or leaving the retina from ectopic locations, instead of from the choroid fissure[122].

4 Limb development

4.1. Common steps on limb formation

The development of a limb relies on a series of morphogenetic events including mesoderm-ectoderm interactions, cell migration and patterning. A key step during limb development is the establishment of the limb field at a precise position in the LPM, in the flanks of the developing embryo[143]. Limb buds are the initial structure formed by the protrusion of the limb mesenchyme precursors covered by an ectodermal layer. Signalling interactions between the two tissues promote limb outgrowth[144]. This process is essential and it precedes the development of all the tissues that conform the adult functional limb: the muscular tissue, connective tissue, epidermis, blood vessels and nerves.

Despite the morphological similitude of forelimbs and hindlimbs, their identity is already specified in the initiation phase of their development[143] (Figure 12). This early determination is established by the differential expression of the paralogue genes *Tbx5* and *Tbx4* in the mesenchyme of the prospective forelimb and the hindlimb, respectively[145–149]. The initiation phase of limb bud outgrowth is dependent on the activation of *Fgf10* (Fibroblast Growth Factor) expression in the mesenchyme, which is critical to ensure subsequent outgrowth[150,151](Figure 12). *Tbx5* null mice are unable to form an upper limb bud and show complete absence of *Fgf10* expression[23,152]. In the case of *Tbx4* null mice however, they still form a hindlimb, although it is significantly smaller[153]. *Fgf10* expression is reduced in *Tbx4* mutants, but not completely lost. In addition, some studies have revealed that a paired-type homeodomain transcription factor, *Pitx1* and *Isl1*, are also necessary for hindlimb outgrowth regulating both *Tbx4* and *Fgf10* directly[154,155].

Fgf signalling is required for limb development in both the initiation and maintenance of outgrowth stages[156]. This signalling pathway is required for proper PD patterning of the limb, and disruption of *Fgf10*, *Fgf8*, or *Fgf4/Fgf8* result in severely malformed or truncated limbs[151,157–161]. After the establishment of *Fgf10* expression in the mesenchyme, cells within this territory signal to the overlying ectoderm where *Fgf8* is induced. Ectodermal FGF8 is in turn responsible of maintaining *Fgf10* expression in the mesenchyme. Thus, bi-directional FGF signalling emanating from both, the mesenchyme and the covering ectoderm, results in the creation of a positive feedback loop between the two tissues that is required to sustain the limb outgrowth[144] (Figure 12).

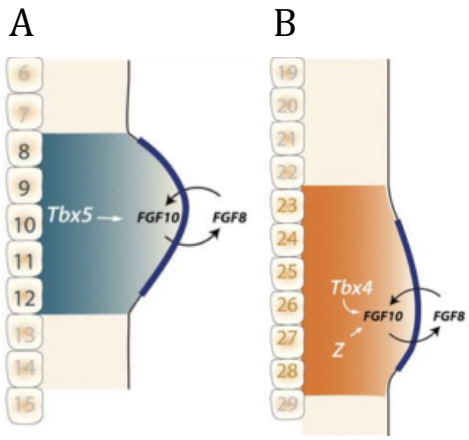

Figure 12 | *The establishment of Fgf positive feedback loop between the mesenchyme and the ectoderm is required to ensure limb development.* *Tbx5 determines forelimb identity and is responsible for the activation of Fgf10 in the mesenchyme (A), whereas Tbx4 confers hindlimb identity and activates Fgf10 in the mesenchyme of this territory (B). Adapted from Duboc and Logan, 2011[143].*

Other signalling pathways such as RA and Shh also play important roles during limb development. RA is implicated in the initiation of both forelimbs and hindlimbs[162–169]. Indeed, blocking RA signalling prevents both forelimb and hindlimb initiation[164,165] [e.g. mouse null mutant for Retinal dehydrogenase 2 (*Raldh2*) do not form limbs and RALDH2 activity blockade inhibits wing bud formation in chicken[170], which can be

rescued by supplying ectopic RA in the LPM[127,166,168]]. Regarding Shh, this pathway is essential for the establishment of the AP pattern and digit number in vertebrate forelimbs and hindlimbs[171]. The expression of Shh, central in AP axis patterning, together with Wnts and Bmps signalling, involved in DV axis formation, are dependent on Fgf signals from the Apical Ectodermal Ridge (AER) in the overlying ectoderm[172].

The role of the key factors that trigger limb development (RA, *Tbx4* or *Tbx5* and *Fgf10*) is conserved among vertebrates[144,173], but the FGF ligands activated in the AER in tetrapods, might vary in different species (e.g. *Fgf8* in mouse or chicken and *fgf24* in zebrafish). Nevertheless, the critical key point is to achieve the establishment of the feedback loop signalling that ensures the outgrowth of the limb[150,174,175]. In addition to the Tbx2 subfamily members *Tbx4* and *Tbx5*, at least seven other T-box genes are expressed during limb development with distinct and dynamic expression patterns: *Tbx2* and *Tbx3* from Tbx2 subfamily, *Tbx1*, *Tbx15* and *Tbx18* from Tbx1 subfamily, *Brachyury* (T) and *Eomes* (Tbr2)[26].

4. 2. Fin development in zebrafish

Similar to what occurs during tetrapod forelimb and hindlimb development, the pectoral and pelvic fins, the equivalent structures in zebrafish, are subject to similar signalling cues during the initiation and outgrowth of these structures. Nevertheless, whilst in other organisms (e.g. mice) both paired limbs are induced at similar stages[143], in zebrafish the pectoral fin is formed much earlier than the pelvic fin. Pectoral fins already become visible as a small protrusion at 28hpf[144], whereas the pelvic fin only emerges at three weeks of development, more than two weeks after completion of somitogenesis[175]. In addition, in contrast to the pectoral fin, the early pelvic fin directly forms the adult fin, without first creating an intermediate larval fin[176]. Therefore, the pectoral fin is a much more suitable model for the study of the early limb development than the

pelvic fin. Indeed, there exist multiple studies using the pectoral fin as a model, whereas the molecular mechanisms for the development of the pelvic fin remain largely unknown[144].

Pectoral fins derive from the LPM and emerge at the level of the 2-3 somites. Fin bud compaction occurs between 18hpf and 28hpf[144] and from this time point onwards, the bud emerges as a small protrusion. Compaction of the fin primordium is apparently the result of a feed-forward mechanism: *tbx5*-expressing mesenchymal cells activate expression of *fgf24* in the fin field (Figure 13), which ensures the subsequent compaction of the *tbx5*-positive cell population within this region[177]. Proper fin outgrowth requires *fgf24* downregulation in the fin mesenchyme with subsequent activation in the AER[175] after the establishment of a positive Fgf feedback loop between the mesenchyme and the surrounding ectoderm. The AER is a transient embryonic structure that consists in an apical thickening of wedge-shaped cells of the basal stratum[176] at the distal part of the fin bud. It is important to highlight that *tbx5a* is the first marker of pectoral fin identity and its expression in the mesenchyme is fundamental for fin bud induction. Thus, interference with *tbx5a* function by MO knock-down or in the *hst* mutants causes total absence of the pectoral fin[86,87]. After *tbx5a* activation by *hox* genes, *fgf10* is eventually activated in the mesenchyme downstream of *fgf24*[178] (Figure 13). Indeed, the *fgf24* gene that belongs to the *fgf8/17/18* gene family, is the first Fgf gene described to be expressed in the fin bud mesenchyme and its mutant ikarus (*ika)* lacks pectoral fins[178]. Therefore, *ika* embryos are unable to activate *fgf10*, and consequently show reduced *tbx5* expression, that will ultimately regress. Subsequent fin outgrowth though, requires *fgf24* downregulation in the fin mesenchyme with subsequent activation in the AER[144].

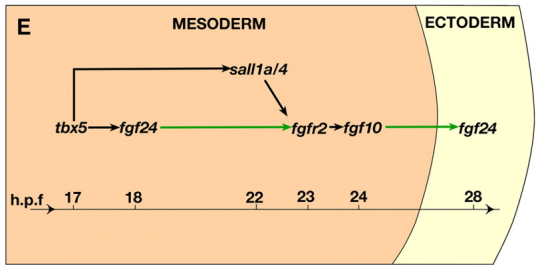

Figure 13 | *Representation of the regulatory relationships between genes required for pectoral fin development.* *Green arrows indicate relationships between FGF receptors and ligands, while black arrows represent transcriptional regulatory relationships. Adapted from Harvey and Logan, 2006*[179].

5. Heart development

5.1. General features

The heart is the first organ to fully develop and function during embryonic development in vertebrates. In addition, it is also the first organ where left-right (LR) asymmetry is evident. In zebrafish, cardiac development can be briefly described as the folding of the lateral cardiogenic layer that gives rise to a tubular heart[180,181]. Then, the tube will loop creating the atrial and ventricular chambers that bloat at the outer curvature. The mesodermal tissues by which the vertebrate heart is mainly composed already specify once gastrulation begins with the ingression of cells from the epiblast[182] (Figure 14A). Heart tube precursor cells originate during early-mid gastrulation[183] (Figure 14B). The endocardial and myocardial lineages are differentiated in the bilateral heart fields while they migrate towards the midline where they will eventually fuse (Figure 14 C-D) and give rise to the cardiac tube[184–187]. The main events that occur during early development of the heart are also shared among vertebrates. These processes include heart tube formation, rightward looping, heart tube elongation by the addition of progenitor cells from adjacent pharyngeal mesoderm, cardiac chamber morphogenesis and cushion and valve morphogenesis[188]. However, the four-chambered heart found in reptiles, birds and mammals contrasts with the much simpler two-chambered struc-

ture with one atrium and a ventricle that fish possess or the three-chambered system, containing two atria partially or completely divided in amphibian tetrapods[189]. The distinct anatomy and functionality of the structure for the different systems though, have specific benefits for each species.

Since the main events taking place during heart morphogenesis are conserved in vertebrates, the study of zebrafish heart morphogenesis is particularly useful. In contrast to avian and mammalian embryos, zebrafish are not totally dependent on a functional cardiovascular system for their development, therefore embryos that lack blood circulation are still able to survive the initial phase of embryonic development thanks to passive diffusion of the oxygen[190]. In zebrafish, heart development starts with the specification of endocardial and myocardial progenitor cells located in the marginal zone at either side of the embryo prior to gastrulation (5hpf, Figure 14 A)[190]. Atrial progenitors occupy a more ventral position in the lateral marginal zone compared to the ventricle progenitors. In the case of the endocardial progenitors, these are scattered throughout the marginal zone without an apparent organization[180]. After involution, during gastrulation and early somitogenesis the cardiac progenitors migrate towards the midline reaching their destination at the level of the hindbrain (by somite 5)[181] (Figure 14 B). Endocardial precursor cells lie most medially, whereas the myocardial precursor cells are situated more laterally[191,192]. By 13SS, the myocardial precursors have segregated into preventricular and preatrial groups (Figure 14 C) and from 19hpf the myocardial precursors begin to merge in the posterior part forming a horseshoe-shaped structure[181] (compare Figure 15 A, A' with Figure 15 B, B'). During mid- and late-somite stages, cardiogenic differentiation and heart morphogenesis occur at once, which difficult to assign specific function to genes during this period of embryonic development[190]. Namely, at this developmental point, the myocardial cells migrate to the midline and begin to assemble while they begin to express genes that are associated with terminal differentiation and start to contract. Thus, within a few hour time-frame myocardial cells expressing *nkx2.5* begin to express sarcomeric genes.

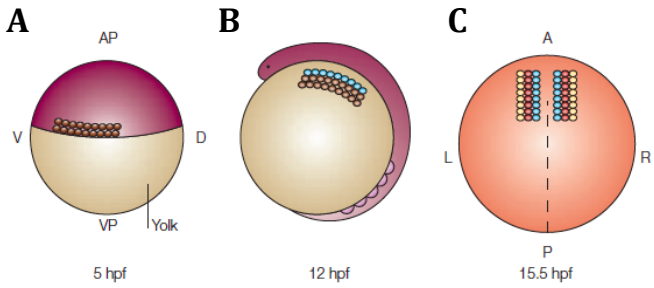

Figure 14 | *First stages of zebrafish heart development.* *Before gastrulation (5hpf) heart progenitor cells are located throughout the ventral and lateral regions of the embryo (A). After involution, the cells converge towards the embryonic axis and reach their final destination at the level of the future hindbrain (~12hpf; 5SS) (B). Myocardial precursors segregated into preventricular (red) and preatrial (yellow) groups (15.5hpf; 13SS)(C). (D). A: anterior, AP: animal pole, D: dorsal, L: left; P: posterior, R: right, V: ventral, VP: vegetal pole. Adapted from Stainier, 2001*[181].

By 19.5hpf the anterior cells migrate in a coherent and medial direction and fuse in the anterior part[181]. Consequently, the horseshoe gets transformed into a cone with the ventricular (arterial) cells at the centre and apex and atrial (venous) cells at its base[181](Figure 15 C, C'). Finally, the endocardial cells lie inside the cone. The formation of this cardiac cone is a critical step in heart morphogenesis. The cone is initially orientated along the DV axis but it rapidly rotates 90º in a clockwise manner to achieve an AP orientation[193] .This rearrangement is potentially led by physical forces exerted in both organ autonomously and organ non-autonomously[181].Then, the cone extends and telescopes out to form the heart tube undergoing the first asymmetric event of its development: cardiac jogging (Figure 15 D, D'). Polarity and epithelial organization are critical for the extension of the cardiac tube, as loss of cell polarity results in an arrest of cardiac morphogenesis at this stage[191,192,194,195]. The ventricular end is the first assembled, followed by the atrial end. This leftward displacement event results in the positioning of the tube along the AP axis at around 24hpf, with the atrial side lying to the left of the midline.

Despite the endocardial and myocardial cells belong to different populations, both migrate towards the left side simultaneously[196]. Nonetheless, myocardial-endocardial interactions have a minor role during myocardial migration. Indeed, in the absence of endocardial cells, the formation of the heart cone is only mildly affected[197,198]. This directed migration requires the extracellular matrix component hyaluronic acid and the Nodal and Bmp signalling pathways, expressed asymmetrically in the anterior LPM, are also essential for the correct directed migration. Nodal and Bmp signalling pathways are also important earlier in heart development, since both are responsible of inducing *nkx2.5* expression and cardiogenic differentiation by *gata5* activation[199].

Later, by 30hpf, the different chambers are morphologically distinct and around 36hpf the heart tube goes through a second asymmetric event: cardiac looping (Figure 15 E, E'), by which the ventricle ends up positioned at the right side of the embryonic midline sitting on top of the atrial chamber, which stays in the left side[190]. According to studies in zebrafish and chick, RA is involved in the chamber formation by encouraging atrial development at the expense of ventricular development[200,201]. These results have also been reported in mouse[202]. The direction of cardiac looping is determined by the previous asymmetric event (cardiac jogging): tubes displaced towards the right side will eventually loop in the reverse direction[203]. At 48hpf, functional valves are formed. Their presence is required to prevent blood to flow back from the ventricular chamber to the atrium when the ventricle contracts.

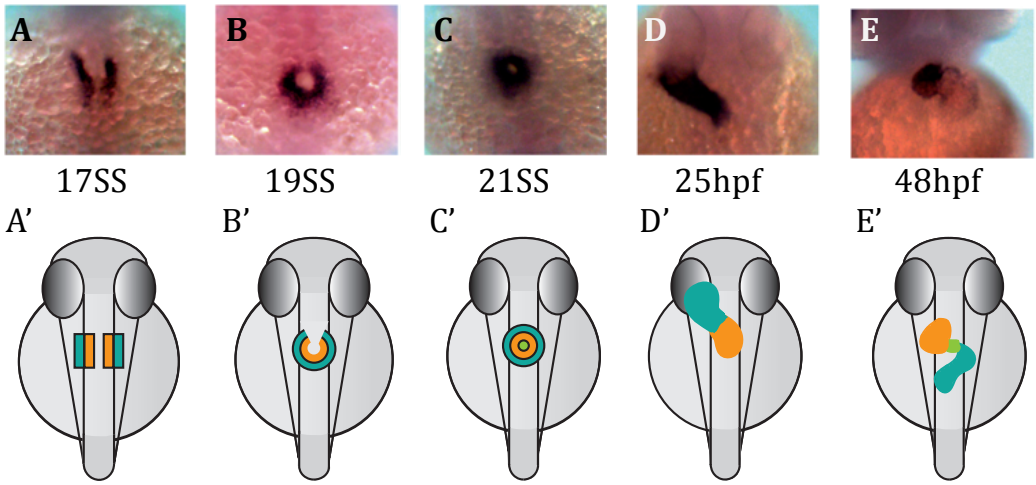

Figure 15 | *Zebrafish cardiac development.* *At 17SS myocardial precursors migrate towards the midline (A-A') and soon after they will fuse at the posterior part (B-B'). At 21SS the fusion also has occurred in the anterior part giving rise to the cardiac cone (C-C'). The cardiac cone then telescopes towards the left side of the embryo (D-D') in the asymmetric event of cardiac jogging. This asymmetric event is followed a dextral torsion, i.e. cardiac looping (E-E') a second asymmetric event after which the ventricle ends sitting on top of the atrial chamber. A-D: Dorsal images with anterior to the top. E is a ventral image with anterior to the top. A-E: CMG lab ISH images for myl7 highlighting the cardiac precursors. In the scheme, orange is for ventricular precursors, while turquoise corresponds to atrial precursors. In green is highlighted the AVC.*

5.2. Signalling during cardiac development

Heart morphogenesis and cardiomyocyte differentiation are complex processes that demand the coordination of multiple signalling pathways. The temporal and spatial integration of all the events is essential to acquire a functional cardiac structure[204]. During the directed migration towards the midline the acquisition of a polarized epithelial organization by the medial myocardial progenitor is fundamental. Myocardial progenitor cells express β-catenin with basolateral localization and aPKC (atypical protein kinase C) and junctional localization of ZO-1 (zonula occludens 1) on the apical surface[194,205]. In addition, the preservation of adherens junctions between the myocardial progenitor population relies on fibronectin deposits which laterally edge

the myocardial progenitor cells[205,206]. As previously mentioned, Bmp and Nodal signalling pathways play relevant roles during heart morphogenesis. Cardiac jogging is controlled by the Nodal co-receptor *oep* (one-eyed pinhead)[207] and the left-sided Nodal signalling cascade[208]. Indeed, cardiomyocytes lacking *oep* move slowly and with reduced directionality[209]. A similar function has been proposed for Nodal in regulating cell migration during cardiac jogging. Bmp4, expressed in the LPM and heart field, depends on Nodal signaling[203,210]. Furthermore, Bmp signalling is needed to repress the nodal-related gene *southspaw* (*spaw*) expression in the right LPM, probably by inducing *lefty1* expression in the midline. Thus, Bmp signalling appears to be acting at two different levels, downstream and upstream of the Nodal signalling pathway[210]. Cardiac cells are extremely sensitive to the dosage of TGFβ (Transforming Growth Factor) signals and possibly complex coordination of Nodal and Bmp signalling pathways control of the differential motility along the LR (Left-Right) axis of the myocardial and endocardial cells[211]. Nevertheless, a study from the Bakker's lab revealed that after gastrulation, Nodal signalling is dispensable for directional heart looping and demonstrate that non-muscle myosin II activity and actin polymerization are essential for cardiac looping[212]. In addition, another recent study supports the existence of a right-handed pathway that conducts differential LR EMT (epithelial-mesenchymal transition) and heart looping in vertebrates. A left-specific Nodal–Pitx2 pathway would confer left identity in the LPM and repress the right-handed pathway, whereas Bmp signalling would activate EMT in the LPM in a LR asymmetric manner to drive heart laterality and the repression of leftward identity on the right side through the repression of the Pitx2 transcription factor[213].

Several T-box genes are involved in the vertebrate heart morphogenesis. These include Tbx1, Tbx2, Tbx3, Tbx5, Tbx18, and Tbx20 and their roles have been linked to early cardiac lineage determination, chamber specification, valvuloseptal development, and diversification of the specialized conduction system in vertebrate embryos[61,214]. To reach adequate levels of T-box protein is key to ensure the functionality of the-

se genes, since haploinsufficiency result in syndromic diseases in humans for *TBX1*, *TBX3* and *TBX5*. In addition, haploinsufficiency phenotypes have also been described in mice with *Tbx1* or *Tbx5* targeted mutagenesis[61,214]. Interactions of T-box proteins with other transcription factors involved in cardiac development add complexity to the regulatory mechanisms that ensure correct morphogenesis. Thus, it is of paramount importance the tight regulation and coordinated expression of T-box proteins with other cardiac genes such as *nkx2.5* or *gata4*. For instance, in mice Tbx20 has been reported to physically interact with the cardiac transcription factors Nkx2.5, Gata4 and Gata5, collaborating to synergistically activate cardiac gene expression[17].

A variety of molecules and signalling pathways affect T-box gene induction, which include Fgfs, Bmps, Wnts and RA. Regarding T-box target genes in the developing heart, these include lineage-specific genes and genes related to growth control. For instance, Tbx2, Tbx3, Tbx5, and possibly Tbx20 are involved in the regulation of atrial and conduction system genes (e.g. *Cx40*, *Cx43*, and *Nppa*)[214–217]. In addition, cardiac restriction of T-box target genes is probably due to protein-protein interactions between T-box, Nkx, and GATA families[218]. It is worth to highlight the role of *Tbx5* during early cardiac development. This transcription factor is a transcriptional activator of genes associated with cardiomyocyte maturation and it also acts upstream of morphological signals for septation[219,220]. During later cardiac development, *Tbx5* is required for patterning of the cardiac conduction system and maintenance of mature cardiomyocyte function[214]. Cardiac expression patterns of *Tbx5* in human, mouse, chick, and frog are very similar. In addition, both paralogues (*tbx5a* and *tbx5b*) in zebrafish are also expressed in the developing heart. In human hearts, TBX5 is expressed in the epicardium, myocardium, and endocardium of embryonic and adult hearts[215]. Functionally confirmed *TBX5* direct targets in the heart are genes implicated in cardiac proliferation, maturation, and function, including *Nppa*, *Gja5*, and *Scn5a*[61,62,185,215,221–226], while no direct effectors of morphology have been uncovered for *TBX5*[214].

6. Left/Right Asymmetry

6.1. Overview and incidence

Despite the external symmetrical appearance of vertebrate organisms, the developing heart together with several other internal organs (e.g. liver, pancreas, gut) and paired structures (e.g. lungs and brain hemispheres) exhibit a defined position in the body plan along the LR axis. Indeed, the establishment of the LR axis during embryonic development, in addition to the DV and AP axes, is crucial for the subsequent proper positioning of organs (*situs solitus*) and their functionality. Impaired LR patterning during embryogenesis results into a partial or total organs reversal (heterotaxia and *situs inversus*, respectively) or other birth defects of clinical relevance (e.g. Kartagener syndrome or Primary Ciliary Dyskinesia (PKD)[227] and Ivemark syndrome or right atrial isomerism[228]). Therefore, understanding the establishment of LR asymmetry is fundamental to understand these human conditions (Figure 16).

Laterality defects in humans are rare disorders, with an incidence of 1:8,000 to 1:10,000[230] and a multifactorial aetiology. To date, many cases of LR asymmetry disorders have been reported, and yet with more than 100 genes that have been identified as playing important roles in the establishment of LR asymmetry in animal models, the aetiology of these human disorders remains unclear[230,231]. Laterality defects arise due to both genetic and environmental factors and phenotypes are highly heterogeneous, ranging from asymptomatic to severe clinical conditions[232]. Interestingly, a wide variety of human syndromes affecting paired organs present a bias for one side[233]. The molecular mechanisms that drive LR asymmetry have been largely unknown up until the last couple decades and some hypothesized that subtle molecular differences may exist between organs which are assumed to be symmetrical (e.g. limbs or eyes)[234]. This idea is also suggested by some human conditions: fibular a/hypoplasia affects the right side more often[233], while HOS presents upper limb malformations which are much

more common on the left side[215,235–237]. Indeed, a recent publication in mouse shows that bilateral suboptimal levels of *Tbx5* fail to reach threshold levels that buffers the inherent asymmetry in the left and right LPM. Thus, it results in abnormalities in limb formation that affects more severely the left limb[54].

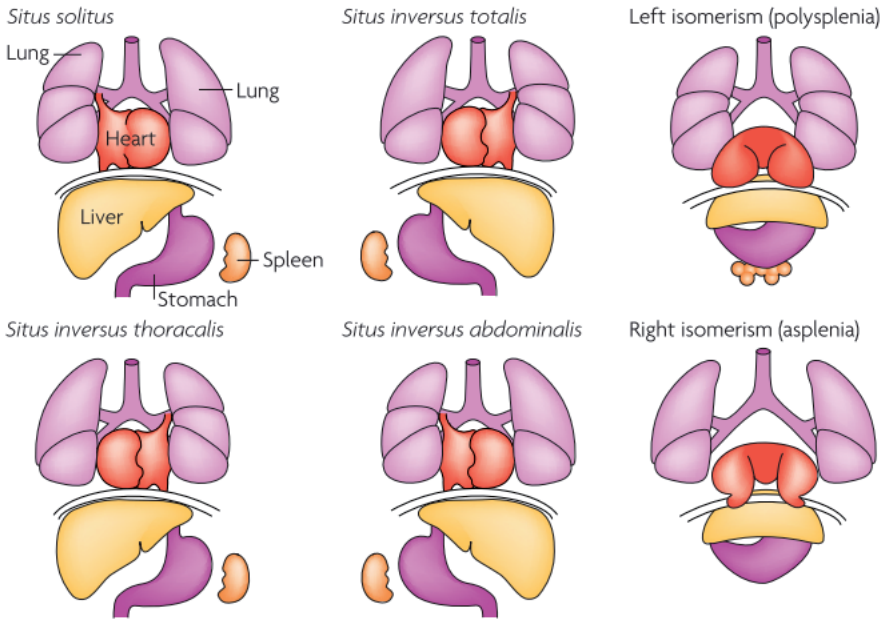

Figure 16 | *Left-Right disorders in humans.* *Schematic representation of the lateral orientation of the asymmetric organs within the body plan in normal conditions and in five different laterality defects that affect the lungs, heart, liver, stomach and spleen. Adapted from Fliegauf et al., 2007*[229].

6.2. Prevailing models for the establishment of LR asymmetry

It is generally accepted that the establishment of LR asymmetry in vertebrates consists of three main phases[238–241]. *Phase* 1: LR asymmetry originates in transient midline structures referred to as left–right organizers (LROs) that appear at the posterior end of the notochord during early somite stages (e.g. node in mouse, gastrocoel roof plate (GRP) in *Xenopus* or Kupffer's Vesicle (KV) in zebrafish). *Phase* 2: asymmetries that originate in and around LROs are then transferred to the LPM. *Phase* 3: final correct position of organs along the LR axis (Figure 17 A).

The first phase is the one that generates more controversy. In the absence of a consistent canonical model, it is widely accepted that a symmetrical embryo distinguishes L from R only after the DV and AP axes have been established, by consistent orientation of some subcellular component inherently chiral[242]. Therefore, the existence of an inherently biophysical origin of asymmetry preceding the asymmetric transcriptional events is accepted[241]. The prevailing model proposes that the movement of cilia present in LROs in the neurulating embryo creates a chiral fluid flow within this transient structure (Figure 17 B). The flow is directional with a strong anticlockwise current due to cilia orientation and biochemical structure[243–245]. Nevertheless, another explanation called intracellular model suggest that the symmetry break arises from cytoplasmic cytoskeletal chirality during the first cell cleavage events. Three different non-mutually-exclusive proposals aim to explain this model: the ion flux model, the chromatin segregation model and the planar cell polarity (PCP) model[241]. These models justify their proposals claiming that a great number of intracellular elements are extensively conserved in LR patterning, including invertebrates and plants[238,246,247.] In addition, in some vertebrates, e.g. chicken, it has been proposed that signalling in the LRO (Hensen's node) is independent of cilia, since there is not an evidence for motile cilia or fluid flow[248]. This is also the case of the pig, whose LRO is not ciliated[249]. Data that support each of the models of LR asymmetry cannot discriminate which is the one

truly responsible for this symmetry break. For example, interference with cytoskeletal proteins affects the intracellular cytoskeleton, but also the cilia, thus not allowing to identify the real cause and to distinguish between the two models. Therefore, here we will consider the cilia model, which has been accepted with higher consensus in the developmental biology community.

Cilia are microtubule-based organelles that protrude from the apical side of cells and, in the case of LROs, are distributed in a one cilium per cell manner. Interestingly, different plausible mechanisms by which the fluid flow created in the LRO is amplified also exist in the cilia model. Consequently, there has also been some discussion in the field to determine which of them could better explain the observed experimental data. One model claims that the accumulation of extracellular morphogens on the left side of the embryo results in the transmission of this signal in the left LPM. Nodal, Fgf, Shh and RA are proposed to act as morphogens[250], although not fully supported by experimental data. For instance, despite in mice Nodal has been suggested to signal from the node to the LPM via an internal route, travelling directly to the LPM via interaction with sulfated GAGs (glycosaminoglycans), this could not be the case in zebrafish, since *spaw* mutants still express *spaw* in the LPM[212,251,252]. Another model, defends that the asymmetric distribution of nodal vesicular parcels (NVPs), small membrane-bound vesicles that transport morphogens in a leftward movement is the responsible mechanism[253–255]. Finally, a last explanation is based on asymmetric detection of fluid flow itself by mechanosensory cilia leading to calcium signalling on one side of the embryo [250,256–260]. All three models have experimental data that support them, and regardless whether there is a prevailing model or it is indeed a combination of the three, the important fact at this developmental point is that left biased signals are transmitted to the peripherally located cells around LROs creating asymmetries in gene expression in this territory. Either way, an increase of intracellular Ca^{2+} concentration on the left periphery of the ventral LRO is ultimately created and then laterally propagated to firmly ensure left side identity[258] (Figure 17 C).

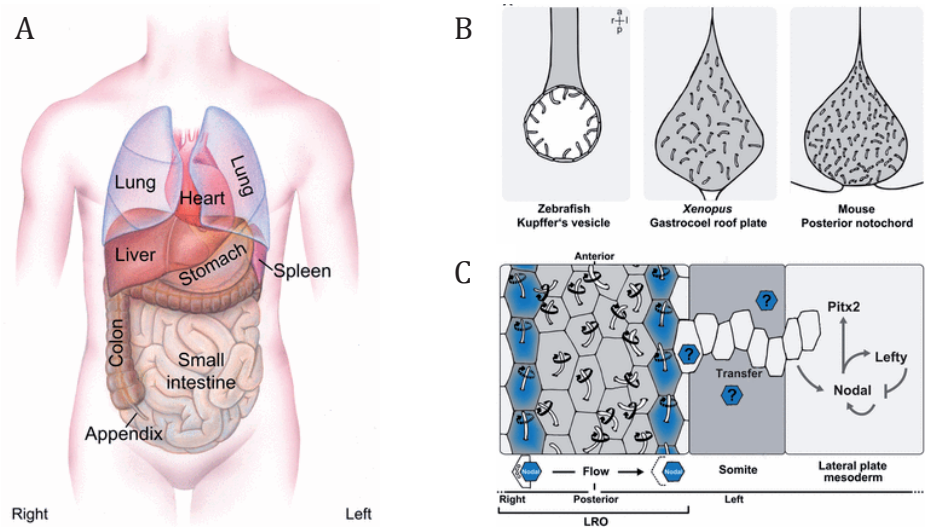

Figure 17 | ***Asymmetrical disposition of organs in human and model for the onset of LR asymmetry.*** *Schematic drawing for asymmetric organs (A). LROs in different organisms differ in shape(B). Depiction of leftward flow at the ciliated epithelium of an LRO (C): motile and polarized cilia (positioned at the posterior pole of cells) rotate in a clockwise fashion to produce a leftward fluid flow in the extracellular space. Flow is sensed by unpolarized cilia on cells bordering the LRO. The asymmetric signal (likely to be Nodal protein; blue octagon labeled with question mark) is transmitted to the left LPM, where the Nodal cascade is induced. Adapted from Blum et al., 2014*[249]*.*

6.3. General features and signalling pathways related to the establishment of LR asymmetry

It is widely accepted that the symmetry break in vertebrates emerges in the LROs at the posterior pole of the notochord and the conserved Nodal signalling pathway has a key role to magnify the biased signalling cues originated. Although LROs have structural differences in terms of shape and cilia[249,257] (Figure 17 B), the main mechanistic features by which LR asymmetry is achieved, are conserved across many vertebrates. Once cilia rotation creates a clockwise flow in the cavity of the LRO, asymmetric gene expression is generated in the vicinity of this structure. A key step in the establishment of left identity is the downregulation of the Nodal pathway repressor *Dand5* (DAN do-

main family member 5) - *charon* in zebrafish - in the left side of the LRO, triggering the activation of left-sided Nodal signalling. Nodal activation induces the expression of its downstream targets (e.g. *Lefty1*, *Lefty2*, *Pitx2*) and Nodal itself[261–263]. In addition, whilst Nodal signalling pathway induces its own expression in the left-side LPM by positive feedback regulation, another member of this pathway, Lefty1, a Nodal antagonist, restricts Nodal activity to the left side by a negative feedback regulation[261,264]. The relation between *Nodal* and *Lefty* has been described to fit into a self-enhancement and lateral-inhibition (SELI) model, in which subtle differences in expression levels are dramatically transformed between two separated regions due to the enhancement of this differences through local activation and long-range inhibition[265]. This model implies that the inhibitor (LEFTY1) spreads faster and diffuses further than the activator (NODAL), which is indeed true[266–268]. Thus, small differences in nodal expression in the LRO are amplified in the LPM (Figure 18). In addition, the antagonistic relationship that these two Nodal signalling members hold seems to be based on the interactions of lefty proteins with EGF-CFC (Epidermal Growth Factor-Cripto/FRL-1/Cryptic) co-receptors and Nodal ligands impeding the establishment of receptor complexes[203,269]. Furthermore, Nodal long-range activity has been shown to be dependent on *Gdf1* in mice, which enhances nodal specific activity by directly binding to it[270].

Vertebrates have two lefty genes, *Lefty1* and *Lefty2*, but while *Lefty2* is mainly expressed in the left LPM, *Lefty1* is primarily expressed in the midline preventing the leak of nodal signalling to the right side of the embryo (Figure 18). Disruption of the midline structure or midline gene expression (e.g. *Lefty1* or *Ntl*) results in the loss of left-side restricted expression pattern and consequently loss of proper organ patterning along the LR axis[271–274]. Nodal signalling in the LRO is fundamental for its own subsequent expression in the left LPM[275,276]. NODAL activates the homeobox transcription factor *Pitx2* in the left LPM, which remains expressed in this region for several hours after Nodal signalling has already ceased[261.] Loss of *Pitx2* in mouse mutant embryos affects the heart vessels and lobation of the lungs[277]. Nevertheless, other asymmetries such

as heart looping or stomach sidedness are not affected in these mutants and strikingly, in zebrafish loss of *pitx2* does not cause any phenotype in organ laterality[278]. Regarding Nodal inhibitors *Lefty1* and *Lefty2*, loss of *Lefty1* result in a bilateral expression of *Nodal* in the LPM after losing its expression in the midline barrier, while in mouse *Lefty2* mutants it has been described that *Nodal* show longer persistency and further expression accompanied by an upregulation of *Pitx2*[268].

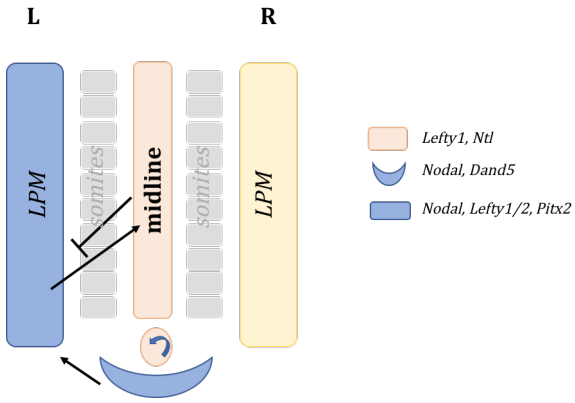

Figure 18| ***Schematic representation of the Nodal signalling pathway during the establishment of LR assymmetry.*** *The directional fluid flow created within the LRO is transmitted to the surrounding territory where Nodal signalling pathway is activated and subsequently induces its own activation in the left LPM. Remarkably, the Nodal target gene Lefty1 together with Ntl are expressed in the midline to prevent signalling leakage from one side to the opposite of the embryo.*

Several studies have also suggested that Bmp signalling has different functions during LR patterning in zebrafish, chick and mouse, probably due to the dynamic expression in different developmental time points and tissues[210,279]. However, the outcome of these studies is quite controversial, since the effect of Bmps on Nodal signalling has been observed to be positive or negative depending on the biological context and animal model. In chicken, Bmps are required for Nodal induction and maintenance in the left LPM[280–282] as has been suggested in mice [279,280]. In contrast, a repressive function of Bmp signalling has been described in *Xenopus*: whilst inactive Bmp signalling on the right

side causes bilateral expression of *Nodal*, constitutively active Bmp signalling causes loss of nodal expression[283]. Besides, misexpression of the Bmp antagonist *Caronte* in the chicken left LPM is sufficient to activate Nodal in the right LPM[284–286]. In mouse, mutant embryos for either *Smad5* or *Alk2* express low levels of *Lefty1* in the midline and hence, *Nodal*, *Lefty2* and *Pitx2* are bilaterally expressed[287,288]. In addition, Bmp antagonists *Chordin* and *Noggin*, restrict Bmp signalling in the left LPM[289]. Similarly, in zebrafish has been proposed that Bmp represses nodal by inducing *lefty1* in the midline, thus preventing nodal expression on the right side[210]. All these results, seem to indicate Bmp signalling has different roles during the establishment of LR asymmetry at different developmental stages. Studies in zebrafish propose that Bmp4 represses *spaw* during early segmentation, right after the formation of the KV. This inhibition would result in the regulation of both visceral and cardiac laterality. Moreover, a second wave of *bmp4* signalling would be responsible uniquely for cardiac laterality[210].

Besides the TGF-β signalling pathways of Nodal and Bmps, a number of intercellular pathways such as Fgfs, Wnts, and Shh, have also been reported to have a role in the control of LR asymmetry[210,253–255,290–293]. Finally, several T-box genes have also been identified to have a role in LR patterning or cilia development. In a screen to identify targets of Ta, one of two zebrafish orthologs of T, *flh* was identified[294], which is required for normal KV and cilia formation[2]. In addition, *Tbx6* regulates LR patterning in mouse embryos through effects on nodal cilia and perinodal signalling[295] and *Tbx3* has been found in primary cilia and localized to the same regions of the cilia where GLI3-repressor is found in mice[87]. In the case of *tbx5*, zebrafish *hst* mutants have been described to show central and linear disposition of the heart[87], in contrast to a directional displacement in the case of the wildtypes. In addition, 70% of HOS individuals exhibit asymmetrical upper limb defects[296]. Hence, the regulatory mechanisms involved in the establishment and maintenance of LR patterning in vertebrates include many signalling pathways and are overall quite complex. Laterality has been reported

to be affected not only by drugs (e.g. cadmium, lidocaine, nitrofurazone) or asymmetrical expressed genes (e.g. *spaw*, *lefty1*, *bmp4*), but also by bilateral expressed genes such as *fli-1*, *hest-1* or *rtk-2*[234].

6.4. Establishment of LR asymmetry in zebrafish

The KV, the LRO in teleosts, is a fluid-filled transient organ located at the posterior end of the notochord during early somitogenesis[271,297] discovered in 1868[298]. In zebrafish, the KV originates from a cluster of 20-30 cells, the dorsal forerunner cells (DFCs), which appear adjacent to the embryonic shield at mid-gastrulation and migrate towards the vegetal pole by late gastrulation[299,300]. DFCs become polarized epithelial cells and create a rosette-like structure at the 1–2SS[271,301]. Then, the lumen of the KV inflates becoming a fluid-filled structure and a single motile cilium protrudes from the apical surface of each cell pointing towards the lumen[302]. Defects in the specification of the DFC, their clustering or migration cause failures in KV assembly, ciliogenesis and LR patterning[297].

Intriguingly, progenitor cells of the DFC/KV lineage remain connected to the yolk cell up until 4hpf, while the contacts between the rest of the embryonic cells and the yolk are closed after 2hpf[297,300,303]. Yet, this fact has provided a unique opportunity to target the cell population that gives rise to the KV without affecting the other embryonic cells and show specific phenotypes of certain genes linked to LR asymmetry. Nevertheless, injecting in this time-frame of 2-4hpf not only delivers the injected solution to the DFCs, but also to the yolk and the yolk syncytial layer (YSL) and therefore, it is extremely important to generate a control by injecting after 4hpf at sphere-dome stages (4-4.3hpf) to demonstrate that the observed phenotype is not due to a signalling alteration in the yolk or the YSL. This approach has enabled to demonstrated a key role for multiple signals during KV morphogenesis (e.g. Fgf, Nodal, Notch, Shh and Wnt).

Correct KV organogenesis is crucial for subsequent signalling and embryonic patterning along the LR axis. Structural defects in the KV, such as smaller size or inability to inflate, or in its cilia (*i.e.* length, number or motility) lead to aberrant signalling and incorrect positioning of the heart, visceral organs and neural structures. For instance, the balance between motile and immotile cilia and their localization in the KV needs to be tightly regulated. Otherwise, an accumulation of immotile cilia at the anterior half of the KV caused by different signalling impairments, such as overexpression of *her12* or Notch intracellular domain (NICD), disrupts the normal intensity of the fluid flow and patterning affecting LR establishment[304]. Other parameters, such as KV size or cilia number, are not that solidly controlled during development, but rather must be hold within a range to secure robust LR patterning. The length of KV cilia had the smallest amount of variability, whereas KV cilia number and lumen size exhibit great diversity within similar stages and genetic backgrounds[305]. In the case of the lumen size, a 1300μm^2 threshold has been reported, below which the KV is no longer able to firmly secure LR patterning[305]. In addition, in wildtype conditions there is a correlation between KV size and cilia number[305].

Like in other vertebrates, Nodal signalling is key for LR asymmetry in zebrafish[263]. *spaw* expressed in the cells surrounding the KV at 4-6SS, where it becomes limited to the left LPM at around 12SS[306] and its positive feedback loop is critical to create LPM asymmetry[262,307] (Figure 19). On the other hand, *charon* is also first expressed bilaterally around the KV at 6SS and it becomes restricted to the right area[308](Figure 19). Since Charon binds to Spaw antagonizing its functions[309], the rightward gradient of Charon around the KV prevents *spaw* expression in the right side. Thus, opposed gradients between Spaw and Charon around KV are proposed to contribute to the asymmetric expression of *spaw* in the left LPM[297] (Figure 19). *spaw* knock-down extinguishes the expression of its target genes in the LPM (e.g. *lefty1*, *lefty2*, and *pitx2*) and *lefty1* in the midline losing left-specific morphogenesis, as observed in mouse[208]. In the case of

the loss of expression of *lefty1*, *spaw* expression leaks to the right side causing a bilateral expression in the LPM[193,310]. Moreover, *lefty1* and *charon* morphants show a faster propagation of *spaw* expression from posterior to anterior in the LPM compared to wild-type siblings[310]. Spaw is, indeed, a long-range activator that might be locally restricted due to the necessity of EGF-CFC co-receptors to activate Nodal signalling through activin receptors[311], thus being slightly different to the consensus definition of a SELI model. So, despite activin receptors are widely expressed, *oep* an EGF-CFP co-receptor is restricted to the LPM and the notochord during early and mid- somitogenesis[311]. Oep together with Lefty1 impedes Spaw to be acting in a longer range and Spaw can only enhance its own expression in *oep* positive cells in the left LPM where Lefty1 is scarce. Nevertheless, further studies are required to better understand the nature of *spaw* signalling expansion in the left LPM and the role of the midline barrier and other signalling molecules to firmly ensure correct LR patterning. Likewise, other signalling pathways (e.g. Bmp signalling[210,312]) have been described to have an important role in the establishment and maintenance of LR asymmetry, but the contribution of additional signalling pathways also needs to be further investigated.

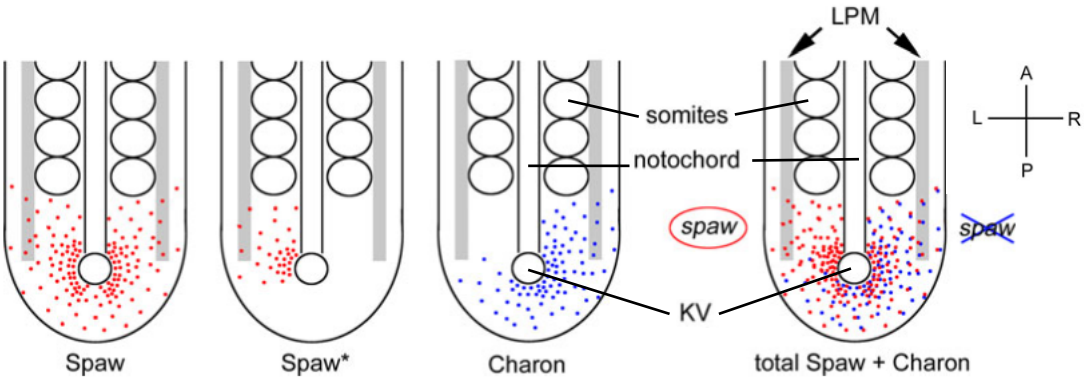

Figure 19 | *Schematic representation of signal transfer from the KV to the LPM.* *spaw is expressed bilaterally around the KV at 4-6SS until 10-12SS where it is restricted to the left side. Charon antagonizes spaw by binding to diffused Spaw*, which cannot activate its own expression in the right LPM. However, Spaw reaches the left LPM without the antagonism from Charon where it stimulates its own expression. A: Anterior; L: Left; P: Posterior; R: Right. Adapted from Matsui and Bessho, 2012[297].*

6.5. Maintenance of LR asymmetry: Organ laterality

The impact of signalling disruptions during development is dependent on the time point when this signalling is altered or interrupted. Hence, it is expected that early interference, when LR patterning is being established will have an embryonic global effect, while the latest the signal is impaired the lesser the impact, this being probably restricted to one or few organs. A key step in the maintenance of LR asymmetry is the interpretation of the LR specific cues that emerge around the KV structure by organ primordia. According to this information, cells undergo specific organ-specific asymmetric morphogenesis by, at least, three different means: looping or rotation out of the midline (e.g. heart and gut), side-specific differences (e.g. lungs) and regression of one side of a bilateral symmetric structure, while the other is maintained (e.g. venous system)[313]. Remarkably, since the establishment of LR identity happens much earlier than asymmetric morphogenesis, LR signalling differences generated by the transiently expressed Nodal and Leftys have to be maintained to secure correct organ laterality[314,315]. *Pitx2* Nodal signalling effector, has been described to have this role in both chicken and mouse[314,315]. Nevertheless, this has been shown not to hold true in the case of the zebrafish (see section 6.3.).

Finally, the orientation of the different organs is highly consonant. In wildtype conditions, the position of the visceral organs can be predicted from the direction of cardiac jogging, which is the first event to take place in asymmetric organogenesis. In addition, the normal development of the midline structures is apparently fundamental for coordinated heart jogging and looping and intestinal looping to occur[316]. Defects in laterality have been observed in human and in model organisms. The degree in discordance in the laterality of each organ respect to the rest is highly variable, hence pointing towards a specific and independent regulation for LR orientation for each organ[317]. One example in zebrafish is Shh misexpression on the right side of the embryo,

that causes both heart and viscera reversal. The reversal events affect each structure independently, suggesting that each organ interprets the signals differently[312]. Also, *bmp4* misexpression on the right side in zebrafish uniquely affects heart positioning, whereas visceral organs remain unaffected[312].

Heart laterality in zebrafish

As previously mentioned in the section related to heart development (see section 5.1), the heart primordia appears in the anterior part of the LPM at around 18-20SS. These bilateral cell populations migrate medially to finally form a cardiac tube, that will experience a series of asymmetric events that give rise to the functional heart. These morphogenetic events during heart organogenesis are controlled by several signalling molecules and pathways, with special relevance of Nodal and Bmp signalling.

After the fusion of the cardiac progenitors in the midline the leftward involution of the right posterior heart field leads to the formation of the ventral floor, whereas the non-involuting left heart field generate the dorsal roof of the primary heart tube[192]. Then, simultaneously to the extension and leftward migration of the myocardial cells, a clockwise rotation of the heart tube occurs regulated by *lefty1*, *lefty2*, *pitx2* and *bmp4*, among others[178,191,207,315]. Thus, all these movements trigger the conversion of the LR axis into the DV axis in the tube[191]. Then, the heart elongates and is displaced over the yolk until the dorsal part of the tube locates on the ventral side of the developing embryo. Later, another rotational movement restores DV polarity to LR polarity, and finally the tube loops creating a multi-chambered structure, in which the left side is positioned on the left side of the looped heart[315]. This second asymmetric event is dependent not only on genetic factors, but also on biophysical mechanisms. The action of mechanical forces together with an important role of extracellular matrix components (ECM) in this process enable correct twisting and bending of the heart[316]. Despite cardiac jogging and subsequent heart looping have a high correlation, a failure

in cardiac jogging not necessarily drives to a failure in looping. It has been reported that indeed, it results in randomized lopping[201], demonstrating that both events share some regulatory mechanisms, but they also possess others that specifically regulates each process.

Visceral laterality in zebrafish

The gut is also generated after a series of looping events. The digestive system is also dependent on LR positional cues that trigger the asymmetric migration of the LPM[317]. In wildtype conditions, the left and right LPM migrate dorsally and ventrolaterally respectively towards the midline, which results to a leftward shift of the intestine (gut looping) at 26-30hpf (Figure 20). Eventually, the liver and the pancreas are asymmetrically positioned in the left and right side, respectively with respect to the midline in the abdominal cavity[297,321,322](Figure 20). Migration or asymmetric cell rearrangement of the adjacent mesodermal tissues are critical for LR orientation of the endodermal organs[320,323]. The movements that drive this asymmetric migration of the LPM are subjected to the control of LR signalling[320]. This has also been confirmed by the results obtained in *spaw* morphants that have randomized LPM migration and gut looping, suggesting that asymmetric LPM migration and gut looping are regulated by LR gene expression in the LPM[297]. In addition to Nodal signalling, bidirectional EphrinB1/EphB3b signalling has been observed as reported as responsible for coordinated liver and LPM movements[324].

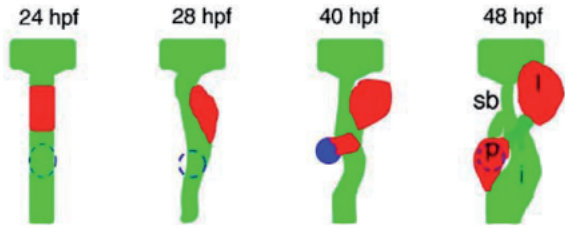

Figure 20 | *Schematic representation of the stages of endodermal organogenesis in wild-type zebrafish embryos.* *Endoderm in green, liver and exocrine pancreas in red, and endocrine pancreas in blue. l, liver; p, pancreas; dotted line, endocrine pancreas; sb, swim bladder; and i, intestinal bulb.. Adapted from Noël et al., 2008[325].*

Neural laterality in zebrafish

LR asymmetry is also a salient feature of the vertebrate central nervous system. Brain asymmetry is indispensable for the expansion of the sub-nucleus in the left habenula by the early larva stage[326]. At the genetic level, Nodal signalling has a central importance with the contribution of the Fgf, Notch, Wnt/bcatenin pathways[327] to build the lateralized embryonic brain (Figure 21). Despite the key role of Nodal in the regulation of neuroanatomical asymmetries in the zebrafish forebrain, the first steps are Fgf-mediated: initial migration of the parapineal from the midline to a lateralized position in the brain is controlled by *fgf8*[328]. Furthermore, reduced Fgf signalling leads to bilateral *lefty1* expression and an increment of cell boundary formation in the brain midline[328]. *spaw* knockdown results in the loss of left-sided activation of Nodal signalling in the diencephalon, suggesting that LPM spaw regulates Nodal activity in the brain[208]. In *abf* (about face) mutants Nodal is activated in the right side of the diencephalon and habenula sub-nucleus asymmetry is reversed, indicating an essential Nodal dependent mechanism for determining habenula laterality[297]. However, mutants in which Nodal is activated bilaterally (*ntl*) or is absent (LZ*oep*), habenula asymmetry is established but laterality of the habenula sub-nucleus is randomized, suggesting that habenula laterality is independent of the nodal handedness in the diencephalon[297].

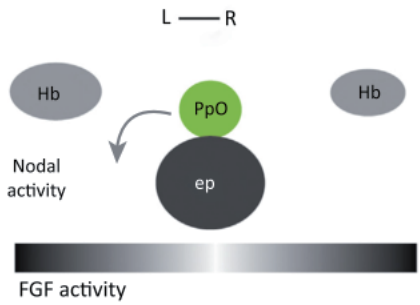

Figure 21 | *Schematic illustration of the epithalamic region of the zebrafish brain showing the left and right Hb, the PpO, and the ep*. *The PpO migrates left toward the left Hb. An FGF gradient that increases from the midline to the lateral sides. Nodal is only active on the left side and promotes left-sided migration of the PpO. ep: epiphysis, Hb: habenulae, PpO:, parapineal organ, L: left and R, right. Adapted from Grimes and Burdine, 2017*[261].

Aims

The present Doctoral Thesis had the following **overall aims**:

1. To uncover the specific *versus* overlapping roles of the *tbx5a* and *tbx5b* genes during zebrafish development.
2. To understand the role of *tbx5a* during left/right asymmetry in zebrafish.

To achieve these **overall aims** I set out to pursue the following **specific aims**:

1. To elucidate the function of the *tbx5* paralogues (*i.e.* *tbx5a* and *tbx5b*) during retina development in zebrafish.
2. To determine the role of the *tbx5* paralogues during pectoral fin development in zebrafish.
3. To characterise the role of the *tbx5* paralogues during heart organogenesis in zebrafish.
4. To analyse the early role of *tbx5a* during the establishment of LR asymmetry in the heart, visceral and neural structures in zebrafish.
5. To understand the mechanism by which *tbx5a* influences the establishment and/or maintenance of LR asymmetry in zebrafish.

Materials
Methods

1. Animal welfare

The local ethics committee approved animal studies and all procedures conformed to the essential ethical rules and the current applicable legislation (Council Directive 86/609/EEC; Law 5/1995/GC; Order 214/1997/GC; Law 1201/2005/SG). Adult fish were kept in a designated fish facility with a designated manager and welfare officers. When animals needed to be euthanized, an overdose of tricaine methane sulfonate (MS222, 200–300 mg/l) by prolonged immersion was used, which is a well-established humane method.

2. Animal maintenance

Adult zebrafish were bred under standard conditions at 28.5ºC with a light/dark cycle of 14/10h. Embryos were obtained by natural spawning and incubated at 28.5°C in E3 medium[329]. They were further staged and fixed in 4% PFA (paraformaldehyde) in PBS at specific time-points[68]. Prior to fixation the embryos were either mechanically dechorionated, using Dumont forceps #5 in the case of the youngest embryos, or by an enzymatic treatment using 2mg/mL pronase (Roche 165921) in E3 medium. In this case, embryos were exposed 1-10' to pronase solution depending on the developmental stage, afterwards rinsed and kept in E3 medium before undertaking the fixation procedure.

3. mRNA synthesis

Transposase mRNA was obtained after linearization of the plasmid pCS2FA, purification of the gel band [QIAquick® Gel Extraction (Qiagen)], transcription (mMESSAGE mMACHINE® SP6 (Ambion®) and purification [MaXtractTM High Density (Qiagen®)].

4. Injection of Morpholino Oligonucleotides (MO)

1-cell injection (full injection)

MO oligonucleotides (Gene Tools LLC) were resuspended to a final concentration of 1mM and, depending on the experiment, 0.5–5ng injected into 1-cell stage embryos. MOs were always co-injected with an anti-*p53* MO (7.5ng) to avoid off-target effects caused by toxicity, and all experiments were performed with at least three independent replicates. The MOs used were: a control MO; an anti-*tbx5a* MO for the coding sequence[86], an anti-*tbx5b* MO against the 5'UTR/coding sequence boundary (*tbx5b*_UTR), an anti-tbx5b MO for the exon 3/intron 4 boundary (*tbx5b*_SP)

DFC-targeted injection

Injections were performed at the 512-cell stage in the same conditions a described for full injection (*i.e.* co-injection with anti-*p53* MO) and using control MO and anti-*tbx5a* MO for the coding sequence[86].

Yolk- targeted injection.

Injections were performed at 4hpf, once the cytoplasmic bridges between the cells and the yolk are closed. The injection conditions were as described in the 1-cell and DFC-targeted injections.

Table 1 | MO sequences

Target	MO sequence (5' --> 3')
tbx5a	GAAAGGTGTCTTCACTGTCCGCCAT
tbx5b_SP	TTAAAAAACTAGGCACTCACCGGCC
tbx5b_UTR	GGATTCGCCATATTCCCGTCTGAGT
p53	GCGCCATTGCTTTGCAAGAATTG
ctrl	CCTCTTACCTCAGTTACAATTTATA

To test the knock-down efficiency of the *tbx5b*_SP MO, RT-PCR (Reverse Transcription PCR) was performed using whole-embryo RNA from 24hpf that had been injected with either control or *tbx5b*_SP MO. RNA was isolated using Trizol reagent (Invitrogen) and a reverse transcription reaction with SuperScript III RNaseH—reverse transcriptase (Invitrogen) was then performed to generate cDNA following the manufacturer's instructions. PCR was performed using the primers zf*tbx5b*_ex3fwd, located in the third exon of the *tbx5b* gene and zf*tbx5b*_ex4rev, present in the fourth exon of the *tbx5b* gene, respectively, to detect spliced and un-spliced *tbx5b* transcripts.

Table 2 | MO specificity assay primers

Primer name	Sequence (5' --> w3')
zftbx5b_ex3fwd	AGTATG GAGGGAATTAAAGTTTA
zftbx5b_ex4rev	CATTTGTTATCTG CAAACTTATAC

As equivalent phenotypes were obtained with both *tbx5b* MOs, for most of the experiments the *tbx5b*_UTR was injected, unless otherwise indicated.

5. MO functionality and specificity

To assess for the functionality of the MOs used, we generated chimeric mRNAs in which the *tbx5a* or *tbx5b* MO recognition sites were fused to EGFP (Enhanced Green Fluorescent Protein) by PCR amplification using a plasmid containing EGFP-polyA as template. The following primers were used: *tbx5a*MO_EGFP_fwd, *tbx5b*MO_EGFP_fwd, in conjunction with the reverse primer: FP_SV40rev. The resulting products were cloned into the pGEMT-easy vector (Promega) and further transferred into the pCS2fl vector to obtain full-length mRNAs. The validity of all products was confirmed by DNA sequencing prior to mRNA synthesis.

Table 3 | MO functionality and specificity assay primers

Primer name	Sequence (5' --> 3')
tbx5aMO_EGFP_fwd	ATGGCGGACAGTGAAGACACCTTTCGGGTGAG-CAAGGGCGAGGAGC
tbx5bMO_EGFP_fwd	ACTCAGACGGGAATATGGCGAATCCAGTGAGCAA-GGGCGAGGAGC
FP_SV40rev	AAGCTTGATGAGTTTGGACAAACCAC

The mMessage Machine kit (Ambion) was used to obtain full length mRNAs according to the manufacturer's protocol. 100pg of mRNA with or without the corresponding MO (3ng) was injected into one-cell stage embryos and the presence of GFP expression assessed at 24hpf.

To assess for the specificity of the MOs used and functionality of *tbx5a* variants, mRNAs to perform rescue experiments were generated. The *tbx5a_fwd* primers was used in conjunction with one of the reverse primers *FLrev*, *hstQ316rev* or *T-boxtruncrev*, to generate full-length, heartstrings or truncated variants of *tbx5a*, respectively. In addition, *tbx5b_fwd* and *FLtbx5b_rev* were used to generate full-length *tbx5b*. Resulting products were cloned into the pGEM T-easy vector (Promega) and further transferred into the pCS2fl vector to obtain mRNAs. The validity of all products was confirmed by sequencing prior to mRNA synthesis. 80pg of mRNA with the corresponding MO (3ng) were co-injected into one-cell stage embryos and heart laterality assessed at 26hpf by means of *myl7* expression.

Table 4 | Primers for *tbx5a* variants for rescue assay

Primer name	Sequence (5' -->3')*
tbx5a_fwd	ATGGCcGAttcaGAgGAtACgTTcaGGCTCAAAACTCTCC-CAGTG
FLrev	TTAGCTGGCTTCATTCCAGTC
hstQ316rev	CTaTGTGTGTCCGTGGTAGGAGC
T-boxtruncrev	CTATGCTTTGGTGATGATCATCTCTG
tbx5b_fwd	ATGGCcAAcCCAATGTTCGAATCTCTACGG
FLtbx5b_rev	TCAACTCCCCCCACACCAGTTG

** mismatched nucleotides are shown in small letters*

6. Whole Mount In Situ Hybridisations

Total RNA was isolated using Trizol reagent (Invitrogen) and a reverse transcription reaction with SuperScript III RNaseH—reverse transcriptase (Invitrogen) was then performed to obtain cDNA following the manufacturer's instructions. Specific probes for each gene were generated by PCR using total cDNA. Resulting products were cloned into the pGEM T-easy vector (Promega). Digoxigenin (DIG) labelled RNA probes were transcribed in vitro from linearized template plasmids using T7, SP6 or T3 Polymerase (Roche) and DIG RNA labelling mix (Roche) according to manufacturer's instructions. The antisense RNA probes used were: *bmp4*[203], *camk2b2*[332], *efnb2a* (kindly provided by J. Terriente), *ephB2* (kindly provided by R. Dorsky) *foxA3* (kindly provided by M. Poulain), *lefty1*[208], *lefty2*, *fgf4*, *fgf8* and *erm* (kindly provided by N. Mercader), *myl7*[333], *ntl* (kindly provided by M. Marsal), *spaw*[208], *tbx5a*[44], *wtip*[334]. Oligonucleotide primers were designed for the rest of the genes tested by in situ hybridisation (ISH) (Table 5). The amplified cDNA fragments were subsequently ligated into pGEM-Teasy (Promega) and sequenced to confirm their validity prior to probe synthesis.

Table 5 | Primers for ISH probe synthesis

Gene	Primer Fwd	Primer Rv
charon	GGAATGGACCAGACGAACCT	CGCCCTGGTTGAGAACTTTT
sox17	ATGTTGAATGAACTGTATGCAC	GCAGGTTTATTGAACTGAGTTG
fgf10a	ATGGAAAGTGACTAAGGGTGC	CTACACGATAGGAATGGGGAG
pea3	AGAAAGAGCCGCAGAGTCCC	TCCTGTTTGACCATCATATGGG
pitx2	AAATGCACCACTCTCTGCGT	TTGGTAGACAGAGAGGCCGA
gdf3	AGAGCCTGTCTTCTGACCCT	CTGGGAGTAACGGGGAGGTA
ephb4b	ATACCACCGAGCAACCAGTG	TATCCGGGTCTGGATCCCTC
prrx1a	AA CTGAAGCGGGCAGCTGGG	TTCATCACTTACATACATGGCC
prrx1b	AACTAAGCCTGAAAAGAGGGAC	CAGATACATATGTCACCATGGG
tbx5aFL	ACGTTCAGGCCAAAACTCTCC-CAG	TTAGCTGGCTTCATTCCAGTC

Chromogenic whole mount ISH were carried out as previously reported[44,335]. Embryos were observed in an OLYMPUS MVX10 macroscope and photographed with the OLYMPUS CELL D software, or alternatively, with a Leica MZ16F stereoscope.
Fluorescent whole mount in situ hybridisations (FISH) were carried out as formerly described[336]. Embryos were embedded in 1% low melting agarose (Sigma) dissolved in PBS and observed in a Leica SP2 confocal microscope. Acquired images are projections of z-stacks.

foxA3 ISH embryos at 48hpf were clarified using the BABB (benzyl alcohol (Sigma B-1042)/ benzyl benzoate (Sigma B-6630); 1:2 ratio) clearing agent.
After following the ISH protocol embryos were gradually submitted to a series of 10' washes diluted in PBT to reach 100% MetOH beginning from a solution of PBT: 25% MetOH, 50% MetOH, 75% MetOH and 100% MetOH.

7. Quantification of retinal phenotype

The extent of retinal markers expression domain was quantified by setting an imaginary hinge in the centre of the lens. The total angle of expression was sub-divided into nasal *versus* temporal by considering the choroid fissure as the ventral-most point. The Kruskal–Wallis test was used to assess statistical differences among experimental conditions.

8. Immunofluorescence

GFP immunofluorescence

ath5:GFP 48hpf embryos were fixed overnight (ON) in 4% PFA [PBS/4% paraformaldehyde (PFA)] at 4ºC, washed with PBST (0.5% Triton), digested with 10 mg/ml of proteinase K for 40'and post-fixed in 4% PFA for 20'. After PBST washes, embryos were blocked in PBST/1% BSA (Bovine Serum Albumin) and an anti-GFP antibody (Invitrogen, 1:600) was subsequently left overnight at 4ºC. The antibody was washed out with 1% BSA washes before adding the secondary antibody (anti-rabbit Alexa488 1:200, Molecular Probes) and left overnight at 4ºC. Secondary antibody washes were performed with PBST. The acquired images are projections of z-stacks taken with a Leica SP2 confocal microscope.

Anti-acetylated tubulin immunofluorescence.

10SS embryos were fixed ON in 4% PFA at 4ºC. Fixed embryos were washed with PBS/0,1% Triton (PBST) and treated with 10 mg/ml proteinase K for 30'' and post-fixed in 4% PFA. After further PBST washes embryos were blocked 2h in PBST/1%BSA. Primary-antibody incubation in PBST/1%BSA (1:1000 monoclonal anti-acetylated tubulin 6-11B-1) was subsequently added and embryos were incubated at 4ºC ON. The primary antibody was washed out with BST/1% BSA washes before adding the

secondary antibody 1:1000 goat anti-mouse Alexa488 (Molecular Probes) and left ON at 4ºC. Secondary antibody washes were performed with PBST. The acquired images are projections of z-stacks taken with a Leica SP2 confocal microscope.

9. RT-PCR

RT-PCR was performed using whole-embryo RNA from shield, 1SS and 48 hpf embryos. RNA was isolated using Trizol reagent (Invitrogen) and a reverse transcription reaction with SuperScript IIITM Reverse Transcriptase (Thermo Fisher Scientific) was then performed to generate cDNA following the manufacturer's instructions. The PCR was performed using the primers *zftbx5a_F 5' AGGCGGATGTTTCCCAGCTTCAAAG 3'* and *zftbx5a_R 5' GATATGGCCGAAGGGATCCAGATG 3'* for *tbx5a* and *zfef1a_F 5' GACATTGCTCTCTGGAAATTCGAG 3'* and *zfef1a_R 5' TCAATCTTCCATCCCTTGAACCAG 3'* for *ef1a* as a reference gene.

10. qPCR

Total RNA was extracted from zebrafish embryos using TRIzol reagent (Invitrogen, Carlsbad, CA, USA), and the extracted RNA was quantified using a NanoDrop 2.0 spectrophotometer (Thermo Scientific; Waltham, MA, USA). Complimentary DNA was synthesized from 1µg of total RNA by using SuperScript IIITM Reverse Transcriptase (Thermo Fisher Scientific) according to manufacturer's instructions. Real-time qPCR was performed using SYBR Green PCR Master Mix (Applied Biosystems, Foster City, CA, USA) on an Applied Biosystems 7500 Sequence Detection System (ABI 7500 SDS). Real-time PCR reaction was a Two-Step Cycling Program and the conditions were as follows: 95 °C for 10 min followed by 40 cycles of 95 °C for 15'' and 60°C for 40''. The qPCR primers used for the reactions were: *bmp2b*[337], *bmp4*[337], *bmpr1aa*[338], *bmpr1ab*[339], *bmpr1ba*[339], *bmpr1bb*[339], *bmpr2a*[339], *bmpr2b*[340], *camk2b2*[341], *cx43.4*[342],

dnah9[304], *fgf4*[343], *fgf8a*[344], *fgf10*[345], *fgfr2*[346], *prrx1a*[347], *spaw*[383] and *ef1a*[341] or *hatn10*[348] as reference genes.

11. Detection of putative binding sites

Putative binding sites for Tbx5 were found in the regulatory regions of the Bmp signalling pathway members analysed in the zebrafish genome using FindM programme from the Signal Search Analysis (SSA) software package. We looked for TBX5 motifs using JASPAR CORE 2016 vertebrate motif library.

12. Image processing

Images taken with the stereoscopes and microscopes were processed using ImageJ/Fiji.

13. Statistical analysis

The Kruskal-Wallis test was used in the experiments to quantify the retinal phenotypic differences after *tbx5a* and/or *tbx5b* knock-down after MO injection.

A $\chi 2$ statistical analysis was used to assess for differences when the *tbx5a* morphants phenotype was compared to control siblings in the LPM or in/around the KV.

Two-tailed Student's T-test statistical analysis was used to analyse the transcriptional levels differences for each gene in the different conditions (ctrl MO and DFC-targeted *tbx5a* MO) for the qPCR results.

Results

Chapter 1

The role of *tbx5* paralogues in the developing retina

Chapter Overview

Despite the role of *Tbx5* has been previously described to a certain extent in the developing heart and forelimb in a number of model organisms, it has not been thoroughly analysed in the retina. In the zebrafish, both copies of *tbx5* are expressed in a similar fashion in the developing retina.

In this chapter I aimed to identify the role of *tbx5* paralogues in the dorsal retina to better understand their putative specific *versus* common roles in this tissue. The knockdown of these genes by using different doses and combinations of both *tbx5a* and *tbx5b* MOs, permitted to identify alterations in the expression pattern of different dorsal and ventral identity markers in the developing retina. Hence, I could define a role for these genes in the DV patterning of the retina as well as ascertain the relationship of these paralogues in the retinal territory.

1.1 MO knock-down efficacy and specificity

Although *tbx5a* is widely used as a marker of dorsal retina identity, its function in this territory, where it is conspicuously expressed, has not been fully investigated. As introduced before, the two copies of the *tbx5* gene in zebrafish are expressed in the eye field from its earliest stages of morphogenesis. It is hence plausible that functional redundancy exists between the two paralogs[44]. All this prompted me to investigate the putative specific *versus* common roles that *tbx5a* and *tbx5b* have in the developing retina following a MO knock-down strategy.

To investigate the function of *tbx5a* and *tbx5b* and their possible redundancy during eye development, MOs against both genes were injected in different doses and combinations into 1-cell stage embryos. Briefly, the MOs used were one against *tbx5a* that had been previously characterised[86], and two different MOs against *tbx5b*: a splicing (SP) MO that binds to a splicing-junction and a UTR MO directed to the 5'UTR of the mRNA blocking the initiation of its translation. The functionality of these MOs was assessed by the generation of chimeric mRNAs containing the *tbx5a* or *tbx5b*(UTR) MO recognition sites fused to EGFP. After the injection of the tester chimeric RNA or the combination of tester RNA and MO, fluorescence or the lack of it was assayed at 24hpf. As shown in Figure 1.1, EGFP expression was observed after injection of 100pg of *tbx5a*-EGFP mRNA into 1-cell stage embryos (Figure 1.1 A, A') or after injecting 100pg of *tbx5b*-EGFP mRNA (Figure 1.1 C, C') at 24hpf, whereas co-injection with *tbx5a* MO (Figure 1.1 B, B') or *tbx5b*(UTR) MO (Figure 1.1 D, D') caused the disappearance of EGFP signal. Finally, *tbx5b*(SP) MO functionality was assayed by RT-PCR. RNA was extracted from injected embryos with a control MO or a *tbx5b*(SP) MO and after the RT-PCR, control embryos showed the expected 215bp (spliced) band in comparison to the 791bp (unspliced) bands in *tbx5b*(SP) MO injected embryos (Figure 1.1 E).

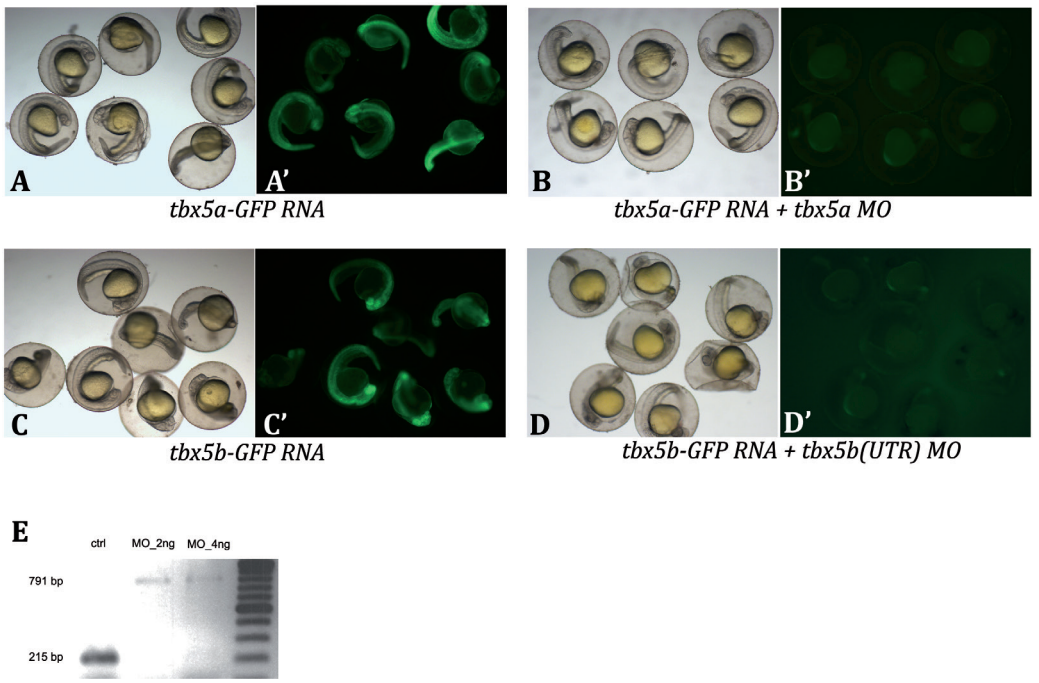

Figure 1.1 | *Efficiency of the MOs used.* *Injection of 100pg of tbx5a-EGFP mRNA (A-A') or tbx5b-EGFP mRNA (C-C') caused detectable expression of EGFP in 24hpf embryos (A'-C'). Chimeric mRNA-driven EGFP expression is abolished by co-injection with tbx5a M0 (B-B') or tbx5b(UTR) MO (D-D'). RT-PCR from injected control MO or tbx5b(SP) MO embryos show 215bp (spliced) band and 791bp (unspliced) bands, respectively.*

1.2 The consequences of *tbx5* knock-down on DV identity of the retina

After confirming the specificity of the MOs used to knock-down *tbx5* paralogues and their functionality, I analysed the effects on retinal DV identity after interfering with *tbx5* paralogues by MO knock-down.

To check whether the knock-down of *tbx5a* and/or *tbx5b* has an effect in the maintenance of the DV retina domains the expression of known dorsal and ventral retina markers was examined. The markers chosen to highlight the dorsal and ventral territories in the retina, *bmp2b* and *vax2*, respectively, are broadly used as read-outs of the-

se identities and therefore, are a good reference to identify defects in DV patterning.

The reference for measuring the reduction/expansion in the expression domain for *bmp2b* and *vax2* was the centre of the dorsal retina and the choroid fissure and, by setting an imaginary hinge in the centre of the lens, the angle of expression was calculated (Figure 1.2 A, D). The total angle of expression was subdivided in nasal and temporal (Figure 1.2 B, E and 1.2 C, F respectively) to assess whether the reduction/expansion of the expression domain was symmetric or it was biased towards one side. ISH experiments showed that, at 24hpf, morphant embryos injected with either 5ng of *tbx5a* MO (Figure 1.2 A-C, G) or 4ng of *tbx5b*UTR MO (Figure 1.2 A-C, G) suffered a subtle but significant down-regulation of *bmp2b* expression with a reduction on the temporal expression domain compared to the wildtype expression shown in the control embryos (Figure 1.2 A-C, G). Injection of lower doses, 1ng of *tbx5a* MO or *tbx5b* MO, did not produce such down-regulation of *bmp2b* expression (non-significant). Co-injection of both MOs resulted in a mild phenotype when 0.5ng of each MO were injected, but after injection of 1.5ng or 3ng of each MO the phenotype resembled the observed in *tbx5a* or *tbx5b* morphants (injected with 5 and 4 ng of MO, respectively) and were also found to be significant Figure 1.2 A-C, G). These results suggest that *tbx5a* and *tbx5b* are required to set-up some dorsal retina characteristics. Nevertheless, the changes in *bmp2b* expression pattern were very subtle, possibly due to the presence of other factors expressed in the retina that might regulate *bmp2b* expression in a complex manner.

In the case of *vax2*, injection of either *tbx5a* (5ng) or *tbx5b* MO (4ng) caused a mild change in the expression pattern. ISH experiments revealed that the ventral *vax2* domain suffered a subtle expansion, which was more evident in *tbx5a* morphants, although both *tbx5a* and *tbx5b* morphants expansion of the *vax2* expression domain was found to be significant. (Figure 1.3 D-F, H). Again, the reference for measuring the

expansion on the expression domain was the choroid fissure, in the ventral retina and as previously described for *bmp2b*, an imaginary hinge was set in the centre of the retina to measure the angle of the expression domain. It is remarkable to point that the expansion of the *vax2* expression domain occurred in the nasal side of the retina. Lower doses (1 ng) of *tbx5a* or *tbx5b* MOs did not cause a significant expansion in the *vax2* expression domain (not shown) and co-injection of both MOs in different doses (from 0.5 to 3ng each, Figure 1.3 D-F, H) resulted in a phenotype that resembled to *tbx5a* or *tbx5b* morphants (injected with 5 and 4 ng of MO, respectively). Hence, it seems that both paralogues act in the same pathway and are both necessary for proper *bmp2b* and *vax2* expression since the injection of single higher doses of MOs and when the two MOs were co-injected a phenotype can be detected in the retina.

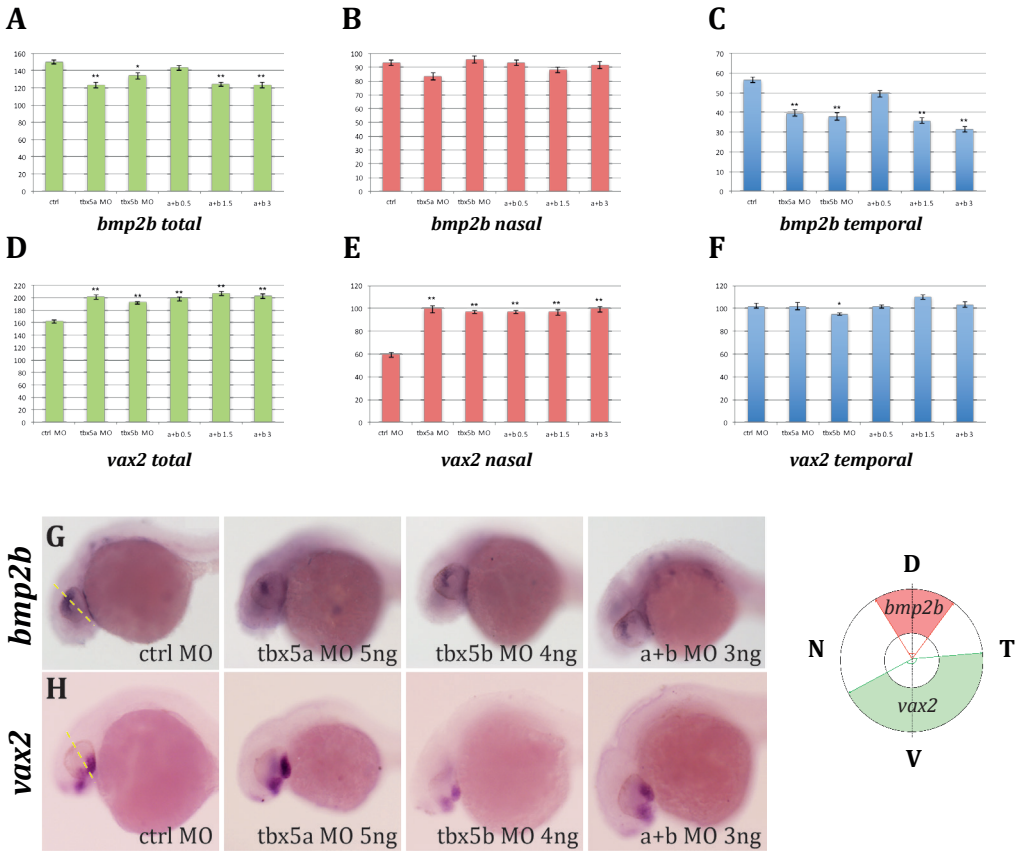

Figure 1.2 | *Expression pattern of bmp2b and vax2 in the retina at 24hpf after the injection of tbx5a and/or tbx5b(UTR) MOs.* *Quantification of total (A), nasal (B) and temporal (C) expression domain for bmp2b. Quantification of total (D), nasal (E) and temporal (F) expression domain for vax2. Data are represented as the mean ± s.e. A Kruskal–Wallis test was used to determine statistical differences among experimental groups (*p < 0.05, **p < 0.001). ISH for bmp2b (G) and for vax2 (H). Lateral views with anterior to the left are shown in G-H. Scheme of the retinal axes references for the quantification (on the right side of the panel). D: dorsal, V: ventral, N: nasal, T: temporal. Yellow discontinuous lines set the centre of the dorsal retina and the ventral choroid fissure.*

In addition, to *bmp2b* and *vax2*, *efnb2a* and *ephB2* expression in the retina was also assessed since both genes have been shown to be fundamental for the maintenance of DV patterning along the retina, which is essential for subsequent correct retinotectal projections. In this case, to be more sensitive to subtle changes in the expression of these markers, FISH was carried out for these genes. To quantify the extent of *efnb2a* expression in the FISH, the angle of expression of this gene was measured by setting an imaginary hinge in the centre of the lens (Figure 1.3 A). In control embryos, the *efnb2a* expression domain was measured to form an average angle of 63º (Figure 1.3 B, H). Knock-down of either *tbx5a* or *tbx5b* caused a reduction of the *efnb2a* angle of expression leading to an average angle of 54º, although this decrease was not found to be statistically significant (Figure 1.3 C, D, H).

To investigate whether both paralogues function in conjunction to determine the extent of dorsal *efnb2a* expression, sub-optimal doses of *tbx5a* and *tbx5b* MOs were co-injected. Remarkably, *efnb2a* expression domain was greatly reduced to an average angle of 37º, a statistically significant 41% reduction compared with control embryos (Figure 1.3 E, H). Injection of increasing concentrations of both MOs caused slightly more severe effects than those observed after co-injection of sub-optimal doses of *tbx5a* and *tbx5b* MOs (Figure 1.3 F, G, H). Notably, further statistical analyses showed that significant differences existed between the injection of single *tbx5a* and *tbx5b* MOs with respect to their co-injection at these higher doses (1.5 and 3ng each; Figure 1.3 H). This suggested that *tbx5* paralogues act redundantly in the dorsal retina to ensure *efnb2a* expression in this territory. To better map the decrease of *efnb2a* expression observed in *tbx5a* and/or *tbx5b*-morphant retinas, the angles obtained were divided into two, a dorso-nasal angle and a dorso-temporal angle, by setting the dorsal-most point as the point lying dorsal to the ventrally located choroid fissure (D in Figure 1.3 A). This showed that both dorso-nasal and dorso-temporal borders of expression similarly decreased according to the total angle of *efnb2a* expression measured (Figure 1.4 A-C).

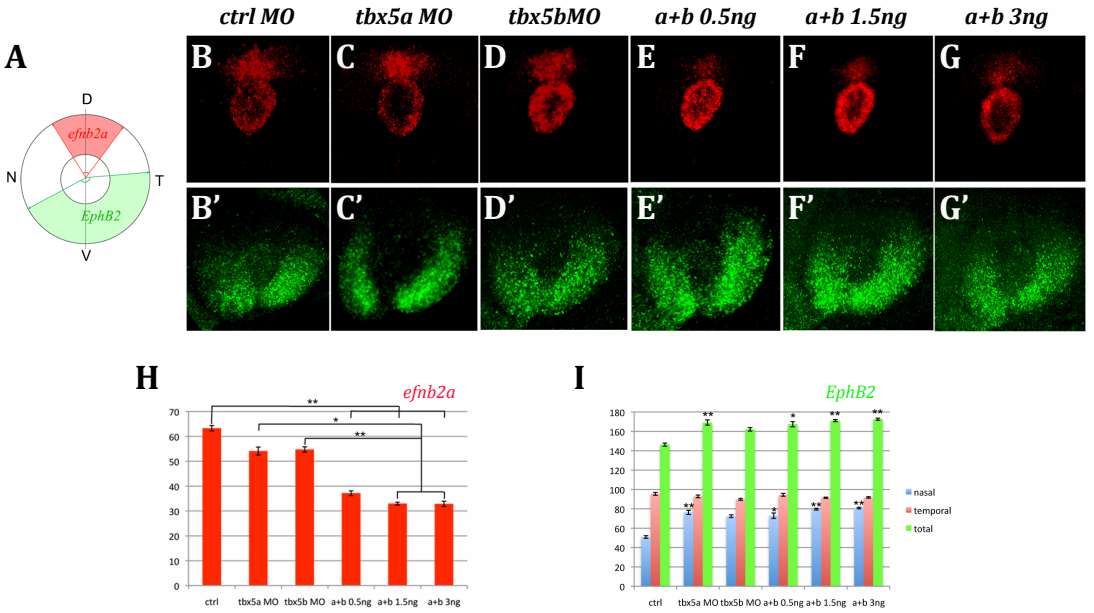

Figure 1.3 | *tbx5 genes are required for DV retina organization.* *Scheme of the quantification method (A). Expression of efn2a and ephB2 in control (ctrl) embryos (B–B', respectively), tbx5a morphants (C–C') and tbx5b morphants (D–D'). Expression of efn2a and ephB2 in embryos co-injected with different concentrations of both tbx5a and tbx5b MOs (E–G'). Quantification of the results obtained for the expression of efnb2a (H) and ephB2 (I). Data are represented as the mean ± s.e. A Kruskal–Wallis test was used to determine statistical differences among experimental groups (*p < 0.05, **p < 0.001). D, dorsal; N, nasal; T, temporal; V, ventral.*

To ascertain whether this decrease in *efnb2a* expression domain was concomitant with a deregulation of *ephB* expression in the ventral retina, the extent of *ephB2* expression was also measured. In control embryos, the expression domain of *ephB2* formed an average angle of 146º (Figure 1.3 B', I). *tbx5a* and *tbx5b* downregulation caused an increase of this angle to an average of 169º (significant) and 162º (non-significant), respectively (Figure 1.3 C'-D', I). Moreover, injection of sub-optimal doses of *tbx5a* and *tbx5b* MOs similarly caused a statistically significant increase in the expression extent of the ventral marker *ephB2* (to an average of 167º, Figure 1.3 E', I). Again, injection of increasing concentrations of both MOs caused similar effects to those ob-

served after co-injection of sub-optimal doses of *tbx5a* and *tbx5b* MOs (Figure 1.3 F', G', I). In contrast to the results obtained for the bilaterally symmetrical reduction of the expression domain of the dorsal marker *efnb2a*, statistically significant expansions of the *ephB2* expression domain towards its ventro-nasal border were large enough to explain the global increase of the domain of *ephB2* expression in the different conditions (Figure 1.3 I).

Hence, downregulation of *tbx5* paralogues was enough to explain the defects in DV-restricted expression of the *ephrinB/ephB*. Notably, dorsal *efnb2a* gene expression was not completely abolished after *tbx5a* and *tbx5b* knock-down (Figure 1.3 G, H), suggesting that other factors might be acting with the *tbx5* paralogues to maintain dorsal retina identity.

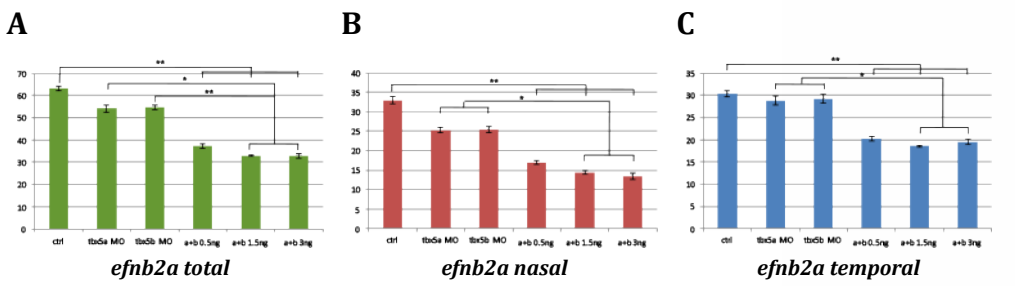

Figure 1.4 | *Quantification of the extent of efnb2a expression*. *Total extent (A), dorso-nasal (B) and dorso-temporal (C) angles measured by setting an imaginary hinge in the centre of the lens, considering the dorsal-most point as the point lying dorsal to the ventrally-located choroid fissure. Data are represented as the mean ± s.e. A Kruskal-Wallis test was used to determine statistical differences among experimental conditions (*p<0.05, **p<0.001).*

1.3 *tbx5* interference affects retinotectal projections

Since defined *ephrinB* and *ephB* expression domains along DV axis are essential for proper topographical map construction in the tectum[136], the alteration of the expression pattern of *efnb2a* and *ephB2* may be causing a misrouting of the retinal projections. To assess this, MOs against *tbx5a* and/or *tbx5b* were injected into one-cell stage *ath5:GFP* embryos that express *GFP* in RGCs under the regulation of the *ath5* promoter, the zebrafish homologue of the *Drosophila atonal* gene[349]. By 48hpf, RGCs have extended their axons to form the optic nerve that crosses the ventral midline to form the optic chiasm and project dorsally to the contralateral optic tectum. Thus, embryos were fixed at this developmental stage and GFP expression was analysed by immunofluorescence to enhance the signal from the retinotectal projections (Figure 1.5 A-D).

Injection of 3ng of *tbx5a* or *tbx5b* MOs did not cause obvious pathfinding errors (Figure 1.5 B, C, respectively). However, these experiments showed that the optic nerve of double morphants (3ng of each MO) was thinner than that of control MO-injected siblings (Figure 1.5 D). Moreover, and in agreement with both *tbx5* genes acting redundantly to ensure proper optic nerve formation, the reduction of the optic nerve diameter in double-morphant embryos was found to be significant (Figure 1.5 E). Altogether, data showed that knock-down of *tbx5* genes caused an alteration of DV *ephrinb/ephB* expression in the retina and the formation of a thinner optic nerve.

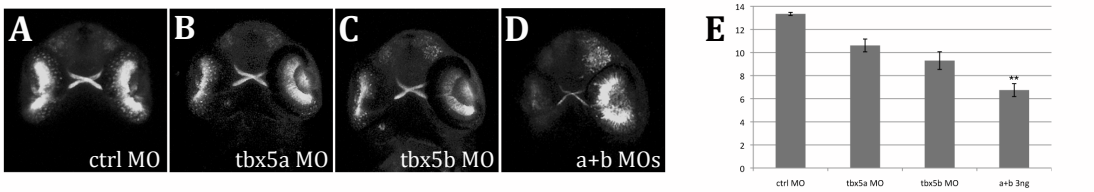

Figure 1.5 | *tbx5 genes are required to ensure correct retinotectal projections.* *Retinal projections of 48hpf ath5:GFP embryos injected with control (A), tbx5a (B), tbx5b (C) or tbx5a and tbx5b (D) MOs. Optic nerve diameter quantifications (E). Data are represented as the mean ± s.e. A χ^2 statistical was used to detect significant differences among experimental conditions (**p<0.01). Images are ventral views with anterior to the top.*

Chapter 2

The role of *tbx5* paralogues during pectoral fin development

Chapter Overview

tbx5 paralogues have been both described to be expressed in the pectoral fin bud during zebrafish development, being *tbx5a* expressed very early and *tbx5b* later, from 36hpf onwards[88]. *tbx5a* had previously been identified to be essential for the initiation of pectoral fin outgrowth: *tbx5a* MO knock-down or the *heartstring* (*hst*) mutation lead to the total absence of pectoral fins. The role for *tbx5b* in this territory had not been fully characterised, although *tbx5b* morphants were described to have smaller pectoral fins[88].

In this chapter I aimed to gain further insight into the role of *tbx5* genes in limb development as well as the functional relationship that exists between these paralogues in the pectoral fin using a MO knock-down approach. Moreover, the use of a series of markers expressed during pectoral fin development in the fin mesenchyme and in the overlying ectoderm, allowed me to identify the mechanism by which fin development is impaired in both cases and to define specific roles for *tbx5a* and *tbx5b* in the pectoral fin field. Briefly, ISH of several members of the Fgf signalling pathway, permitted to understand how Fgf signals that emanate from both fin mesenchyme and the surrounding ectoderm were affected, thus interfering with the creation of the positive Fgf feedback loop between these two tissues and the maintenance of this signalling to ensure sustained pectoral fin outgrowth.

Finally, according to the obtained results, a model for *tbx5a* and *tbx5b* role during zebrafish pectoral fin bud initiation and outgrowth was proposed.

2.1. Consequences of *tbx5b* knock-down in pectoral fin development

To assess the phenotype that results after interference with the function of *tbx5b*, a MO against *tbx5b* was injected. After injecting 3ng of *tbx5b* MO, morphant embryos showed much-reduced pectoral fins compared to control MO injected embryos at 3dpf (Figure 2.1, compare the black line in ctrl MO with the ones in *tbx5b* MO), which was reminiscent of the phenotypes observed after subtle downregulation of *tbx5a* function or downregulation of *tbx5* target genes[144,179,332]. Therefore, despite *tbx5b* morphants could initiate pectoral fin initiation outgrowth, they were unable to reach the normal fin size, suggesting that the signalling responsible for the maintenance of pectoral fin outgrowth was impaired. Regarding *tbx5a* knock-down by MO injection, the already-described phenotype of total loss of pectoral fins was obtained, as shown in Figure 2.1.

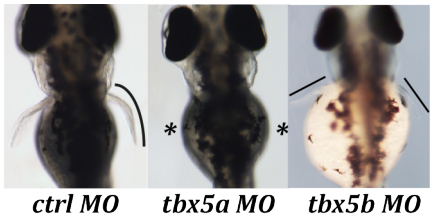

Figure 2.1 | *tbx5 knock-down results in defects in pectoral fin development.* *Pectoral fin morphology at 3dpf. Dorsal views are shown with anterior to the top. tbx5a morphants show total absence of pectoral fins, whereas tbx5b morphants exhibit smaller pectoral fins compared to control MO injected embryos. Asterisks label the lack of pectoral fins in tbx5a morphants. Black lines highlight the pectoral fins in control and tbx5b morphants.*

2.2. Characterization of *tbx5b* knock-down phenotype in the pectoral fin

To get further insight into where in the limb developmental pathway *tbx5b* function was required, I used a series of markers to assess the state of the two tissues required for and involved in the process of fin outgrowth: the fin mesenchyme and the overlying fin ectoderm. Briefly, bi-directional Fgf signals emanate from and are received by both tissues, creating a positive feedback loop that is required to sustain pectoral fin outgrowth. First of all, I tested that the initiation of pectoral fin bud outgrowth occurred normally. Before pectoral fin bud, protrusion it is essential that the mesenchymal cells in this territory condense and get compacted. In control embryos, compacted pectoral fin territories could be observed by means of *tbx5a* expression at 26hpf (Figure 2.2A) and expression of the *tbx5a* target gene, *fgf24*, was activated in this territory, namely the pectoral fin mesenchyme (Figure 2.2B-B'). By contrast and as already shown, *tbx5a* morphants failed to compact the *tbx5a*-labelled mesenchymal tissue (Figure 2.2O) and *fgf24* expression was never activated in the mesenchyme, although its expression was readily detected in other tissues such as the branchial arches (Figure 2.2P, arrow). Similar to control embryos, *tbx5b* morphants displayed compacted expression of *tbx5a* and *fgf24* expression was activated in this territory (Figure 2.2H, I-I'). *fgf24* expressed in the pectoral fin bud mesenchyme is required to activate the expression of another Fgf, namely *fgf10a*. Activation of *fgf10a* expression was observed in both control and *tbx5b* morphants (Figure 2.2C-C', J-J'), indicating that the fin bud outgrowth initiation programme was properly established in *tbx5b*-compromised embryos. However, in contrast to the similarities observed between control and *tbx5b* morphants regarding mesenchymal Fgf expression, it was striking to note that at 36hpf, when *fgf24* expression had been downregulated in this tissue and activated in the overlying fin ectoderm in control embryos, this did not occur after *tbx5b* depletion (Figure 2.2D-D', K-K'). To determine whether the only tissue with active Fgf signalling was the fin bud mesenchyme and not the overlying ectoderm of *tbx5b* morphants,

pea3 expression was used as a marker since it is a direct read-out of cellular exposure to Fgf. In control embryos, *pea3* expression was detected in both mesenchymal and ectodermal compartments of the fin bud (Figure 2.2E-E'), whereas only mesenchymal *pea3* was detected after *tbx5b* knock-down (Figure 2.2L-L', the asterisk labels lack of ectodermal expression). Interestingly, ectodermal *fgf24* was observed in 48hpf *tbx5b* morphant fins (Figure 2.2M-M') and these fins resembled to the control 36hpf ones (Figure 2.2D-D'). In agreement with Fgf signalling being active in both mesenchymal and ectodermal tissues of *tbx5b*-depleted fins, *pea3* expression was now evident in these two tissues (Figure 2.2N-N', the arrow marks expression in the *tbx5b*-morphant ectoderm), similar to what was found in control MO-injected embryos (Figure 2.2G-G'). Taken together, these data showed that pectoral fin development has a different requirement for each of the *tbx5* paralogues: *tbx5a* function is required for the earliest steps of initiation of fin outgrowth, whereas *tbx5b* functions later to ensure properly timed and sustained fin outgrowth. Both these requirements are linked by the connection between *tbx5* genes and the downstream regulation of Fgf signalling.

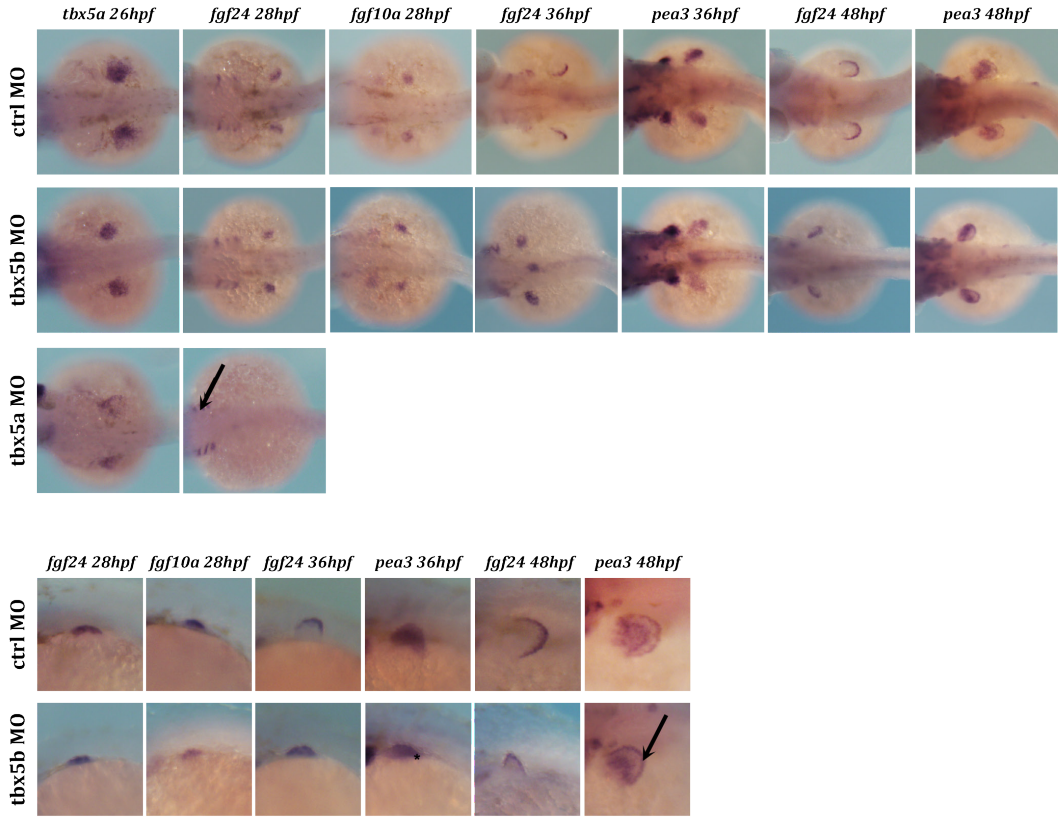

Figure 2.2 | *tbx5b knock-down causes a delay in pectoral fin growth.* *Expression of the developing pectoral fin markers in ctrl MO-injected embryos (A-G). Higher magnifications of ctrl MO-injected embryos (B'-G'). Pectoral fin markers expression in tbx5b-morphant embryos (H-N). Higher magnifications of tbx5b MO-injected embryos (J'-N'). tbx5a morphants (O-P). A-P are dorsal views with anterior to the left. B'-G', I'-N' are lateral views with anterior to the left. Arrow in P highlights expression in the branchial arches. Asterisk in L' shows lack of expression in the ectoderm and arrow in N' highlights expression in the ectoderm.*

In summary, during the initiation phase of pectoral fin outgrowth, *tbx5a* expressed prior to overt fin outgrowth is required to initiate *fgf24* expression in the pectoral fin mesenchyme, and hence in the absence of *tbx5a* the limb initiation programme is never established and pectoral fins fail to form. Later, once the limb initiation programme has commenced and Fgf signalling is active in the pectoral fin mesenchyme, *tbx5b*

is required for the maintenance of pectoral fin growth. *tbx5b* morphants have a delay in pectoral fin growth: these embryos fail to downregulate *fgf24* expression in the fin bud mesenchyme and activate the expression of this gene in the overlaying ectoderm at 36hpf (Figure 2.2K-K'). Nevertheless, 12h later, *fgf24* expression is no longer detected in the mesenchyme and becomes clearly observed in the ectodermal tissue (Figure 2.2M-M'). Strikingly, 48hpf *tbx5b*-morphant pectoral fins resemble younger (36hpf) control fins, suggesting that *tbx5b* is required to setup a certain threshold of Fgf activity in the mesenchyme that is necessary to signal to the overlying ectoderm and activate Fgf signalling in this tissue and downregulate *fgf24* expression in the mesenchyme. Thus, owing to this delay in Fgf signalling activation in the ectoderm, *tbx5b*-deficient pectoral fins appear smaller than control fins (Figure 2.1).

Chapter 3

The role of *tbx5* paralogues during heart development

Chapter Overview

tbx5 paralogues have recently been described to have a role during cardiac looping in zebrafish[88]. Analysis at 48hpf showed that both genes are required to ensure the complete looping of this structure to obtain the correct display of the heart chambers[88].

In this chapter I aimed to further analyse the cardiac phenotype observed after interfering with either *tbx5a* or *tbx5b*, or with both genes to better understand the morphogenetic events that the anterior LPM cell population undergo during heart development until this organ is displayed in the right place along the embryonic axes. Knock-down interference with *tbx5a* and/or *tbx5b* function by MO knock-down with subsequent analysis of the key events during cardiac morphogenesis (*i.e.* jogging and looping) led to determine that, due to the highly similar phenotypes observed in *tbx5a* and *tbx5b* morphants, these genes may act cooperatively during heart morphogenesis. In addition, *tbx5a* knock-down also affected the previous event of directional migration towards midline of the LPM bilateral population of cardiac precursors.

Finally, to understand the existing discrepancies in the phenotype described for the *hst* mutant compared to the results obtained here after MO knock-down for either *tbx5a* or *tbx5b*, a series of injection and rescue experiments for different versions of *tbx5a* gene *versus* the full-length form of *tbx5a* version or the *hst* version were carried out.

3.1. *tbx5* genes knock-down causes cardiac looping defects

As others previously described, *tbx5a* or *tbx5b* knock-down leads to an incomplete looping event in morphant embryos (Figure 3.1) in comparison to the characteristic looping observed in control morphants that results in the positioning of the ventricle and the atrium parallel to each other (Figure 3.1A)[88]. To consider the event of cardiac looping complete, the ventricle must be located at the right-hand side of the embryo with the atrial and ventricular chambers sitting side by side. Nevertheless, the unavailability to properly complete the cardiac looping event was not the only defect that could be observed after *tbx5a* and/or *tbx5b* MO knock-down. In *tbx5a* and/or *tbx5b* morphants, defects in the orientation of the cardiac torsion were also evident. In other words, in contrast with previous data, the defects detected were more profound than the degree (or extent) of looping. *tbx5* morphants exhibited a randomized cardiac looping orientation and they could be readily classified into three distinguishable heart looping orientation groups [D-loop (right, normal), L-loop (left, reversed) and no-loop]. After MO knock-down the characterisation of the cardiac looping phenotypes was performed by ISH at 48hpf using *myl7* expression to reveal the position of the heart.

Injection of a control MO resulted in over 99% (n = 158) of the embryos displaying an S-shaped heart with the ventricle lying to the right-hand side of the embryo (D-loop; Figure 3.1A, I). By contrast, 88% (n = 121) of the *tbx5a* MO-injected embryos had incomplete cardiac looping and within these, 57% showed D-loop, 24% showed L-loop and 19% showed no looping at all (Figure 3.1D-D'', I, J). Likewise, injection of *tbx5b* MO also caused heart looping defects (81%, n = 108), and these embryos displayed D-looped (52%), L-looped (16%) and no-looped (34%) cardiac morphologies (Figure 3.1E-E'', I, J).

The phenotypic similarities observed after *tbx5a* or *tbx5b* knock-down prompted to investigate whether these genes cooperatively regulate cardiac looping. To this end, both paralogues were simultaneously knocked-down by co-injecting sub-optimal doses of *tbx5a* and *tbx5b* MOs (0.5ng of each MO). Remarkably, when injected alone these MOs did not affect cardiac looping (Figure 3.1B, C, I; n = 75 for *tbx5a* MO and n = 71 for *tbx5b* MO). In contrast, over 56% (n = 110) of the double-morphants had looping defects and the three D-loop, L-loop and no-loop phenotypes were detected (68%, 11% and 21%, respectively; Figure 3.1F-F'', I, J) suggesting that indeed, both genes act in the same pathway and cooperate with each other to ensure the completeness and orientation of looping of the zebrafish heart.

Similar to the results obtained after single and double-MO injection with sub-optimal doses of the *tbx5a* and *tbx5b* MOs, double-morphant embryos after injection with 1.5 and 3ng of each MO also exhibited looping orientation defects since the three orientation phenotypes were also detected (Figure 3.1G-H'', J). Moreover, injection of increasing concentrations of both MOs caused an increase in the percentage of looping phenotypes, with 87% (n = 99) and 96% (n = 105) of double-morphants displaying looping phenotypes after injection with 1.5 and 3ng of each MO, respectively. Although, in agreement with previous reports, the severity of the phenotype was not enhanced by double knock-down, downregulation of both genes increased the penetrance of the phenotype (Figure 3.1I).

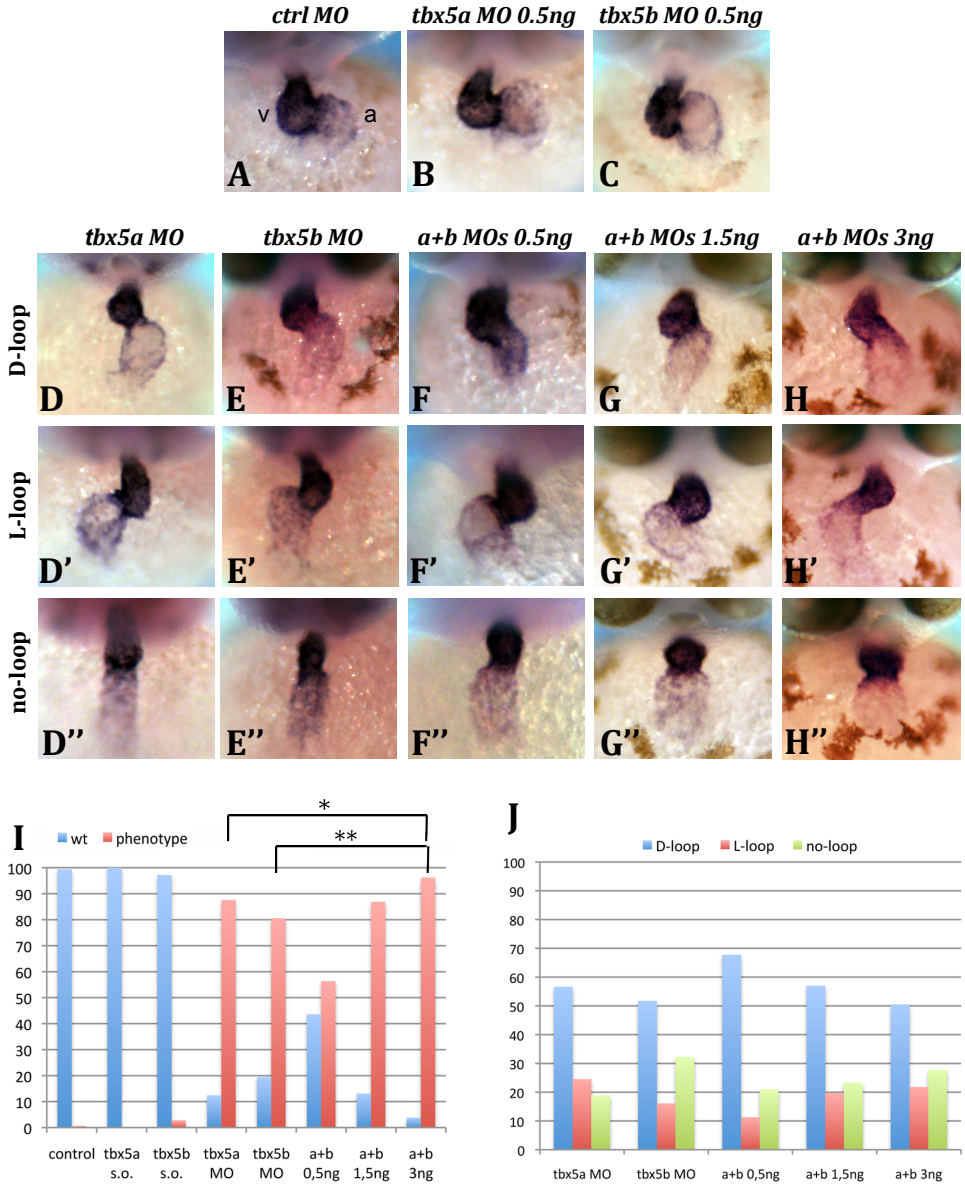

Figure 3.1 | *Knock-down of tbx5 genes causes cardiac looping defects.* *Embryos injected with control (ctrl) MO (A) or sub-optimal concentrations of tbx5a (B) or tbx5b MO (C). tbx5a morphant phenotypes (D–D″). tbx5b-morphant phenotypes (E–E′). Double knock-down of tbx5 genes (0.5ng each MO (F–F″), 1.5ng each MO (G–G″) and 3ng each MO (H–H″). Quantification of the percentage of looping phenotypes: wt, complete; phenotype, incomplete looping s.o., sub-optimal (I). Quantification of the looping orientation phenotypes (J). A χ^2 statistic has been calculated to assess significant differences between groups (**p < 0.01, *p < 0.05). Images are frontal views of 48hpf embryos with anterior to the top, and myl7 expression is used to highlight the developing heart.*

3.2. *tbx5* genes knock-down results in cardiac jogging defects

As heart looping orientation phenotypes are indicative of cardiac LR asymmetry defects, the previous and first apparent morphological breakage event in LR symmetry (*i.e.* heart jogging) was also assessed. To check whether the directional migration of the heart tube was disrupted, MOs against both *tbx5* paralogues were injected and the laterality of the heart tube was evaluated at 26hpf by ISH using *myl7* expression to reveal the position of the heart tube. Cardiac jogging was classified as left (normal), right (reversed) or midline (no jog). After injection of 3ng of control MO, 99% (n = 197) of the embryos developed normal left jogging (Figure 3.2F, G). Conversely, right as well as midline jogging phenotypes were observed after *tbx5a* knock-down (Figure 3.2A-A'', G; n = 183). Similarly, *tbx5b* morphants displayed left as well as right and middle jogging of their linear heart tubes (Figure 3.2B-B'', G; n = 90).

Once again, the phenotypic similarities between *tbx5a* and *tbx5b* morphants suggested these genes cooperatively regulate heart jogging. To confirm this, sub-optimal doses of *tbx5a* and *tbx5b* MOs were injected. This showed that, in agreement with both genes cooperating to ensure the normal left-sided jog of the heart tube, 12.5% (n = 96) of these morphant embryos had a defective middle or right jog of the heart (Figure 3.2C-C'', G). Moreover, and similar to the heart looping defects results mentioned in the previous section, increasing concentrations of both MOs increased the percentage of phenotypes observed, with nearly 30% (n = 94) and 40% (n = 71) of double-morphant embryos showing defective heart jogging after injection of 1.5 and 3ng of each MO, respectively (Figure 3.2D-E'', G). The cardiac phenotypes caused by *tbx5a* and/or *tbx5b* knockdown (namely cardiac jogging and looping orientation defects) demonstrated that *tbx5* genes are required to direct both asymmetric events the zebrafish heart undergoes.

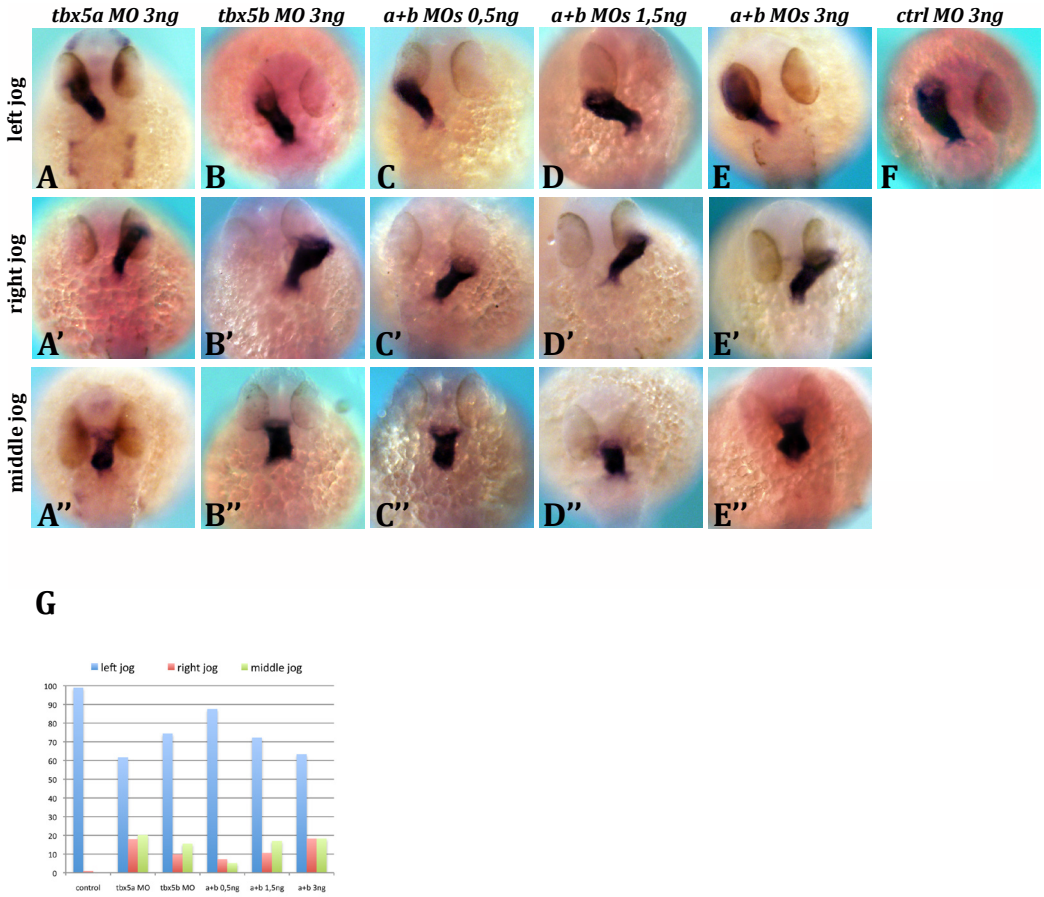

Figure 3.2 | *tbx5 morphants exhibit cardiac jogging defects.* *tbx5a morphant phenotypes (A-A''). tbx5b morphants (B-B''). Co-injection of tbx5a and tbx5b MOs at 0.5ng (C–C″), 1.5ng (D–D″) or 3ng (E–E″) of each MO. Control MO-injected embryo (F). Quantification of the jogging phenotypes (G). All images are dorsal views with anterior to the top, and myl7 expression is used to highlight the developing heart tube.*

3.3. *tbx5* knock-down results in medial migration and fusion defects

Considering the aforementioned phenotypic defects in both asymmetric events during cardiac LR asymmetry establishment (*i.e.* heart jogging and heart looping), medial migration, the process that precedes these asymmetric events during cardiac morphogenesis, was also analysed to assess whether the directional migration and fusion of the cardiac precursors in the midline was impaired. To assess this, MOs against both *tbx5* paralogues were injected and the ability to complete the medial migration towards the midline to form the heart cone of the cardiac precursors was analysed at 21SS by ISH using *myl7* expression to label the cardiac population (Figure 3.3 A-A''). In this case, the phenotypes observed were classified as heart cone, when no defects were observed in the consecution of the fusion of the cardiac population in the midline, *cardia bifida*, when the bilateral LPM populations were unable to complete their migration towards the midline, and fusion defects, when the anterior fusion of the cardiac populations was achieved but heart cone formation was not completed. All control-MO injected embryos displayed a perfectly formed heart cone (100%, n = 119, Figure 3.3 A'', D, D'). In contrast, after injection of 3ng of *tbx5a* MO injection (3ng, n = 97) only 69.07% of the embryos were able to fully complete the whole migration process while within the embryos that showed a phenotye (30.93%), the majority showed *cardia bifida* (73.33%, Figure 3.3 B', D, D') or a milder phenotype: anterior closure without previous posterior fusion to complete the heart cone formation (30.93%, Figure 3.3 B, D, D'). These phenotypes were not observed in the case of *tbx5b* MO injection. Despite the co-injection of both MOs using sub-optimal doses (0.5ng each) did not result in LPM fusion defects either (Figure 3.3 D, D'), co-injection of 3ng of each MO caused midline fusion defects like in *tbx5a* morphants, but with a higher penetrance. The 72.73% (n = 121) of the embryos presented a migration phenotype: *cardia bifida* in 66.64% of the embryos (Figure 3.3 C', D, D') and posterior fusion defects in 36.36% of them (Figure 3.3 C, D, D'). These results were statistically significant at $p<0.01$ after using a χ^2 statistical analysis.

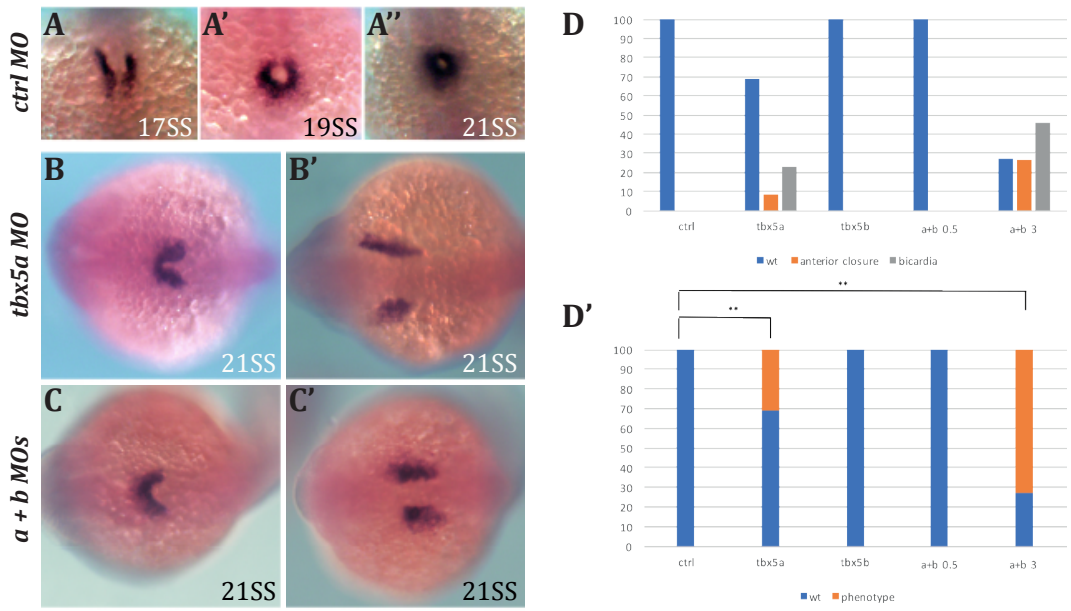

Figure 3.3 | *tbx5a morphants have defects in the midline fusion of the anterior LPM at 21SS*. *Cardiac development in wildtype conditions (17SS: A, 19SS: A', 21SS: A''). tbx5a morphants (B-B') and embryos co-injected with tbx5a and tbx5b MO (3ng each) (C-C') result in posterior fusion defects (B, C) and cardia bifida (B'-C'). Quantification of the phenotypes (D-D'). A χ^2 statistic has been calculated to assess significant differences between groups (**p < 0.01). Images are dorsal views with anterior to the top (A-A'') and dorsal views with anterior to the left (B-C'). myl7 expression is used to highlight the developing heart.*

The observed results suggested that either *tbx5a* has a role during the migration of the rostral population of the LPM towards the midline to fuse correctly to form the heart cone, or that *tbx5a* has an earlier role that eventually results in defects in directional medial migration of the cardiac precursors and subsequent cardiac laterality defects. In contrast *tbx5b* knock-down did not result in any observable phenotype at this earlier stage indicating that it is not required for midline migration of cardiac cell precursors. Nevertheless, a migration phenotype was obtained when both *tbx5a* and *tbx5b* MOs were co-injected with 3ng each. In this case, there was a higher penetrance of embryos with medial migration defects. Hence, this pointed towards a possible mi-

nor role for *tbx5b* during cardiac precursors directional migration towards the midline. The results suggested that *tbx5b* could have mildly rescued *tbx5a* after *tbx5a* MO injection, but it failed to do so when both paralogues are knocked-down in the double morphants.

3.4. *hst* phenotype *versus tbx5* knock-down phenotype

The defects observed after *tbx5* paralogues knock-down during heart development showed some discordance with previous results obtained using the *hst* mutant as a model for *tbx5a* loss-of-function. The intriguing differences were analysed by performing rescue experiments to ascertain the nature of the differences observed.

The reason for the discrepancies between the roles of the *tbx5* paralogues described here, as *tbx5* genes being implied in the asymmetric events the zebrafish heart undergoes (namely cardiac jogging first and looping later), and those of others remained unclear. One possibility is that we used a MO against *tbx5a* to downregulate its function, whereas Parrie and colleagues used the *tbx5a* mutant line *hst* to analyse the effects of this gene loss-of-function[88]. The *hst* mutant is characterized by a stretched heart tube that is unable to loop and exhibits bradycardia. The *hst* mutation introduces a premature STOP codon at residue 316 of the *tbx5a* open reading frame (ORF), which leaves the mutated protein with intact N-terminal and T-box (DNA binding) domains and part of the C-terminal domain. It is therefore possible that the *hst* mutation behaves as an hypomorphic allele with regard to the LR asymmetric development of the heart. In agreement with this hypothesis, most of the *TBX5* mutations causing a clear HOS phenotype lie upstream of the predicted *hst* mutation.

To test whether in fact the *hst* mutation behaves as an hypomorphic allele with regard to cardiac development, we developed an assay to check whether the laterality phenotype of *tbx5a* morphants could be rescued by introducing specific MO-insensitive forms of the *tbx5a* mRNA (Figure 3.4 A):

I. A full-length *tbx5a* mRNA that should be able to rescue the *tbx5a* MO-mediated phenotype.

II. *tbx5a* mRNA that is identical to that produced in *hst* mutant embryos.

III. A severely truncated version of *tbx5a* the T-box domain.

Notably, both the full-length and the *hst*-like forms of *tbx5a* were able to partially rescue the cardiac jogging phenotype when co-injected with the *tbx5a* MO (Figure 3.4 B, n = 65 and n = 168, respectively). Similarly, a full-length *tbx5b* form was able to rescue the jogging phenotype of *tbx5b* morphants when co-injected with our *tbx5b* MO (Figure 3.4 B; n = 117). By contrast, the severely truncated form of *tbx5a* was not able to rescue the laterality phenotype (Figure 3.4 B, n = 79). Overall, these data demonstrated not only the specificity of the cardiac phenotypes caused by MO-mediated knockdown of *tbx5a* and/or *tbx5b*, but also that the *hst* mutation behaves as a hypomorphic allele regarding cardiac laterality. When heart tube jogging was analysed in *hst* mutants (n = 38), all of them displayed a normal left-jog as visualized by *myl7* expression in 26hpf embryos (Figure 3.4 C). These results underline the need for caution when using the *hst* mutation as a *tbx5a* loss-of-function allele.

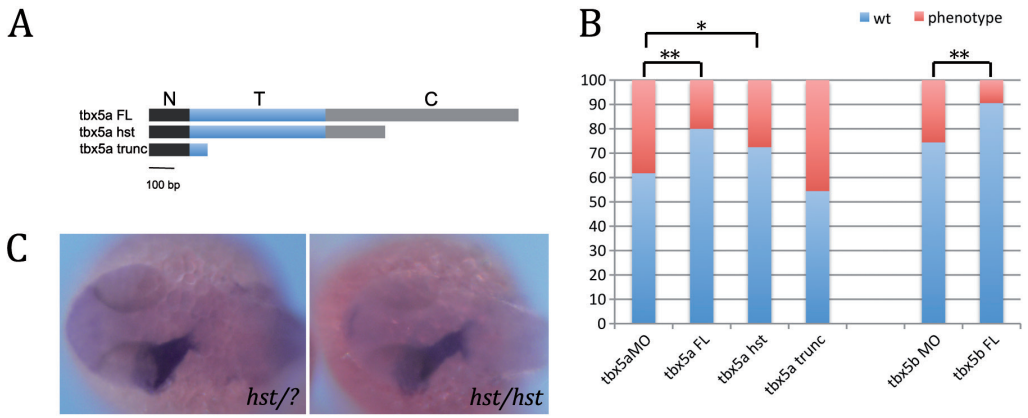

Figure 3.4 | *The hst mutation is a hypomorphic allele with regards to cardiac laterality.* *tbx5a variants generated to perform the rescue experiments: a tbx5a full-length (tbx5a FL) version includes the whole N-terminal (N, black rectangle), T- (T, blue rectangle) and C-terminal (C, grey rectangle) domains; a heartstrings version (tbx5a hst) containing the whole N-terminal domain and T-domain and a truncated C-terminal domain; and a tbx5a severely truncated version (tbx5a trunc) that contains the whole N-terminal domain and a truncated T-domain (A). Quantification of the rescue experiments (wt, left jog; phenotype, right and middle jog) (B). A χ^2 statistic has been calculated to assess significant differences between groups (**p < 0.01, *p < 0.05). Dorsal views with anterior towards the left of 26hpf +/+ or +/hst and hst mutant embryos showing normal leftward jogging of the embryonic heart tube highlighted by myl7 expression (C).*

Chapter 4

The role of *tbx5a* in the establishment of left-right asymmetry

Chapter Overview

After uncovering a new role for the *tbx5* genes during the asymmetric morphogenesis that cardiac precursor cells undergo, further questions about the mechanism by which this asymmetry defects were originated arose. Since the *tbx5a* paralogue was shown in our experiments to have an earlier role than *tbx5b*, affecting also the directional migration towards the midline of the cardiac precursors, in this chapter I focused on this paralogue and the consequences of its knock-down during zebrafish development in a broader sense, including the assessment of the specificity of the phenotypes observed and the analysis of other structures, where LR asymmetry is also of paramount importance.

In this chapter I aimed to ascertain whether the phenotype observed in the cardiac field was due to an early specific effect of targeting the DFCs that eventually give rise to the left-right organizer (KV), or by contrary, these defects emerge much later in development as a consequence of an impaired signalling in the LPM. To shed some light into this question, after *tbx5a* MO knockdown I checked the expression pattern of several left-LPM markers. In addition, I also examined whether these laterality defects were restricted to the heart or the knock-down of *tbx5a* affected the laterality of other organs; the neural structure of the diencephalon and the endodermal organs liver and pancreas.

Finally, I injected *tbx5a* MO during the time-frame when only DFCs and the yolk cell are affected and analysed whether the heart phenotype was disrupted to confirm whether *tbx5a* knock-down has a specific effect on DFCs/KV lineage.

4.1 The expression of left-side markers is altered after *tbx5a* knock-down

After observing defects in both asymmetric events of cardiac morphogenesis as well as in the migration towards the midline of the LPM population in *tbx5a* morphants, I aimed to examine whether the signalling cues that drive organ primordia positioning were also impaired when *tbx5a* was knocked-down. Since Nodal signalling pathway has been described to be key for the establishment of the left-identity in the LPM, the nodal-related gene *spaw* and its feedback inhibitors *lefty1* and *lefty2* expression was analysed in both control and *tbx5a* morphant conditions. In all the markers analysed, the typical left-side expression was randomized. The embryos were classified in four categories: left expression, right expression, bilateral expression and absence of expression.

The expression pattern of *spaw* in the LPM was assessed at 16SS and 21SS and, in both cases, the results were alike. Injection of a control MO resulted in 90.05% (n = 191, Figure 4.1 A, F) and 93.67% (n = 158, Figure 4.1 H, M) of the embryos with the typical expression of *spaw* at the left LPM at 16SS and 21SS, respectively. By contrast, after injection of 3ng of *tbx5a* MO morphants exhibited *spaw* expression in the left LPM in only 45.50% (n = 189, Figure 4.1 B, F) and 46.63% (n = 193, Figure 4.1 I, M) of the cases at 16SS and 21SS, respectively. The rest of the *tbx5a* morphants at 16SS (Figure 4.1 G) showed an altered expression of *spaw* in the LPM and within these, 22.33% (Figure 4.1 C, F) showed expression on the right side, 19.42% (Figure 4.1 D, F) showed bilateral expression and 58.25% (Figure 4.1 E, F) of the embryos did not have expression in the LPM. Similarly, at 21SS, 53.37% of *tbx5a* morphant embryos showed altered *spaw* expression (Figure 4.1 N) and within these, 50.46% of the embryos expressed *spaw* on the right side (Figure 4.1 J, M), 16.50% bilaterally (Figure 4.1 K, M) and 33.00% of the embryos lacked expression (Figure 4.1 L, M) in the LPM. These results were found to be statistically significant at both stages at $p<0.01$ after a χ^2 statistical analysis (Figure 4.1 G, N).

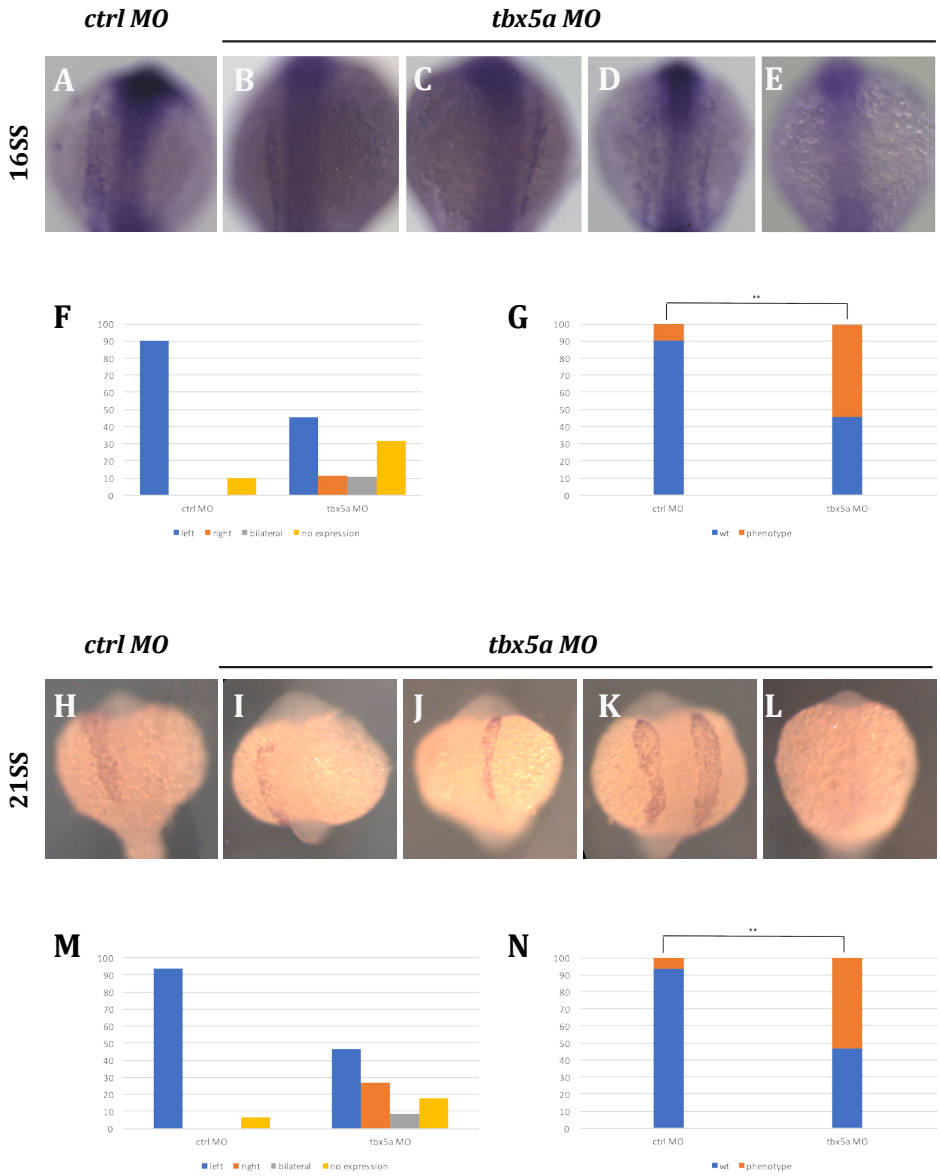

Figure 4.1 | *tbx5a morphants have randomized expression of spaw.* *Control (ctrl) morphant (A and H for 16SS and 21SS, respectively) showing the typical left-side expression of the marker. Left, right, bilateral and no-expression phenotypes were obtained after injection of tbx5a MO (3ng) at 16SS (B-E) and 21SS (I-L), respectively. Quantification of the laterality phenotypes (F and M for 16SS and 21SS, respectively). Quantification of the embryos exhibiting a phenotype compared to the ones showing the typical expression pattern (G and N, for 16SS and 21SS). A χ^2 statistic has been calculated to assess significant differences between groups (**p < 0.01). All images are dorsal views with anterior to the top.*

Similar to *spaw*, expression of *lefty1* was randomized in the LPM of *tbx5a* morphants. In control morphants *lefty1* is normally observed at the left LPM in 92.08% of the embryos (n= 202, Figure 4.2 A, F). In contrast, after injection of 3ng of *tbx5a* MO at 1-cell stage embryos, only in 32.47% (n = 231, Figure 4.2 B, F) of the embryos *lefty1* was expressed in the left LPM. The rest of the *tbx5a* morphant embryos (67.53%) exhibited right (26.28%, Figure 4.2 C, F), bilateral (26.92%, Figure 4.2 D, F) or absence (46.79%, Figure 4.2 E, F) of *lefty1* expression. A χ^2 statistical analysis showed that the number of *tbx5a* morphants with altered *lefty1* expression was significant with respect to the control counterpart at $p<0.01$ (Figure 4.2 G). Finally, it is worth mentioning that expression of *lefty1* in the midline of *tbx5a* morphants remained unaffected, thus preventing signalling leakage to the right side of the embryo (Figure 4.2 B-E).

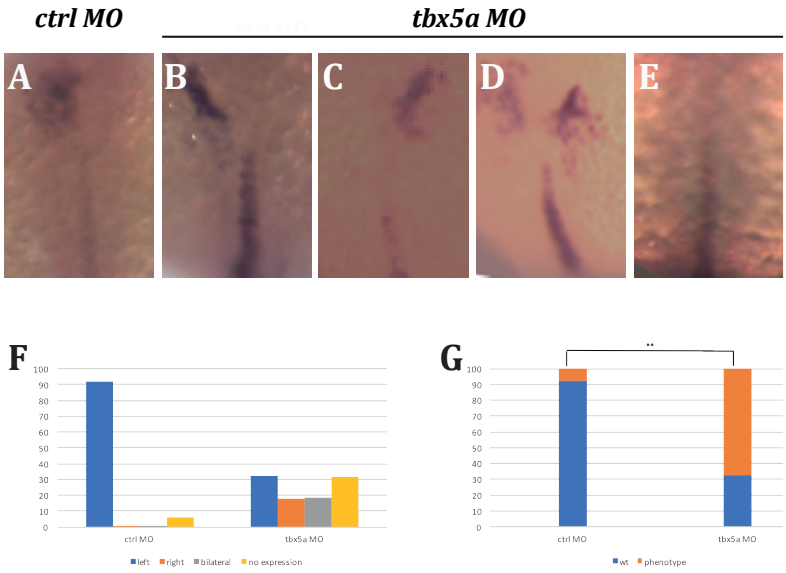

Figure 4.2 | *tbx5a morphants show randomisation of lefty1 expression in the LPM at 21SS.* *Control (ctrl) siblings (A) have the typical left-sided expression of lefty1 marker. Left, right, bilateral and lack of expression phenotypes were found after injection of tbx5a MO (3ng) (B-E). Quantification of the phenotypes (F). Quantification of the embryos exhibiting a phenotype compared to the ones showing the wildtype expression pattern (G). A χ^2 statistic has been calculated to assess significant differences between groups (**p < 0.01). All images are dorsal views with anterior to the top.*

The expression of *lefty2*, another downstream target of the Nodal signalling pathway and also a feedback inhibitor, was analysed. The expression pattern of this left-side marker in the cardiac field at 21SS was affected after *tbx5a* MO knock-down. Control embryos showed the typical *lefty2* expression in the left LPM in 98.69% of them (n = 152, Figure 4.3 A, F), whereas injection of 3ng of *tbx5a* MO resulted in the randomization of *lefty2* expression with only 41.75% (n = 194, Figure 4.3 B, F) of the embryos showing left-side expression of *lefty2*. Within the rest of the morphant embryos (58.25%), the 64.60% of them expressed *lefty2* in the right-side (Figure 4.3 C, F), 20.35% of them had bilateral expression (Figure 4.3 D, F) and 15.04% showed no *lefty2* expression in this territory (Figure 4.3 E, F). The statistical analysis (χ^2) of the quantification of the embryos presenting a phenotype *versus* the ones that retained the typical left-side expression was found to be significant at $p<0.01$ (Figure 4.3 G).

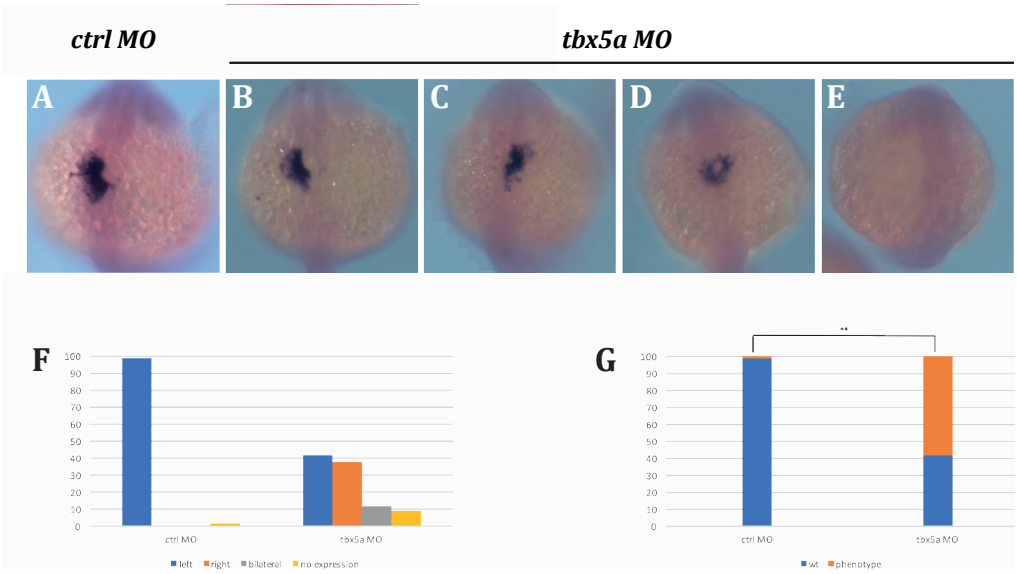

Figure 4.3 | *tbx5a morphants have randomized expression of lefty2 in the LPM at 21SS.* *Control (ctrl) siblings (A) showed the typical left-sided expression of lefty2. Left, right, bilateral and no-expression phenotypes were observed after injection of tbx5a MO (3ng) (B-E, respectively). Quantification of the phenotypes (F). Quantification of the embryos exhibiting a phenotype compared to the ones showing the endogenous expression pattern (G). A χ^2 statistic has been calculated to assess significant differences between groups (**p < 0.01). All images are dorsal views with anterior to the top.*

The randomization of the expression of members of the Nodal signalling pathway in the LPM prior to the initiation of the first cardiac morphogenesis asymmetric event (*i.e.* heart jogging) suggested that this earlier LR defect could be resulting in a more general phenotype in the developing embryo, affecting other structures in which correct laterality signalling cues are also crucial to achieve their proper directional display along the LR axis. It was hypothesized that the diencephalon and the positioning of the endodermal organs of the liver and pancreas with respect to the gut could also be impaired after interfering with *tbx5a* function.

4.2 *tbx5a* knock-down affects LR asymmetry in the diencephalon

To determine whether the effect on LR asymmetric events during zebrafish development after *tbx5a* knock-down was limited to cardiac morphogenesis or it also affected the laterality of neural structures, the expression of a diencephalic maker was assessed.

lefty1 was once more used as a left-side marker to study its expression in the diencephalon. The vast majority (96.67%) of control MO-injected embryos (n = 120) had *lefty1* expression in the left diencephalon of the embryos (Figure 4.4 A, F). In contrast, only 30.72% (n = 166) of the embryos injected with 3ng of *tbx5a* MO showed left-sided expression of *lefty1* (Figure 4.4 B, F). Surprisingly, in *tbx5a* morphants *lefty1* expression in this structure was also randomized and from the 69.28% of the morphant embryos with altered expression (Figure 4.4 C-G), 20.87% of them displayed *lefty1* expression on the right side (Figure 4.4 C, F), in 49.57% the expression was bilateral (Figure 4.4 E, F) and in 29.56% *lefty1* expression could not be detected in this territory (Figure 4.4 D, F). Statistical significance of these results was assessed using a χ^2 statistical analysis, which was found to be significant at $p<0.01$ (Figure 4.4 G).

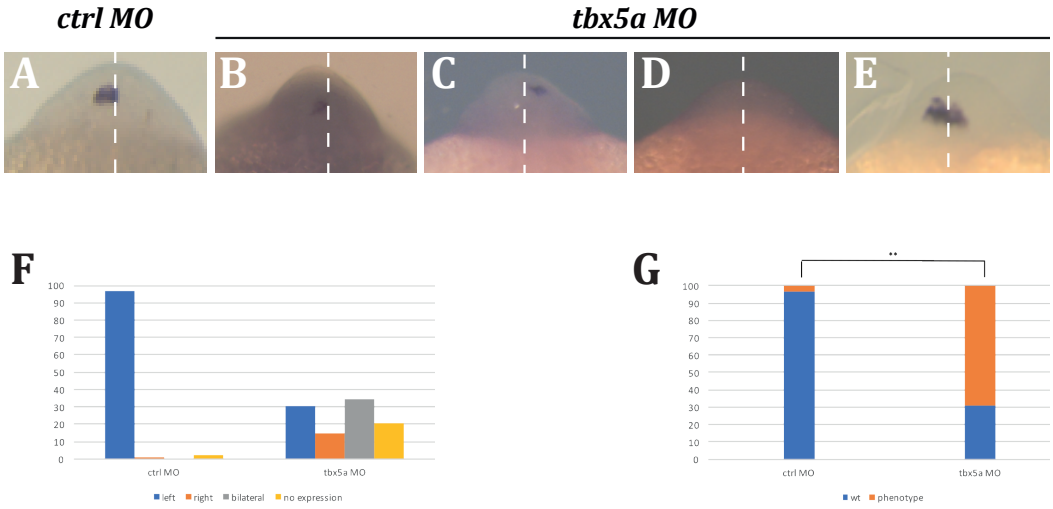

Figure 4.4 | *tbx5a knockdown leads to neural laterality defects.* *Left, right, no-expression or bilateral expression was observed (B, C, D, E, respectively) in tbx5a morphants, whereas control morphants showed lefty1expression restricted on the left side (A). Quantification of the laterality phenotypes at 21SS (F). Quantification of the embryos showing a phenotype compared to the ones expressing a wildtype expression pattern (G). A χ^2 statistic has been calculated to assess significant differences between groups (**p < 0.01). Images are dorsal views with anterior to the top (A-E). Dashed white lines divide the embryos into left and right halves (A-E).*

Once confirmed that the laterality of the diencephalon was impaired after *tbx5a* knockdown, supporting the hypothesis of a more widespread effect upon reduction on *tbx5a* levels, laterality was assessed in the developing pancreas and liver to check whether LR defects were extended to the positioning of these visceral organs.

4.3 *tbx5a* knock-down affects visceral organs disposition along the LR axis

The observation that *tbx5a* MO knock-down had also an effect on neural laterality prompted to investigate whether visceral laterality was also under the scope of *tbx5a* roles. The extent of the effects of *tbx5a* interference was studied in the asymmetric positioning of the attached organs (namely liver and pancreas) with respect to the midline and the bending of the gut. In wildtype conditions, the liver lies on the right side of the embryo, whereas the pancreas is located in the left. The endodermal marker *foxA3* enabled the observation of these organs at 48hpf (Figure 4.5 A-E). The position of these visceral organs was the expected in the control embryos (Figure 4.5 A, G) in 95.72% of the cases (n = 122), while 72.87% of the embryos injected with 3ng of *tbx5a* MO (n = 129) showed the wildtype position of these organs. Other *tbx5a* morphants showed the following phenotypes: totally reversed, partial reversal and absence of attached organs. The different categories assigned to the embryos exhibiting a phenotype correspond to the specular image of the wildtype conditions in the case of totally reversed (8.57%, Figure 4.5 C, G), the incorrect positioning of the pancreas or liver and the duplication of one or both structures in partial reversal (34.29%, Figure 4.5 D, E, G) and the absence of the attached organs refers to the sole presence of the gut structure (57.14%, Figure 4.5 F, G).

Although the laterality of the endodermal organs appeared to be less sensitive to *tbx5a* knock-down than heart or neural laterality, that showed more than 80% and around 70% of the *tbx5a* morphant embryos with LR laterality defects, respectively, the percentage of *tbx5a* morphant embryos showing a laterality phenotype in the display of the liver and pancreas was also significant at $p<0.01$ after χ^2 statistical analysis (Figure 4.5 H).

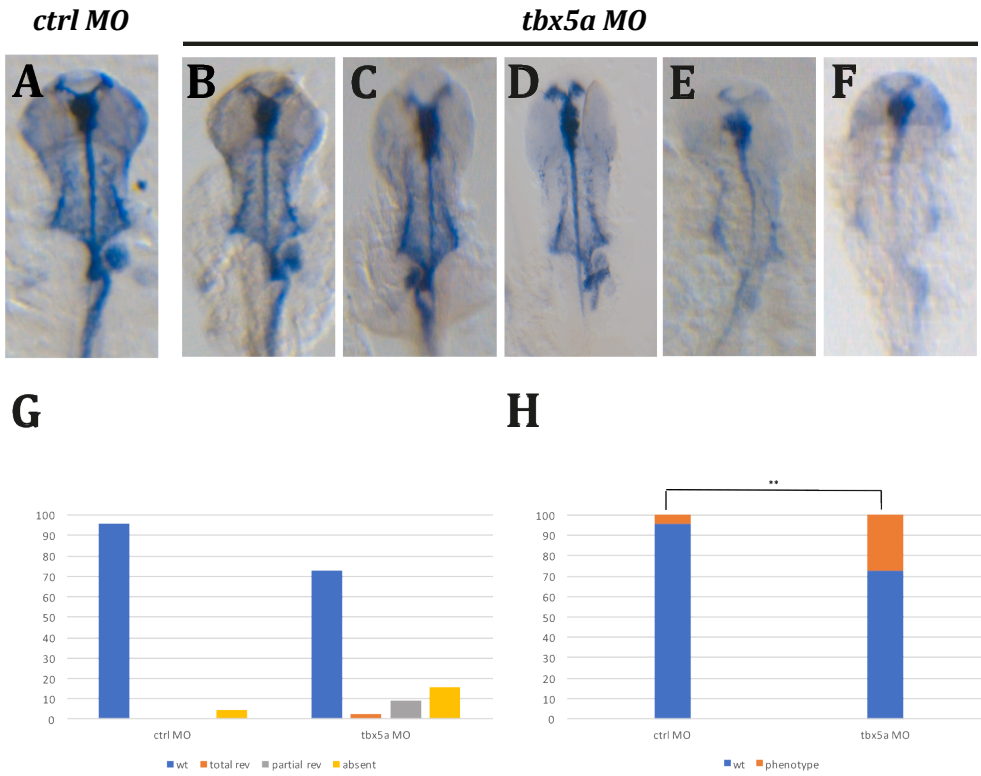

Figure 4.5 | *tbx5a knock-down affects liver and pancreas positioning along the LR axis.* *foxA3 expression at 48hpf highlights distribution of the visceral organs (A-F). Normal positioning of the organs (B) together with total reversal (C), partial reversal (D-E) and absent attached organs (F) was observed in tbx5a morphants, whereas control embryos showed normal distribution of these organs (A). Quantification of the laterality phenotypes (G). Quantification of the embryos exhibiting a phenotype with respect to the wildtype positioning (H). A χ^2 statistic has been calculated to assess significant differences between groups (**p < 0.01). Images are ventral views with anterior to the top (A-F).*

These results were also verified by analysing GFP expression in the *gut:GFP* line, a stable transgenic line that expresses GFP throughout the developing digestive system[325]. At 48hpf, control MO injected embryos showed the pancreas and liver correctly positioned along the LR axis in 96.84% of the embryos (n = 95, Figure 4.6 A, H). *tbx5a* morphant embryos displayed the liver and the pancreas correctly in 71.62% of the cases (n = 74, Figure 4.6 B), while an aberrant position of the pancreas and liver was obser-

ved in 28.38% of the embryos (Figure 4.6 C-H): 9.52% totally reversed, 42.86% with partial reversal and 47.62% with absence of the structures. The χ^2 statistical analysis was also found to be significant at $p<0.01$ (Figure 4.6 I). Hence, despite the percentage of *tbx5a* morphants exhibiting laterality defects in the visceral organs compared to the previous structures analysed is lower, the statistical analysis indicate that the results were still significant in both approaches (*foxA3* ISH, Figure 4.5 H and and *gut:GFP* line, Figure 4.6 I).

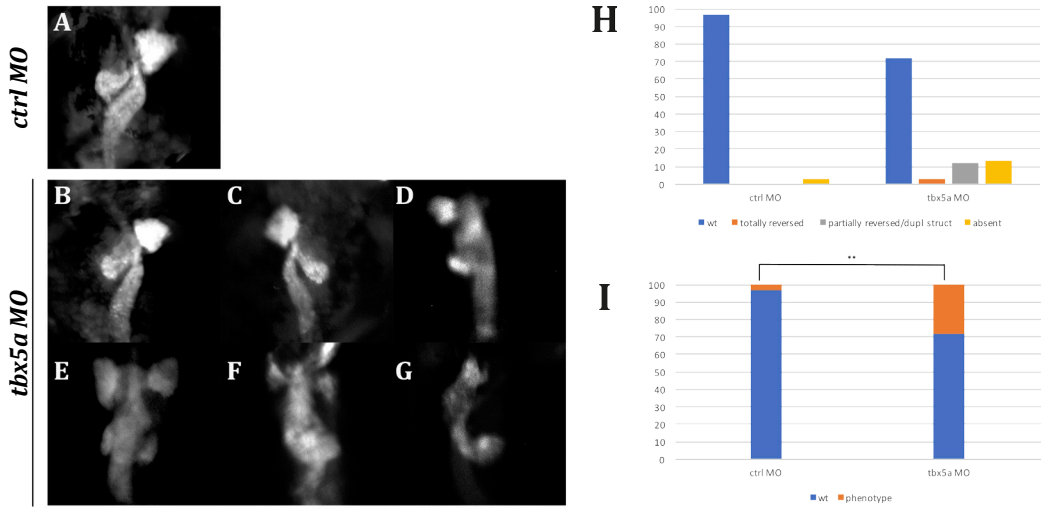

Figure 4.6 | *tbx5a knock-down affects liver and pancreas positioning.* *GFP expression at 48hpf in gut:-GFP transgenic embryos highlights the distribution of the visceral organs (A-G). Normal positioning of the organs (A-B), total reversal (C), partial reversal (D-G) Quantification of the laterality phenotypes (H). Quantification of the embryos exhibiting a phenotype with respect to the wildtype positioning (I). A χ^2 statistic has been calculated to assess significant differences between groups (**p < 0.01). Images are ventral views with anterior to the top (A-G).*

Overall, it is clear that *tbx5a* has a relevant role during zebrafish embryonic development for the proper positioning along the LR body axis of multiple organs and structures. Of note, this role is not restricted to heart morphogenesis but also to neural and visceral structures. Therefore, all these observations suggested that the onset of the

consequences of *tbx5a* knock-down might be at very early stages during zebrafish development and might be explained by specifically targeting the lineage that give rise to the KV, the LRO in zebrafish.

4.4 *tbx5a* specific knock-down in the DFCs lineage leads to laterality defects

The observation of the randomized expression of the left-side expression markers in the LPM together with the fact that laterality defects were not limited to the heart, prompted to check whether the *tbx5a* phenotype was a result of an early interference with the establishment of LR asymmetry.

The DFC/KV lineage cells maintain cytoplasmic bridges between the yolk up to 4hpf, while these cytoplasmic bridges are closed after 2hpf between the yolk and the other cells[303]. Taking advantage of this fact, the *tbx5a* MO was injected during this time-frame (2-4hpf), at 512-cell stage, and the direction of cardiac jogging was assessed at 26hpf (Figure 4.7 H-G'). Once again, after *tbx5a* MO knock-down (n = 103) in addition to the normal left-jogging (42.72%, Figure 4.7 A), midline (20.39%, Figure 4.7 B) and right-jogging (13.59%, Figure 4.7 C) phenotypes were observed. Moreover, DFC-targeted injection also resulted in more severe phenotypes classified as *cardia bifida* (16.50%, Figure 4.7 D) and other fusion defects (6.80%, Figure 4.7 E), for embryos that although a medial migration of the anterior LPM cell population is observed, they were unable to culminate the migratory process with the midline fusion. As a positive control, the expression of *fgf24* was checked in the pectoral fin bud and branchial arches, which remained unaffected (Figure 4.7 F). Additionally, it is worth to notice that the phenotypes identified after injection targeted to the DFCs were more severe than the ones observed after global injection with 3ng *tbx5a* MO (compare Figure 4.7 H, H' with Figure 4.7 G, G'). This apparent paradox could be explained by the fact that the same dose of MO is injected targeting a much-reduced cell population, thus causing a stronger phenotype in the morphant embryos.

Furthermore, to complete this analysis *tbx5a* MO was injected after 4hpf as a negative control. At this time-point the cytoplasmic bridges are already closed between the DFCs and the yolk cell. Hence, an injection after this developmental stage solely targets the yolk cell. Yolk-targeted injections did not result in laterality defects during the cardiac jogging either in the control or in the *tbx5a* morphants (n = 67 and n = 102, respectively; Figure 4.7 I, I'), demonstrating that the LR phenotype after *tbx5a* knockdown resulted from specifically affecting the DFCs.

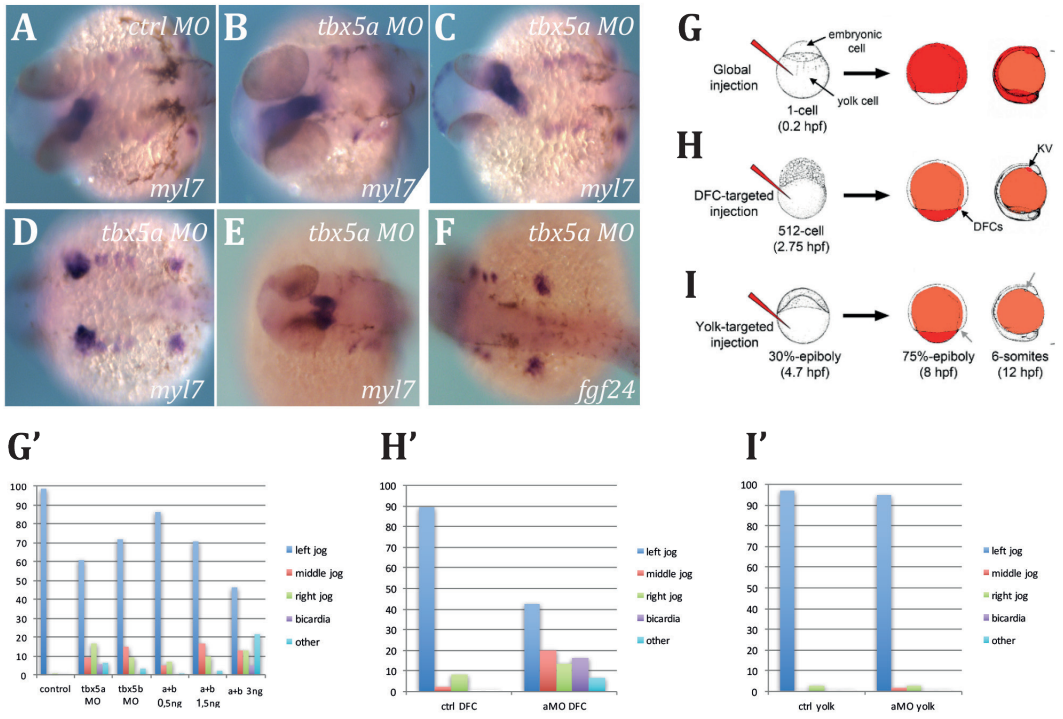

Figure 4.7 | *DFCs-targeted injection with tbx5a MO results in a jogging phenotype.* *tbx5a knock-down targeting the DFC lineage result in morphants that exhibit not only left, right, no-jogging (A, B, C, respectively), but also cardia bifida (D) and other severe phenotypes (E). (B-E). Expression of fgf24 in the pectoral fin bud and branchial arches as a positive control (F). Scheme of the different injection strategies adapted from Wang et al., 2013[303]: global injection (G), DFC-targeted injection (H), yolk- targeted injection (I). Quantification of the jogging phenotypes at 24hpf obtained after tbx5a MO global injection (G-G'), DFC-targeted injection (H-H') and yolk-targeted injection (I-I'). Yolk-targeted injection morphants do not exhibit laterality defects (I') phenotypes (F). Images are dorsal views with anterior to the left (A-F).*

Chapter 5

A novel and early role for *tbx5a* during zebrafish development

Chapter Overview

The results described in chapter 3 and 4 regarding the laterality defects in the organs analysed, together with the specific LR asymmetry jogging phenotype after interfering with *tbx5a* function specifically in the DFCs, strongly suggested that *tbx5a* is expressed earlier than what it had been previously described.

In this chapter I aimed to demonstrate an early *tbx5a* expression pattern and to investigate the possible mechanism by which *tbx5a* plays a role in the establishment of the correct signalling and positioning along the LR axis. To this end, I assessed the expression pattern of several genes expressed in the KV or on its vicinity that have been previously described to have either a role in LR asymmetry or to be involved in *tbx5a* signalling by ISH. In these experiments, expression was compared between control embryos and embryos with compromised *tbx5a* function. In the ISH experiments control embryos expression pattern was compared to the *tbx5a* morphants at 10SS. For the most promising genes, I carried out qPCR to seek for significant variation in their expression levels comparing control embryos *versus* DFC-targeted *tbx5a* MO injected embryos. In addition, I searched for putative binding sites in the regulatory region of those genes that showed a significant change in their transcriptional expression after *tbx5a* knock-down that could explain the defects identified. Finally, I also checked the morphology of the KV and its cilia in control and *tbx5a* morphant embryos.

5.1 *tbx5a* is expressed during early zebrafish development

The onset of *tbx5a* expression had been described to be at around the 6-7SS in the posterior halves of the optic cup and faintly in the LPM[85]. Nevertheless, the fact that DFC-targeted *tbx5a* MO injection resulted in cardiac asymmetry defects, suggested an earlier expression for *tbx5a* in development related to LR asymmetry. Hence, RT-PCRs using RNA from early developmental stages were performed. RNA was extracted from embryos at shield, 1S and 24hpf stages (the latter as a positive control for *tbx5a* expression). Strikingly, after running a RT-PCR for *tbx5a* and *ef1a* (elongation factor 1 a), as a positive control, a band could be detected for all the developmental stages analysed (Figure 5.1 A) that could not be detected in a negative control RT-PCR with water. In addition, the RT-PCR results were confirmed by ISH for the same developmental stages. The probe previously described by Begemann and Ingham[85] did not reveal any signal at shield or at 1SS (Figure 5.1 C, C'). Hence, another probe that includes the 5' region of *tbx5a* (*tbx5a* 5') was designed. This probe did not reveal any specific signal in any of the stages analysed either (Figure 5.1 D, D') and therefore, a longer *tbx5a* probe [*tbx5a* FL (full length)] as well as its complementary sense probe were designed. Remarkably, this FL probe, which spans a greater region than the probes previously used, reported signal in both shield and 1S stages (Figure 5.1 E-E'), in addition to the typical expression pattern obtained at 24hpf (Figure 5.1 E''). As expected, no staining was obtained with the sense probe (Figure 5.1 B-B''), indicating that the signal detected with the FL *tbx5a* probe was specific. At shield stage, expression was specially detected on the dorsal side, in the area where the shield develops (Figure 5.1 E). The embryonic shield is a thickening of the leading edge of the blastoderm during the formation of the germ ring and is one of the first signs of DV polarity in the embryo. Later, at 1SS, the expression seemed to be more homogenous throughout the embryo (Figure 5.1 E').

Moreover, by using the same FL *tbx5a* probe some faint expression around the KV at 10SS (Figure 5.1 F'') together with the previously described expression pattern in the OC and LPM (Figure 5.1 F') could be detected. This evidence, enforced the hypothesis of *tbx5a* having an early role during the embryonic development of the zebrafish that ensures the consecution of the correct arrangement of the organs along the LR axis.

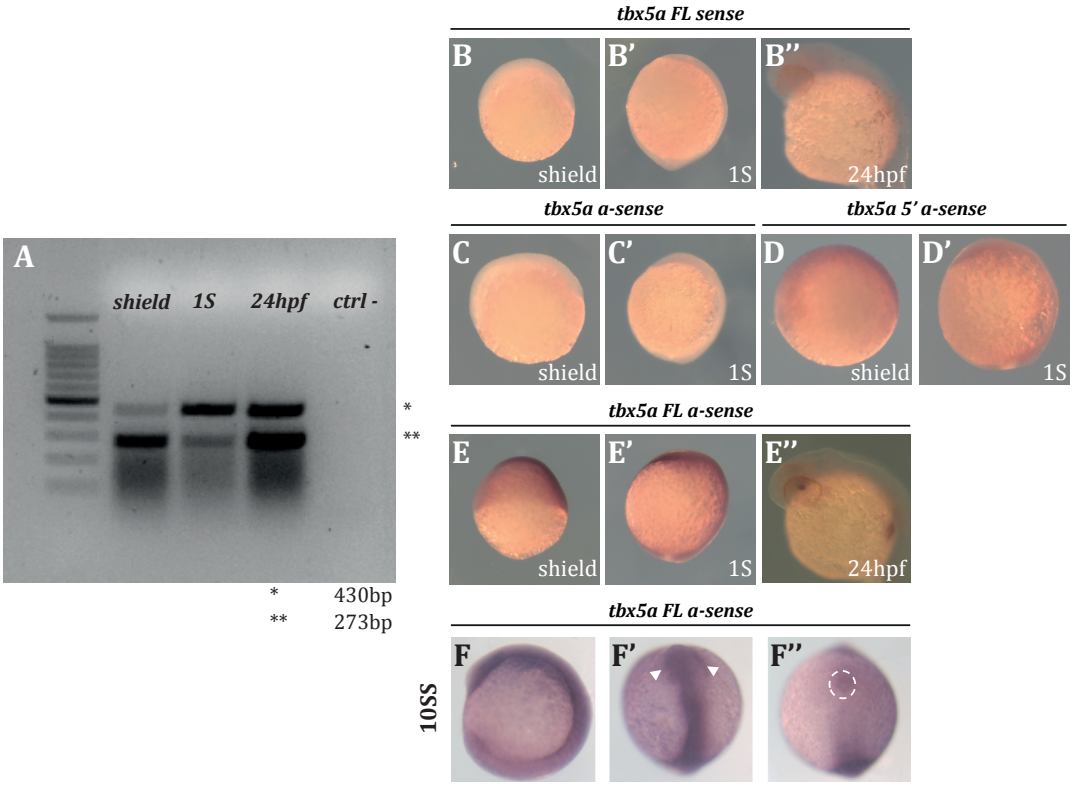

Figure 5.1 | *tbx5a is expressed at shield and 1S stages.* *RT-PCRs show a band for both ef1a (positive control: 430bp (*) and tbx5a (273bp (**)) at all lanes except for the negative control (ctrl -) (A) .tbx5a (C-C') and tbx5a 5' (D-D') probes do no detect tbx5a expression in the zebrafish embryos at shield (B-E) and 1S (B'-E') stages. tbx5a FL probe (D-D''') retrieves signal at all stages analysed (shield: E, 1S: E'-E''', 24hpf; E''), whereas FL sense probe does not show any signal (shield: B, 1S: B', 24hpf: B'').). tbx5a expression pattern at 10SS using FL tbx5a probe for ISH (F-F''). Images are animal views B-E with dorsal to right, lateral views in B'-E', F, with anterior to the left, dorsal view in F' with anterior to the top and ventral view in F'' with anterior to the top. White arrowheads point to the OCs, whereas the white dashed circle define the area containing the KV structure.*

5.2. Analysis of the expression pattern of putative effectors of *tbx5a*

Once *tbx5a* expression was confirmed to be expressed as early as shield stage and also been detected in the surroundings of the KV at 10SS, the expression of a series of putative targets was analysed at 10SS. This analysis was performed by comparing the ISH signal of the control-MO injected embryos with tbx5a morphants (injected with 3ng of *tbx5a* MO at the one-cell stage).

The criteria to select the genes to be included in this analysis took different aspects into consideration. Genes should be described as expressed in the KV or in its vicinity around 10SS. To this end, the literature and zfin.org database were thoroughly searched to select candidates. In addition, genes reported to be regulated by T-box genes in other structures that were also found in the first selection process were prioritized.

5.2.1. The Fgf signalling pathway

After the aforementioned search, the Fgf ligands *fgf4* and *fgf8a* were found to be expressed in the KV[350]. In addition, *fgf10a* and *fgf24* were also analysed since they have been described to act downstream of *tbx5a* during pectoral fin morphogenesis and they are also faintly expressed in the KV at this stage[351]. Finally, *pea3* and *erm* were also examined since both are direct read-outs of cells to Fgf levels.

fgf4 and *fgf8* are expressed in the KV (Figure 5.2 A and 5.2 B, respectively), specially *fgf4*, which expression gets further extended towards the posterior notochord. Both genes have been previously described to result in defects in LR asymmetry after their knock-down using MO injection[350], but their expression was not found to be altered after *tbx5a* MO knock-down (compare Figure 5.2 A, B with 5.2 A', B' and 5.2 A'', B''). For *fgf10a* and *fgf24*, which are expressed in lower levels in the KV area, similar results

were obtained. Both Fgf ligands did not exhibit a significant change in their expression pattern or levels (Figure 5.2 C-C'' and 5.2 D-D'' for *fgf10a* and *fgf24*, respectively). Finally, despite no significant changes were observed in any of the Fgf ligands, *erm* and *pea3* expression pattern was also assessed as a general read-out for Fgf signalling. No differences were observed for these genes either (Figure 5.2 E-E'' and 5,2 F-F''), indicating that *tbx5a* does not play its role in LR asymmetry via regulation of Fgf signalling.

The quantification of the embryos exhibiting a fainter expression compared to the ones showing the typical expression pattern was submitted to a χ^2 statistical analysis for all the genes checked by ISH (Figure 5.2 A''-F''). The analyses demonstrated that there were no significant differences between control MO injected embryos and *tbx5a* morphants.

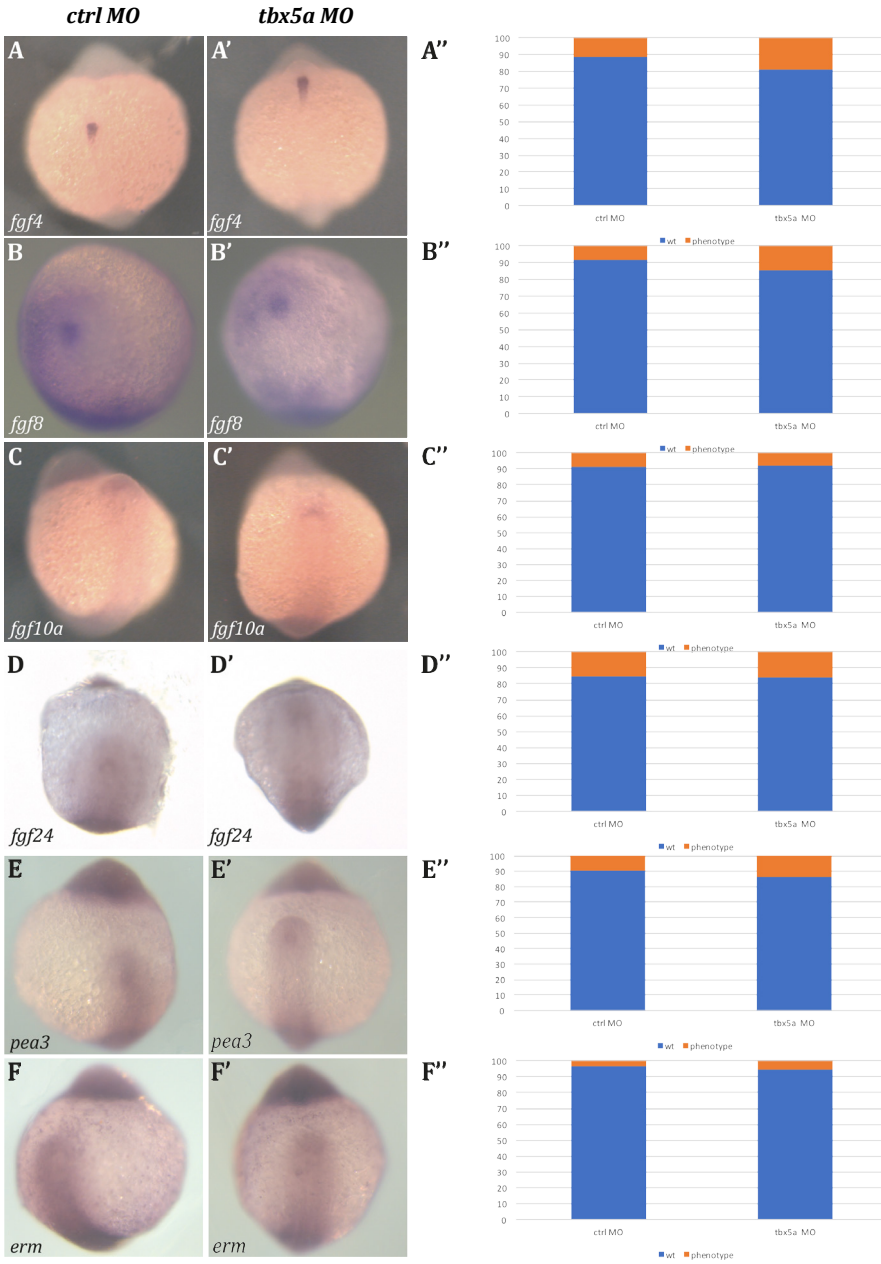

Figure 5.2 | The *Fgf signalling pathway is not affected by tbx5a MO knockdown.* *Fgf ligands fgf4 (A), fgf8 (B), fgf10a (C) and fgf24(D) do not change their expression pattern after tbx5a MO injection (A', B', C', D', respectively). erm and pea3 FGF signalling read-outs do not have any significant modifications either (E vs E' and F vs F'). Quantification of the expression pattern (A''-F''). A χ^2 statistic has been calculated to assess significant differences between groups, but no significant differences were found. Images are ventral views with anterior to the top (A-F').*

5.2.2. The Bmp signalling pathway

Bmps have been described to be related with *tbx5* in several developmental processes including cardiovascular development and limb and retina morphogenesis. From this family of signalling molecules, I chose to analyse *bmp4* since it is expressed around the KV area and had previously been demonstrated to be required for proper LR development[210]. As shown in Figure 5.3, *bmp4* expression in the periphery of the KV gets reduced after *tbx5a* MO injection: 43.50% (n = 246) of the *tbx5a* morphants showed a reduced expression in the vicinity of the KV compared to the control morphants (compare Figure 5.3 A, C with 5.3 B, C). The quantification of the embryos exhibiting a fainter expression compared to the ones showing the typical expression pattern was submitted to a χ^2 statistical analysis and the differences between control injected embryos and *tbx5a* morphants were found to be significant at $p<0.05$ (Figure 5.3 C).

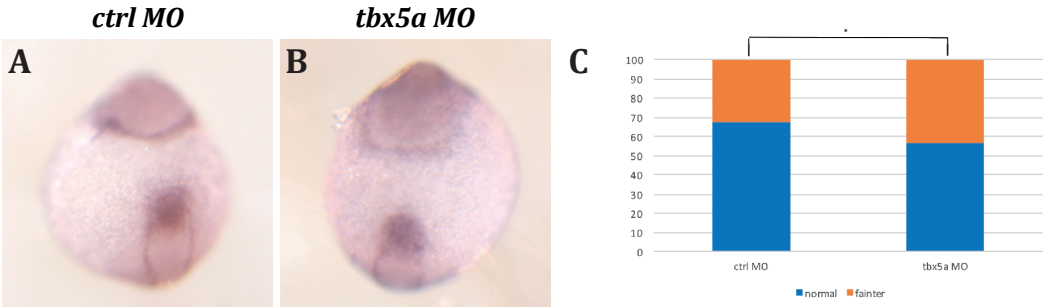

Figure 5.3 | *bmp4 expression levels are reduced after tbx5a knock-down.* *The typical expression around the KV is significantly reduced in tbx5a morphants (B) compared to the control embryos (A). Quantification of the phenotype (C). A χ^2 statistic has been calculated to assess significant differences between groups (*p<0.05).*

5.2.3. Eph/ephrin signalling

Among the ephrin ligands and Eph receptors, *ephb4b* was selected since it had been previously reported to be expressed in the DFC[352]. In addition, the *efnb2a* ligand was also included in these analyses since, as described in the chapter 1 of the results, its expression domain gets reduced in the double knock-down of *tbx5* genes. In addition, Zhang and colleagues also demonstrated that Eph signalling inhibition results in LR defects[352]. By overexpressing s-*efnb2a* mRNA, which encodes the extracellular domain of Efnb2a and binds to Eph receptors antagonizing Eph signalling[353,354], they observed the randomization of the heart looping and the liver position[352].

Despite a faint ring-shaped expression could be detected for *efnb2a* in the border of the KV (Figure 5.4 A), its expression did not change in *tbx5a* morphants (Figure 5.4 A', A''). No changes were either detected for *ephb4b*, which was highly expressed in the KV in both control and *tbx5a* morphant embryos (Figure 5.4 B-B''). The differences in the expression pattern (*i.e.* reduction on the detected signal) were quantified and a χ^2 statistical analysis was done for both genes. Nevertheless, the differences were not significant (Figure 5.4 A'', B'').

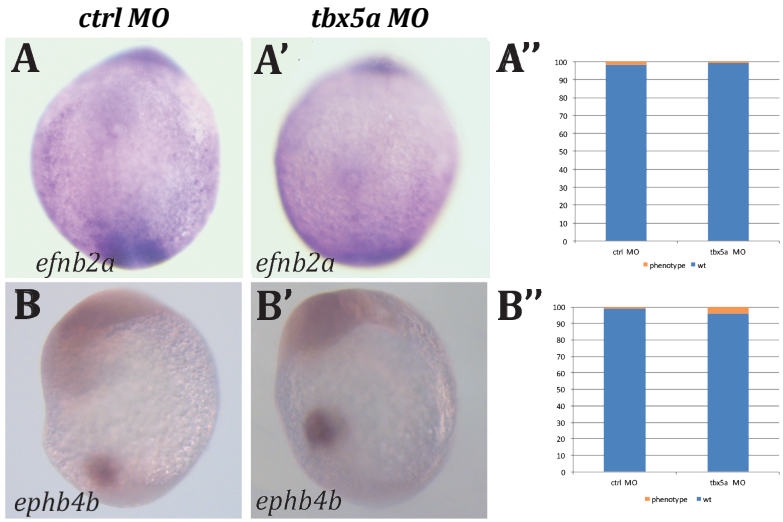

Figure 5.4 | *Expression of efnb2a and ephb4b in the KV area is is not affected by tbx5a knock-down.* *efnb2a expression in the periphery of the KV in tbx5a morphant (A') and controls (A). ephb4b remains expressed in the same domain in tbx5a morphants compared to control embryos (B' and B', respectively). Quantification of the expression pattern (A''-B''). A χ^2 statistic has been calculated to assess significant differences between groups but no significant differences were found. Images are ventral views (A-A') and frontal views (B-B') with anterior to the top.*

5.2.4. Additional tbx5a putative downstream effectors

In addition to members of Fgf, Bmp and Ephrin/Eph signalling cascades, other genes previously described as *tbx5a* targets were included in these analyses. Among them, *prrx1a* and *prrx1b* which have Tbx5 binding sites in their regulatory region[355]. Also, *camk2b2* expression was checked, since its regulation by *tbx5* is required for proper pectoral fin and cardiac morphogenesis[332] and *cx43.4*, which is under Tbx genes regulation during cardiac development[356].

With regard to the *prrx1* paralogues, only *prrx1a* was found to be expressed surrounding the KV. *prrx1a* was a promising candidate since, in addition to the putative binding sites for Tbx5 in its regulatory region, ISH experiments at a later stage of embr-

yonic development (18SS) showed higher levels of *prrx1a* expression and asymmetric expression in the LPM[213,355]. Yet, the expression levels for *prrx1a* in this area at 10SS were found to be quite faint and did not experience significant expression changes after *tbx5a* MO injection (Figure 5.5 A-C).

Similarly, the expression of *camk2b2*, which was faintly detected in the KV, in agreement to the essential role of calcium in the establishment of LR asymmetry, did not change in *tbx5a* morphants (Figure 5.5 D-F). Finally, the expression of *cx43.4* did not suffer any noticeable changes to be reported (Figure 5.5 G-I). Any detected reduction on expression levels was quantified for the three genes and submitted to a χ^2 statistic to assess differences between groups, but no significant differences were detected (Figure 5.5 C, F, I). Nevertheless, it cannot be ruled out that this lack of significance could be due to the sensitivity of the probes, which may not be good enough to detect subtle changes in the expression domain/level.

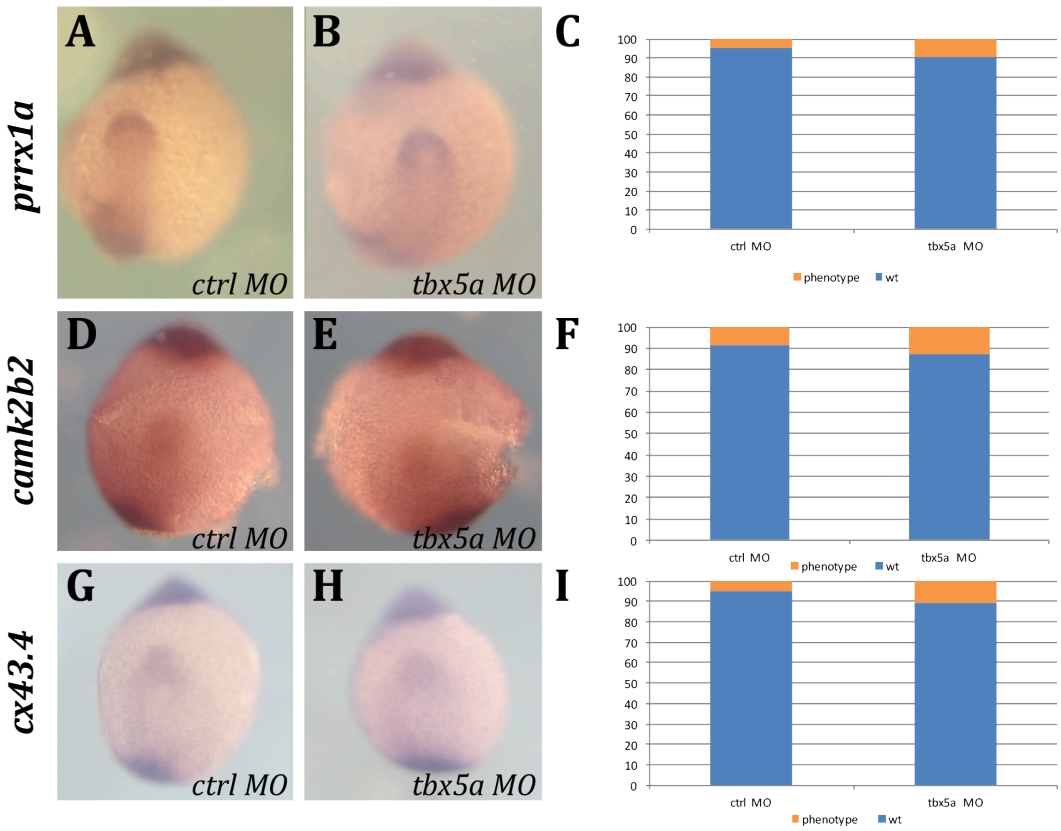

Figure 5.5 | *prrx1a, camk2b2 and cx43,4expression in the vicinity of the KV is not altered in tbx5a morphants*. *prrx1a expression around the KV (A), camk2b2 in the KV (D) and cx43.3 in the vicinity of the KV (G) are detected in low levels in this territory. tbx5a knock-down does not cause significant changes in their expression pattern (B, E, H, respectively). Quantification of the expression (C, F, I). A χ^2 statistic has been calculated to assess significant differences between groups, which retrieved no significant differences. Images are ventral views with anterior to the top.*

5.2.5. The Nodal signalling pathway

Several members belonging to the Nodal signalling pathway were examined, since this pathway has been extensively reported to be linked with LR asymmetry establishment. The Nodal-related gene *spaw*, its downstream effectors *pitx2* and *lefty1* and *charon*, a negative regulator of Nodal signalling, were analysed. In addition, *gdf3*, previously known as *dvr1*, that potentiates the activity of Nodal was also checked. Interestingly, despite no significant differences in the expression levels were detected by ISH for *spaw* (Figure 5.6 A-A''), expressed around the KV, or for *lefty1* (Figure 5.6 B-B''), which maintained its expression in the midline preventing LR cues leaking from the left side of the embryo, *charon* expression domain suffered an obvious change in its typical expression domain (Figure 5.6 C-C''). In control conditions, *charon* is expressed in the periphery of the KV surrounding this structure with a horseshoe shape (with the anterior side opened, Figure 5.6 C), but after *tbx5a* MO injection 44.67% (n = 244) of the embryos exhibited an impaired expression in this territory (Figure 5.6 C'). Since *pitx2* is not expressed in the KV area and *gdf3* is only faintly expressed in this area, to detect whether there were any differences in the expression of these genes pattern in *tbx5a* morphants compared to controls, expression was checked in the LPM. Expression of *pitx2* (Figure 5.6 D-D'') and *gdf3* (Figure 5.6 E-E'') remained unaltered after *tbx5a* MO knock-down. Hence, from all the members belonging to Nodal signalling pathway analysed, only *charon* was altered after interfering with *tbx5a* suggesting that this gene is directly or indirectly regulated by *tbx5a*.

The differences in expression levels or expression domain for all the members of Nodal signalling pathway genes analysed were quantified and submitted to a χ^2 statistical analysis (Figure 5.6 A''-E''). In the case of *charon*, the differences between control and *tbx5a* morphant groups were found to be significant at $p<0.01$ (Figure 5.6 C'').

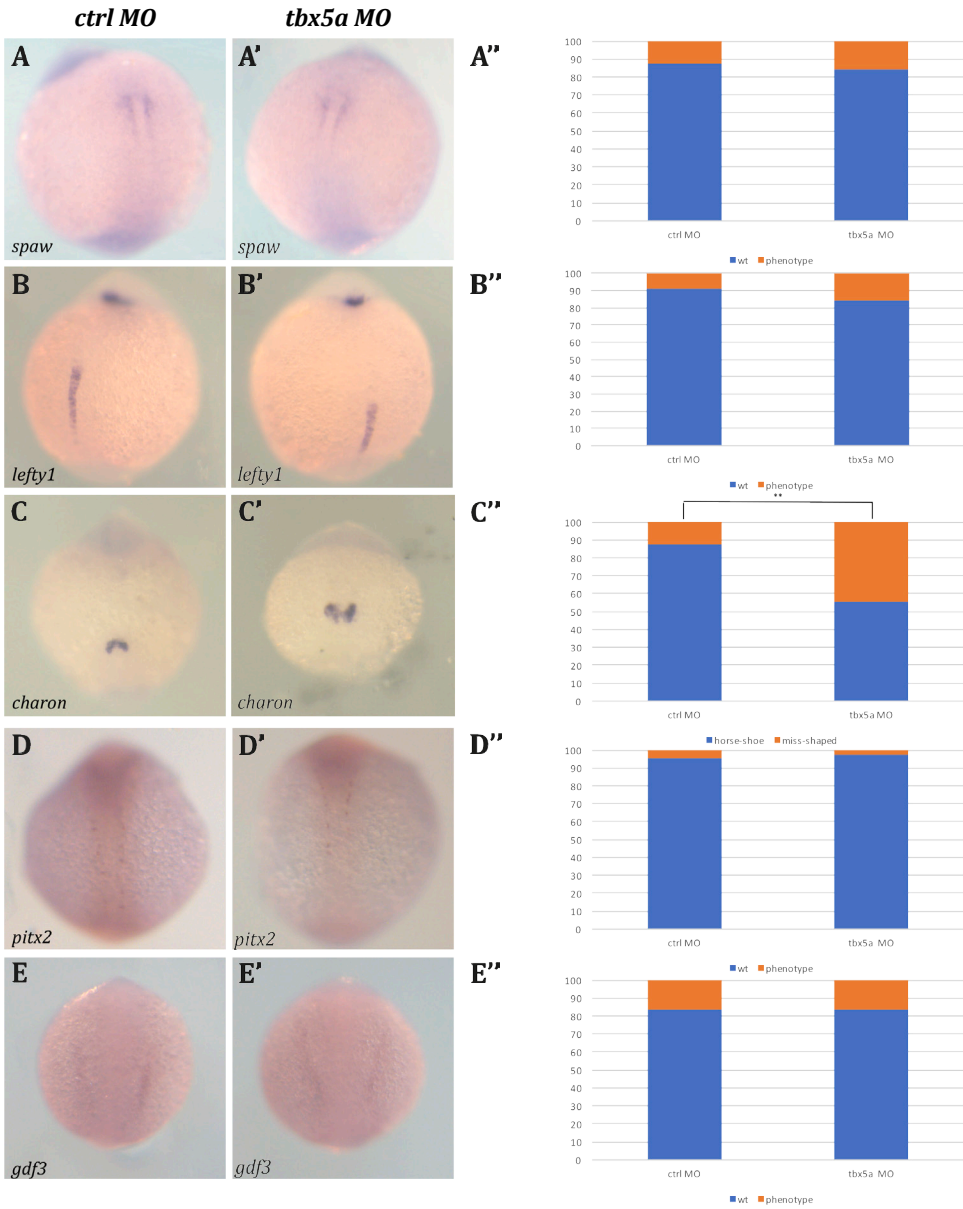

Figure 5.6 | *charon typical expression pattern is misshaped around the KV when tbx5a is knocked down.* *spaw (A-A') and its inhibitor lefty1 (B-B') expression remain unaltered after MO knockdown, whereas nodal-inhibitor charon loses its typical horseshoe-shaped (C) pattern around the KV in tbx5a morphants (C'). pitx2 (D-D') and gdf3 (E-E') in the LPM also were unaffected by tbx5a knock-down. Quantification of the phenotypes (A''-E''). A χ^2 statistic has been calculated to assess significant differences between groups (**p < 0.01). Ventral images with anterior to the top (A-C'). Dorsal images with anterior to the top (D-E'). Control embryos (A-E) and tbx5a morphant embryos (A'-E').*

5.2.6. Other genes expressed in the vicinity of the KV

Finally, several other genes previously described in zfin.org or reported in the literature to be expressed in the KV or in its immediacy were checked. Many of them showed extremely low signal or were basically undetectable. Hence, only few more genes were included in the present expression pattern analyses in the KV after *tbx5a* knock-down. A special case was considered for *wtip*, (Wilm's tumor 1 interacting protein) and *ntl*. *wtip* is expressed in the basal bodies of cilia[357] and its knock-down by MO injection results in the randomization of *spaw* and *lefty1/2* expression in the LPM and the randomization of the cardiac looping[334]. In additon, its bilateral expression at 10SS in the LPM resembles that of *tbx5a*. Regarding *ntl*, its expression in the midline is important to preserve the left and the right side as independent compartments, acting as a physical barrier that prevents signal leakage from one side to the other of the embryo. Consequently, its expression was also checked to assess whether it is affected after *tbx5a* knock-down.

Therefore, expression pattern in this area was checked for *cav1* (Figure 5.7 A-A''), which is expressed in the territory surrounding the KV, *sepw1* (Figure 5.7 B-B''), which also exhibits its expression surrounding the KV but in lower levels, *wtip* (Figure 5.7 C-C'') and *ntl* (Figure 5.7 D-D'').

After comparing the expression pattern of the *tbx5a* morphant embryos to their respective control siblings, no significant observable changes in the expression pattern could be detected in any of the genes (Figure 5.7 A''-D''). These results, are especially relevant in the case of *ntl*, because this indicates that the midline barrier is not lost after *tbx5a* interference (Figure 5.7 D-D''). Regarding the rest of the genes, the observations point towards a regulation independent of *tbx5a*, at least in this territory and developmental stage. The quantifications (Figure 5.7 A''-D'') indicate the percentage

of embryos in which the levels of expression were found to be fainter compared to the expected expression pattern. A χ^2 statistic was calculated to assess significant differences between groups, but no significant differences were detected.

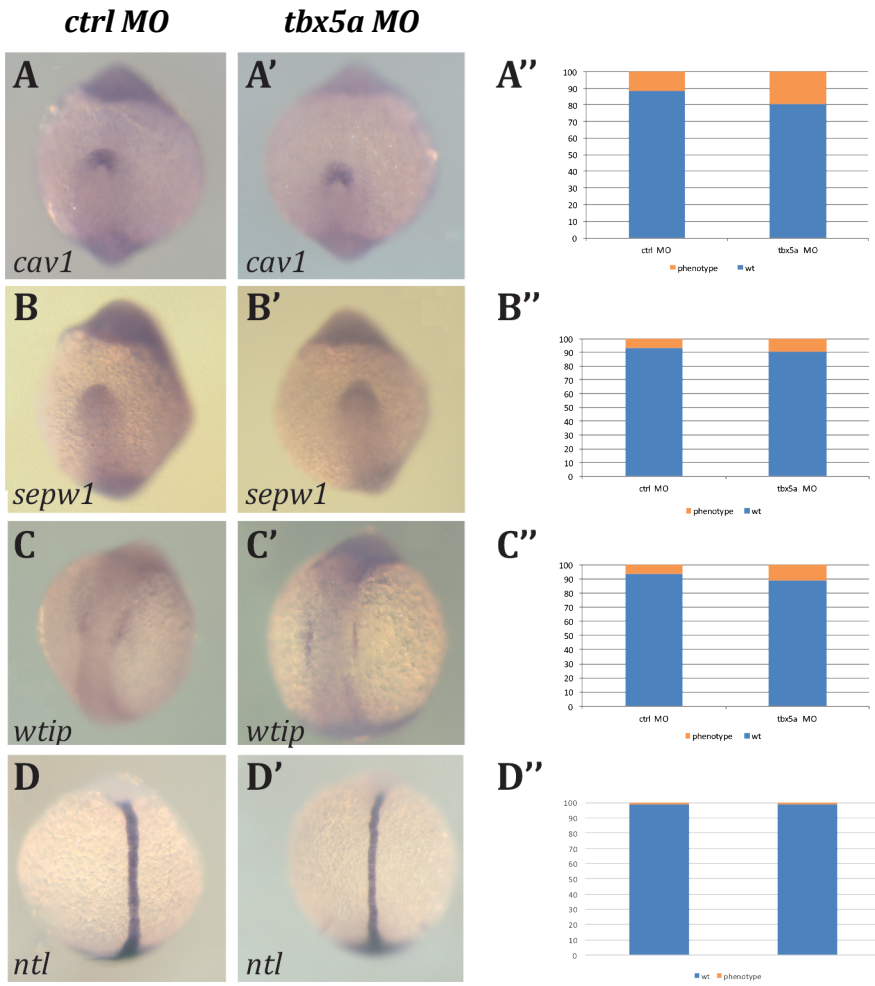

Figure 5.7 | *cav1, sepw1, wtip and ntl expression levels do not change after tbx5a MO knock-down.* *Cav1 expression pattern around the KV in control and tbx5a morphants (A,A', respectively), sepw1 expression for control (B) and tbx5a morphants (B'), wtip expression in the LPM in control and tbx5a morphants (C vs C') and ntl expression in the midline in control and tbx5a morphants (D vs D') remain unaltered. Quantification of the expression pattern for the genes (A''-D''). A χ^2 statistic has been calculated to assess significant differences between groups. Images are ventral views (A-B') and dorsal views (C-D') with anterior to the top.*

In summary, the analysis of the expression pattern of several putative downstream effectors for *tbx5a* in both control and *tbx5a* morphant conditions showed that only *bmp4* and *charon* expression around the KV structure were significantly altered in terms of expression levels and expression domain, respectively. The rest of the candidates checked by ISH did not retrieve any significant differences, although some of them were quite promising due to its previous relationship with *tbx5a* or its role in LR asymmetry described in the literature, such as the Fgfs, *camk2b2*, *cx43.4* or *prrx1a.* However, it has to be considered, that ISH may not be sensitive enough to detect subtle differences in the expression levels or in the expression domain. For this reason, I aimed to perform qPCR for the most promising genes in order to obtain a quantitative approach for the expression of these genes in order to achieve more conclusive results.

5.3. Quantitative analysis of putative *tbx5a* downstream effectors

Although some significant differences were already found in the expression pattern of two genes by ISH, this method confers lower sensitivity than qPCR. Thus, the expression of several genes from the Fgf, Bmp, Nodal signalling pathways, among others, was analysed by qPCR. The samples to be compared were control MO-injected embryos *versus* DFC-targeted injected embryos with 3ng of *tbx5a* MO, which would allow to directly link variations in the expression levels to interference with *tbx5a* in the DFC/KV lineage. For all genes analysed, a technical and a biological triplicate was performed and *ef1a* was selected as a reference gene. From Bmp signalling pathway, the ligands *bmp4* and *bmp2b* were included in these analyses as well as their receptors *bmpr1aa*, *bmpr1ab*, *bmpr1ba*, *bmpr1bb*, *bmpr2a* and *bmpr2b*. Interestingly, many of the genes assessed suffered a significant reduction on their transcriptional levels after using a two-tailed Student's T-test statistical analysis, e.g. both ligands and several of *bmpr1* receptors: *bmpr1ab*, *bmpr1ba* and *bmpr1bb* (Figure 5.8 A, B).

In the case of the Fgf signalling pathway, none of the genes analysed (*fgf4*, *fgf8*, *fgf10a* and *fgfr2*) exhibited significant differences in their expression levels (Figure 5.8 A, C). Finally, for the Nodal-related gene *spaw* there was a reduction on its expression levels, whereas in the case of *cx43.4* and *prrx1a*, no significant differences could be detected (Figure 5.8 A, D).

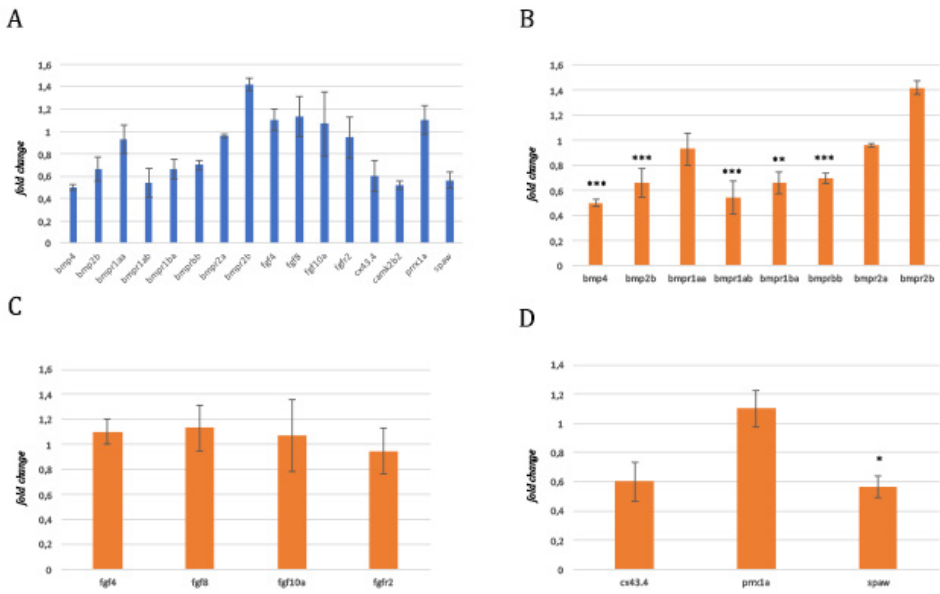

Figure 5.8 | ***Quantification of the transcriptional levels by qPCR at 10SS of DFC-targeted tbx5a morphants compared to control embryos.*** *Summary of fold change for all the analysed genes (A). Bmp signalling pathway genes (B), Fgf signalling pathway genes (C) and other tbx5a related genes (D). Error bars represent the standard error. Data were analysed by Student's T-test (* p<0.05, ** p<0.005, *** p<0.0005). Y axis represents fold change.*

To confirm the observed results, the experiments were repeated using another reference gene: *hatn10*, a repetitive sequence in the genome (ERE: Expressed Repetitive Element). *hatn10* has been reported to be one of the most reliable reference gene in many biological scenarios (e.g. comparison of different developmental stages, or-

gans or drugs)[348]. After doing this further analysis the results were quite similar those obtained in the analysis using *ef1a*. All the genes that were found to be significantly downregulated in the first analysis were also found downregulated in this second analysis although with some variation in the level of significance (compare Figure 5.9 B with 5.8 B). An exception was detected in *spaw*, which expression levels in the morphants appeared to be non–significantly altered in this second analysis (Figure 5.9 D *versus* 5.8 D).

From all the genes analysed, Bmp signalling pathway members were the most profoundly affected after *tbx5a* knock-down, suggesting that this pathway acts downstream of *tbx5a* to ensure proper consecution of LR asymmetry (Figure 5.9 A, B).

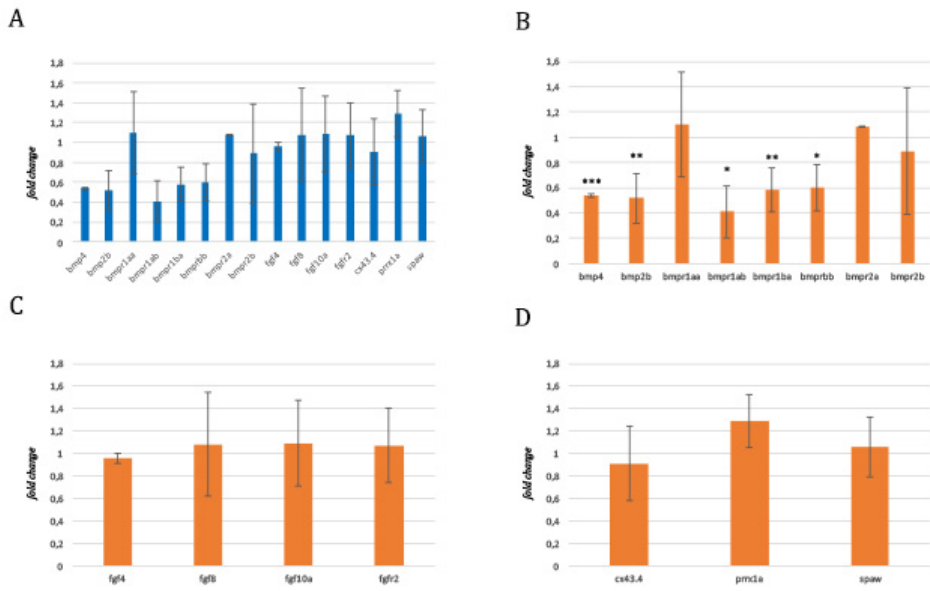

Figure 5.9 | *Quantification of the transcriptional levels by qPCR at 10SS of DFC-targeted tbx5a morphants compared to control embryos.* *Summary of fold change for all the analysed genes (A). Data are dissected in Bmp signalling pathway genes (B), Fgf signalling pathway genes (C) and other tbx5a related genes (D). Error bars represent the standard error. Data were analysed by Student's T-test (* p<0.05, ** p<0.005, *** p<0.0005). Y axis represents fold change.*

5.4. Analysis of the regulatory region of the Bmp signalling pathway members

The fact that several members of the Bmp signalling pathway (both ligands and receptors) were downregulated after interference with *tbx5a* in the DFCs prompted to investigate whether there were any binding sites for Tbx5 in the regulatory region of these genes. To do so, the FindM software was used. FindM is a tool from the Signal Sequence Analysis Server that finds motifs around functional sites. The putative regulatory region encompassing 30kbp upstream and downstream of every gene as well as the gene sequence for all the members of the Bmp pathway previously analysed by qPCR were submitted to this *in silico* analysis. In the search, the TBX5 motif from the motif library JASPAR CORE 2016 vertebrates (Figure 5.10 A') was the target sequence to be detected in the input sequences. Strikingly, the regulatory regions for all Bmp signalling members analysed contained a putative binding site for TBX5 (Figure 5.10 A). Thus, the stringency of the analysis was increased to find which of the putative binding sites obtained in this first *in silico* analysis appeared to be conserved along vertebrate evolution, which resulted in a more refined output. No conservation was found for any of the Bmp receptors 1 and, in the case of receptors 2, conservation was only found to be preserved in teleosts (Figure 5.10 A''). In contrast, for *bmp2b* and *bmp4* ligands conservation was extended to mammals: both ligands were found to be conserved in mouse and *bmp4* was also found to be conserved in human (Figure 5.10 A''). Due to the high conservation of the Tbx5 putative binding site in the *bmp4* regulatory region, the regulatory region of zebrafish *bmp4* gene was further dissected to precisely locate the putative Tbx5 binding site along its sequence. After this analysis, the binding site sequence (AGGTGTGA) was found to be located beginning at position -3930 in the + strand (Figure 5.10 B).

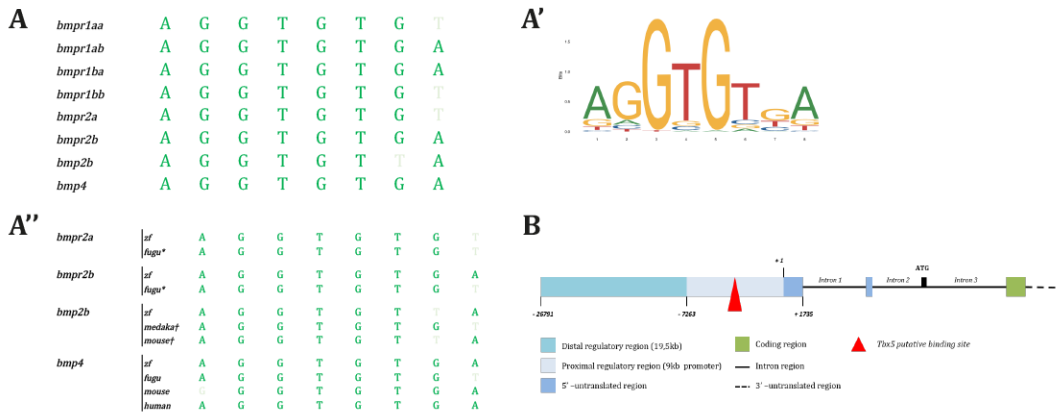

Figure 5.10 | *Bmp signalling members contain a putative binding site for Tbx5*. *Schematic representation of TBX5 binding site in the Bmp pathway members (A), its conservation (A'') and the reference sequence used by FindM to locate TBX5 putative binding sites along the regulatory region of these genes (A'). Schematic representation of the zebrafish bmp4 regulatory region (B): the drawing includes the distal and proximal regulatory regions, 5'- and 3' untranslated regions, exons 1-4 and intron 1-3. The sequence highlights a putative binding site for tbx5 (AGGTGTGA) beginning at position -3930 in the + strand with a red triangle.*

Once it was confirmed by a quantitative approach that some members of the Bmp signalling pathway appeared downregulated and that putative binding sites for Tbx5 were found in their regulatory region, several parameters of the KV were checked to investigate whether there were other additional defects that could contribute to the *tbx5a* knock-down phenotype.

5.5. Morphology of the KV of *tbx5a* morphants

I next analysed other parameters of the KV such as its size and functionality to detect whether there were any physical and biological aspects of KV development that were also affected by *tbx5a* downregulation. The analysis included the measurement of the diameter and area of the KV, the migration of the DFC cohesiveness and some parameters related to the KV cilia.

The diameter of the KV at 10SS in control and *tbx5a* DFC-targeted morphants was similar in terms of maximum length (around 75µm), while the mean size of the KV was reduced in *tbx5a* morphants (Figure 5.11 A-C). In addition, the minimum size detected for *tbx5a* was also smaller (Figure 5.11 A-C). Previous publications reported that the KV size expands between 1SS and 10SS[301,302] and it has been described that an essential feature of KV size/morphology is to achieve a luminal area bigger than 1300µm^2 at 8SS[305]. This size ensures the correct creation of the directional fluid flow to initiate LR asymmetry establishment and subsequent correct expression of *spaw* in the LPM. Therefore, this parameter was also analysed in both conditions (control and *tbx5a* morphants). The mean value for the KV area of *tbx5a* morphants was around 2281µm^2 in contrast to the 3277µm^2 for the control siblings. In addition, a higher variation of KV size was observed in *tbx5a* morphants (Figure 5.11 D) and some embryos presented an area under the minimum KV threshold size between 1300µm^2 and 1700µm^2 or even under the critical size of 1300µm^2 (< 1700µm^2: 42.31%, < 1300µm^2: 16,67%), below which the KV can no longer function to generate robust LR asymmetric development[305]. Thus, the observed reduction in the KV size could impede the consecution of a correct/consistent fluid flow in the KV and the subsequent proper LR asymmetrical disposition of the internal organs.

Additionally, to assess whether cilia motility was impaired in *tbx5a* morphants, *dnah9* (dynein, axonemal, heavy polypeptide 9), also known as *lrdr1* (left-right dynein-rela-

ted 1) expression levels were checked. *dnah9* is a marker for cilia functionality in the KV since its expression is under the control of *foxj1a*, a master regulatory gene for motile cilia production[358]. After comparing control embryos with *tbx5a* DFC-specific morphants by qPCR using *hatn10* as a reference gene, no differences were detected (Figure 5.11 E), suggesting that cilia motility remained unaffected after *tbx5a* knock-down. Therefore, despite the reduction in size of the KV, the functionality of the cilia seems to be preserved after *tbx5a* interference.

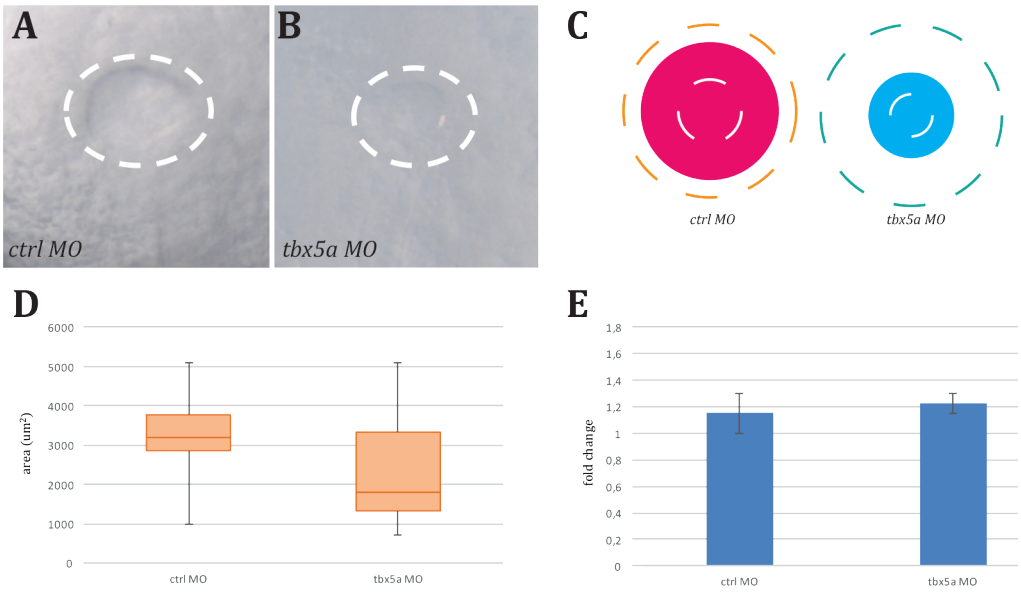

Figure 5.11 | *tbx5a morphants have a smaller KV at 10SS.* *In vivo imaging of the KV at 10SS, which in comparison to ctrl MO injected embryos (A) is smaller in tbx5a MO injected embryos (B). Schematic representation of the KV (C) with its maximum (outer dashed lines), minimum (inner dashed lines) and mean diameter (colour-filled circumference) detected in both control and DFC tbx5a-depleted embryos. Quantification of the KV lumen area variation in control embryos and tbx5a morphants (D). Quantification by qPCR of dnah9 expression in tbx5a morphants compared to control MO injected embryos (E). Error bars in E represent the standard error. Data were analysed by Student's T-test (E). Dashed white lines encircle the KV.*

Migratory defects in DFC could explain the diminishment in KV size since a smaller population of DFC lineage would be contributing to the formation of this structure. To assess this, DFC migration was assessed by examining *sox17* expression during epiboly in the DFC population. When *sox17* was checked in control embryos (Figure 5.12 A) and *tbx5a* morphants (Figure 5.12 B-B'') at 50% epiboly no significant differences were detected (Figure 5.12 C). Control morphants showed subtle defects in their cohesive migration only in 5.88% of the embryos (n = 102), whereas 13.40% (n = 97) of *tbx5a* morphants exhibited defects. After a χ^2 statistical analysis, the differences were found to be non-significant. Thus, since the migratory process seems to be unaltered in *tbx5a* morphants, the fact that these embryos had a smaller KV might be due to a reduced capacity of the inflation of the vesicle or the reported defects of Bmp signalling downregulation alone or together with some other signalling impairments. Finally, in order to visualize the cilia within the KV structure at 10SS, an immunofluorescence against acetylated tubulin was performed, but after analysing 10 cilia per embryo (n = 5 for each condition) the length of the cilia within the KV was found to remain unaffected after *tbx5a* knock-down (Figure 5.12 D, D').

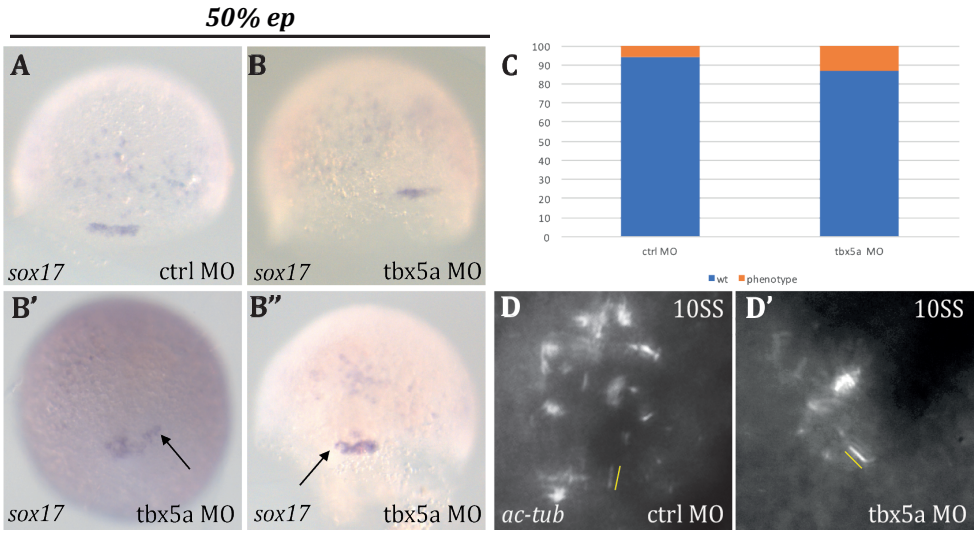

Figure 5.12 | *tbx5a morphants do not show significant DFC migration defects.* *ISH for sox17 at 50% epiboly in control (A) and tbx5a morphant (B-B'') embryos. Quantification of the embryos showing a non-cohesive expression of sox17 (C). A χ^2 statistic has been calculated to assess significant differences between groups. Cilia length in control (D) and tbx5a morphants (D') at 10SS. Images are lateral views with animal to the top (A-B) and ventral views (D-D'). Black arrow points towards mild migratory defects in B'-B''. Yellow lines highlight cilia with the same length in D-D'.*

In summary, the reduction in KV size might be responsible of the creation of a less robust flow within the KV followed by an altered expression of *charon* expression domain around the KV together and a reduction on Bmp signalling levels. The decrease in the Bmp signalling expression levels could be either a direct consequence of *tbx5a* knock-down, as downstream effectors of *tbx5a* (indicated by the putative binding sites) or an indirect effect, as a consequence of lack of a stable directional flow than can be sensed and transmitted by the KV cilia. These defects would trigger the laterality phenotypes observed later in development in the LPM signalling and during the morphogenetic events that resulted in organs that exhibited a LR phenotype when *tbx5a* was knocked-down.

Discussion

1. Consequences on retinal DV patterning after interference with *tbx5a* and *tbx5b* genes function

The MO knock-down approach to assess the function of the *tbx5* paralogues in the developing retina shed some light into their function in the retina by means of the analyses of marker gene expression. The dorsal retina marker *bmp2b* suffers a subtle reduction of its temporal expression domain when either *tbx5a* MO (5ng), *tbx5b* MO (4ng) or both MOs are injected. In addition, the ventral retina marker *vax2* experiences an expansion of its nasal domain especially significant after *tbx5a* knock-down, although a significant expansion is also observed after injection of *tbx5b* MO (4ng) or different combinations of both MOs. These results indicate that retinal identities are affected after interfering with *tbx5* genes. In addition, the results highlight the relevance of *tbx5* paralogues to maintain the dorsal identity in the retina. Indeed, the maintenance of the dorsal identity in this territory is key to acquire a correct retinotectal map and a proper visual function.

Changes in the expression domain of dorsal and ventral retinal markers were further analysed by checking *efnb2a* and *ephb2* expression domains in the dorsal and ventral retina, respectively, which are crucial to ensure DV identity along the retina and the subsequent proper retinotectal projections. The *efnb2a* expression domain is symmetrically shrunk in both dorso-nasal and dorso-temporal borders after both *tbx5* genes were knocked-down. Significant differences are found when single *tbx5a* or *tbx5b* MO injections and their co-injection at high doses are compared, suggesting that these paralogues act redundantly in the dorsal retina to ensure the expression of *efnb2a* in this territory. Remarkably, *efnb2a* expression is never completely abolished after co-injection of both MOs at high doses, indicating that some other factors are acting together with *tbx5* paralogues to maintain dorsal retina identity. Indeed, the other members of Tbx2 subfamily genes are also expressed in the developing retina and functional redundancy between these genes may explain the lack of complete inhibition of the

expression of dorsal retina markers, since Tbx genes have been shown to cooperatively interact in many developmental processes[6,359]. *ephB2* expression in the ventral retina suffers an asymmetric expansion in *tbx5a* and *tbx5b* double morphants. More specifically, the ventro-nasal domain is largely expanded in *tbx5* double morphants while the temporal domain remains unaltered, similar to the control embryos. This DV patterning phenotype was observed both in single *tbx5a* or *tbx5b* MO injection or combined injection of *tbx5a* and *tbx5b* MOs at different increasing doses.

2. Consequences of *tbx5* knock-down on retinotectal projections

The importance of ensuring proper DV patterning in the retina is reflected at 48hpf, when double morphants for *tbx5a* and *tbx5b* display significantly thinner retinotectal projections compared to those of control siblings, which are probably associated with impaired visual function. Related with this observation, *rb1* mutants exhibit a much thinner optic nerve compared to their control siblings and they also present a delay in RGC axonal outgrowth, leading to a delay in optic nerve development and reduced innervations of the optic tectum[360]. Tbx2 has been shown to molecularly interact with Rb1[361]. Hence, it is tempting to hypothesize that, since Tbx5 is closely related to Tbx2, it could likewise be interacting with Rb1 to regulate the normal formation of the optic nerve in zebrafish embryos (Figure 22).

It is relevant to highlight that the homeodomain-containing *meis1* transcription factor has been reported to be involved in the establishment of proper retinotectal map of the developing zebrafish. Similar to tbx5 genes down-regulation, *meis1* knock-down results in a reduction of dorsal *efnb2a* expression in the retina and an expansion of *ephB2* in the ventral domain. *meis1* knock-down has also been associated with *tbx5a* downregulation[136], hence it is plausible that downregulation of *tbx5* (and *tbx5b*) is enough to explain the DV expression defects observed in *meis1* morphants. This

prompts to think of a model in which *meis1* acts upstream of *tbx5* genes to ensure the correct DV expression of *ephrinb2a* and *ephB2* in the zebrafish developing retina (Figure 22).

gdf6a has been described to be necessary and sufficient to activate *tbx5a* and *efnb2a* in the retina and that impaired expression of *gdf6a* results in defects in DV patterning positional information and subsequent formation of the retinotectal map[132]. Therefore, the down-regulation of *tbx5* paralogues could be causing the same phenotype one level downstream of the described effect for *gdf6a* interference (Figure 22).

Finally, *Bmp2* knock-down has been described in chicken to cause altered retinotectal projections[129]. *Bmp2* expression is critical for the maintenance of regional specificity along the DV axis, suggesting that the dorso-temporal reduction of *bmp2b* expression domain after *tbx5* paralogues knock-down could also influence into the retinotectal phenotype observed in *tbx5* double morphant embryos at 48hpf (Figure 22). Additionally, mouse *Vax2* mutants have been described to exhibit impaired DV and NT gradient of *EphB5*, *EphB2*, EphB3, *EphrinB1* and *EphrinB2* axon guidance cues[126]. Therefore, if this signalling mechanism is also conserved in zebrafish, the ventro-nasal expansion of the *vax2* expression domain in the retina after *tbx5* genes knock-down could also contribute to the retinotectal defects observed (Figure 22).

Apart from the speculations suggested by the results of the experiments, it is clear that the observations reported in the eye field indicate that a synergistic effect of *tbx5a* and *tbx5b* is necessary for proper *efnb2a* expression in the dorsal retina. Also, that *efnb2a* expression is not significantly affected in *tbx5a* or *tbx5b* morphants, whereas it is decreased by 50% in double *tbx5a* and *tbx5b* morphants, suggesting these two genes act together to guarantee the proper extent of *efnb2a* expression in this domain.

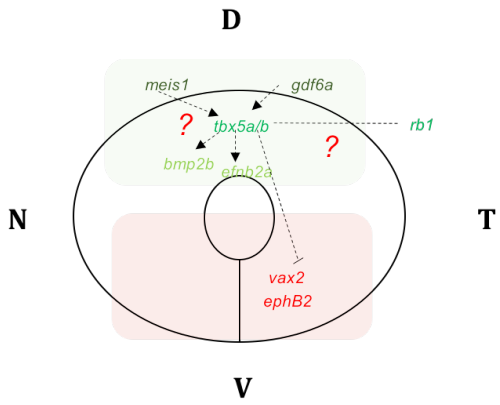

Figure 22 | *Model for tbx5 genes function in the dorsal retina.* *meis1 and gdf6a result in a reduction on efnb2a expression probably through the downregulation of tbx5 genes. Tbx5 genes knock-down by MO injection cause a reduction on bmp2b and efnb2a and an expansion on vax2 and ephB2 expression ventral domains. In the case of efnb2a, only after the knock-down of both paralogues a significant decrease in the expression domain is observed. Tbx5 might be interacting with Rb1 to ensure proper retinotectal projections as it is described in the case of Tbx2. D: dorsal, n: nasal, T: temporal, V: ventral.*

3. Consequences of interfering with *tbx5* genes in the developing pectoral fin

In contrast to the synergistic role for the *tbx5* paralogues identified in the developing retina, pectoral fin development shows different (and specific) requirements for *tbx5a* and *tbx5b*. *tbx5a* is required for the earliest steps of initiation of pectoral fin bud outgrowth (Figure 23 A), whereas *tbx5b* function is related to a later stage ensuring properly timed and sustained fin growth, so that the pectoral fin achieves its final normal size (Figure 23 B). The distinct roles executed by the different *tbx5* paralogues are linked by Fgf signalling, which is key to establish a crosstalk between the mesenchymal and ectodermal territories that secures a positive feedback loop signalling between the two tissues to promote and sustain pectoral fin outgrowth.

The total absence of pectoral fins in *tbx5a* morphants shows the essential role of this paralogue for the compaction of the cells in this territory for the subsequent protru-

sion of the fin bud and formation of this structure. The lack of activation of *fgf24* by *tbx5a* in the mesenchyme impedes the pectoral fin development programme to initiate. By contrast, *tbx5b* knock-down results in the formation of shorter fins compared to the control embryos. The mechanism that explains the *tbx5b* morphants phenotype is the delayed achievement of a threshold in the Fgf signalling feedback between the mesenchyme and the ectoderm, as shown by the expression pattern of several Fgf signalling members at different stages during the development of the pectoral fin (Figure 23 B).

Given the critical requirement of *tbx5a* to establish the pectoral fin bud outgrowth initiation programme, it is not clear whether *tbx5a* may function, similarly to *tbx5b*, during these later stages of fin outgrowth. It is tempting to speculate that this is indeed the case, because as mentioned before, the subtle downregulation of *tbx5a* function or its target genes is reminiscent of the *tbx5b* loss-of-function shown here[144,179,332]. Nevertheless, Parrie and colleagues showed that the phenotype of *tbx5b* morphants could not be rescued by injection of *tbx5a* mRNA[88]. Injection of *tbx5a* mRNA into *tbx5b* morphants made the fin phenotype more severe and most embryos failed to even initiate pectoral fins. However, since *tbx5* doses are extremely critical to ensure to correct development of the structures where they are expressed an "overexpression" could also result in defects in the pectoral fins, which could explain the lack of rescue of the *tbx5b* morphants. To decipher which is the case, different doses of *tbx5a* mRNA should be injected in a *tbx5b* morphant background to see whether there exist any conditions that allow to significantly rescue the fin outgrowth phenotype.

Related to forelimb outgrowth, it is worth mentioning that experiments with mice that carry a tamoxifen-inducible allele for *Tbx5* show that, although *Tbx5* is essential for initiation of the forelimb and its misexpression results in limb truncation, the requirement of this transcription factor is restricted to a specific time frame[362]. Hence two

distinct phases of limb development are defined, equivalent to the ones defined in our model for pectoral fin outgrowth. The first one would be the *Tbx5*-dependent limb initiation phase, which would be followed by the subsequent limb outgrowth phase, which is *Tbx5*-independent. In this second phase the Fgf feedback loop between the mesenchyme and ectoderm is already established and, in contrast to what is observed in zebrafish, it does not rely on the expression of *tbx5* to maintain the signalling between the two structures[362].

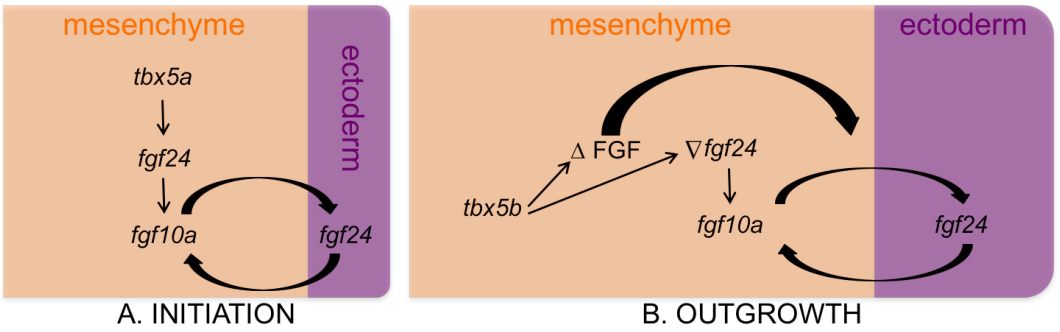

Figure 23 | *Model for the differential requirements for the tbx5 genes during pectoral fin development.* *tbx5a is required for the initiation process (A), while tbx5b is essential to maintain the outgrowth of the structure (B).*

4. Consequences of *tbx5* genes knock-down in the asymmetric development of the zebrafish heart

Cardiac looping is affected in both *tbx5a* and *tbx5b* morphants, and downregulation of both *tbx5* genes does not increase the severity of the looping phenotype, indicating the essential function of these genes to achieve the complete looping of the zebrafish heart. Moreover, both genes must act in the same pathway and cooperate with each other to ensure looping morphogenesis, since co-injection of sub-optimal concentrations of *tbx5a* and *tbx5b* MOs similarly causes looping phenotypes and increasing con-

centrations of both MOs result in an increase in the percentage of embryos with a laterality phenotype. Regarding the first cardiac asymmetric event, both paralogues are also essential for normal leftward heart tube jogging to occur, since *tbx5a* and *tbx5b* morphants show jogging orientation defects and co-inhibition of both genes does not result in either more severe or higher phenotypic penetrance.

Despite this is a quite unexpected phenotype for a gene that is bilaterally expressed in the LPM, laterality defects have been previously described after interference of other genes expressed symmetrically along the LR axis (e.g. *fli-1*, *rtk-2*). Furthermore, these results are in conflict with the cardiac phenotypes described in previous publications where the *hst* mutant and/or *tbx5a* MO were used to interfere with *tbx5a* gene function and *tbx5b* MO to knock-down *tbx5b* paralogue[87,88].

5. The *hst* phenotype differs from the *tbx5* knock-down phenotype

The *hst* mutant was originally described as having a severe cardiac dysfunction due to *tbx5* premature termination at aminoacid 316. The characteristic phenotype consists in failure of cardiac looping completion, cardiac edema with a central linear heart (string-like) and a slow heart rate[87]. In addition, in *tbx5b* morphants Parrie and colleagues only reported its inability to completely loop[88].

Our rescue experiments for *tbx5a* MO injected embryos show that the *hst* form of *tbx5a* is an hypomorph that is able to partially rescue the phenotype caused after *tbx5a* MO injection. Related to the controversy generated by the different phenotypes observed after different approaches for *tbx5* paralogues knock-down, two new CRISPR mutants for *tbx5a* have been recently reported[366]. Both mutants exhibit *tbx5a* frameshift alleles in the first coding exon: *tbx5a* c.21_25del (*tbx5a*Δ5) and *tbx5a* c.22_31del (*tbx5a*Δ10). Interestingly homozygous and transheterozygous combinations of these alleles result

in loss of pectoral fins and cardiac defects. However, these frameshift mutants do not exhibit the characteristic stretched *hst* heart phenotype. An evident difference between the two types of mutants is the location of the mutation that in the case of the *hst*, is an ENU-induced stop codon in the second-last coding exon, hence being able to translate into a C-terminally truncated protein with residual or dominant-negative activity compared to the CRISPR mutants obtained in this study that contain the mutation in the first exon. These CRISPR mutants exhibit fully penetrant cardiac defects in homozygous and trans-heterozygous mutants that range from inflow tract defects to mis-looped chamber, but never an *hst* heart phenotype.

All this variability in the cardiac phenotype after interfering with *tbx5* paralogues is of critical importance since the high sensitivity of *tbx5* dosage might be greatly influencing the different phenotypes reported under different conditions. It is also important to consider whether activation of a compensatory network to buffer against deleterious mutations influences the final phenotype, which normally does not occur after translational or transcriptional knockdown[367]. It is therefore extremely important to consider recent publications related to the use of MOs as a knock-down strategy that recommend extreme caution when analysing mutant and morphant phenotypes[71,367]. The phenotypes induced by MO are often more severe than those obtained with the equivalent mutant, probably due to phenotypic rescue of zygotic mutants by maternally provided wild-type mRNAs, which translation can be inhibited by MOs, the hypomorphic nature of the mutant allele or the genetic compensation in the mutant conditions but not in the morphant animals. Also, MO could exhibit a stronger phenotype due to off-target effects of the MO[367].

Hence, in all the experiments performed with *tbx5* MOs, they were co-injected with *p53* MO to avoid unspecific phenotypes that do not present any link to the real phenotype caused by the reduction of the endogenous levels of the target gene. Finally, in

the case of the existence of different paralogues that share their expression pattern in different developing tissues, like the *tbx5* paralogues, it is important to test functional compensation by co-injection of MOs that simultaneously knock-down both genes and analyse the phenotype obtained at different injection doses. Similarly, using this strategy it can be demonstrated genetic interaction between the paralogous genes by knockdown of both genes at subthreshold levels[368].

6. Consequences of *tbx5a* knock-down for cardiomyocyte medial migration

The early defects during the migration of myocardial precursors in the anterior LPM are only detected after *tbx5a* MO knock-down or when co-injected with *tbx5b* MO (3ng each). The fact that not only randomization of the asymmetric events of the heart, but also defects in the migration of the cardiac precursors towards the midline are found, indicates that *tbx5* may be regulating migratory cues. Nevertheless, it is striking that in the case of the midline fusion defects to form the cardiac cone the phenotype only arises after *tbx5a* MO injection or when both paralogues are knocked-down at high doses (3ng each). Hence, the results suggest a role for *tbx5a* during the medial migration of the cardiac towards the midline, while *tbx5b* would only have a minor role that fails to rescue *tbx5a* when both paralogues are knocked-down in the double morphants.

Interestingly, the LR cardiac determinant *Bmp4*, have been isolated in screens that aimed to find *Tbx5*-induced genes[363]. Bmp signalling to the endocardium non-autonomously decreases myocardial migration rates on the right and potentially tempers Nodal-induced increases in velocity on the left, therefore leading to the anterior and left positioning of the atrial cells with respect to the ventricular cells[211]. Hence, *tbx5* knock-down could be affecting Bmp signalling in the LPM leading to migration defects.

In addition, the posterior fusion defect in the cardiac cone formation resembles to the phenotype obtained after *snail1b* MO knock-down. Both *snail1a* and *snail1b* paralogues have been described to be implicated in the anterior migration of axial mesoderm[71,365-367] and *snail1b* has been shown to have a key role in the migration of cardiac precursors. *snail1b* morphants have a delay in the migration towards the midline and defects in the myocardial fusion. The phenotype observed in *snail1b* morphants is not surprising, since *snail* genes are known to regulate cell adhesion and migration. In addition, at 48hpf *snail1b* morphants result in a string-like heart[365], so it is tempting to speculate that both genes (*i.e. tbx5a* and *snailb*) may be related to secure the correct migration towards the midline during cardiac morphogenesis to ensure the final correct positioning of the looped heart.

7. Consequences of *tbx5a* knock-down on the expression of left-side LPM markers.

As evidenced by the randomization of all three Nodal-related genes analysed, *spaw* and its downstream effectors and inhibitors *letfy1* and *lefty2*, LR asymmetry is already altered before the morphogenetic migratory events that take place during cardiac development (Figure 24 B).

Regarding the randomization of the expression of *spaw*, *lefty1*, *lefty2*, there are several aspects to consider. First of all, the maintenance of the *lefty1* expression in the midline that indicates that the physical and genetic barrier which impedes signalling cues to diffuse from one side of the embryo to the other is preserved. Otherwise, only total absence or a bilateral expression pattern for *spaw* and *lefty1/2* would be observed in the LPM. This suggests that laterality establishment is impaired earlier in development, at the KV level or on its vicinity or, alternatively, that the expression pattern in the LPM for these genes results altered after interfering with *tbx5a* because this

genes has a buffering role in the LPM as described in mice. Interference with *Tbx5* in mice shows the inherent LR asymmetry in the formation of the forelimbs, since after *Tbx5* knock-down the left limb is more severely affected than the right[54]. Similarly, another possibility could be that *tbx5a* would be buffering some signalling molecules that ensure the correct consecution of all the asymmetric events that occur during cardiac morphogenesis. In addition, the fact that the randomized expression for *spaw* was also observed at 16SS indicates that this phenotype in the LPM is evident in early somitogenesis stages. It is also interesting to note that when *spaw* expression pattern is compared in both stages (*i.e.* 16SS and 21SS) in the LPM of *tbx5a* morphants, despite showing a similar penetrance of embryos exhibiting a LR phenotype, the proportion of the embryos displaying expression in the right side, bilaterally or lack *spaw* expression in the LPM varies. Curiously, the proportion of embryos exhibiting total absence of *spaw* signal decreases at 21SS. A suitable explanation would be that the onset of Nodal-related genes in the LPM is delayed in *tbx5a* morphants and consequently, embryos lacking expression are later classified as left, right or bilateral expression.

8. Consequences of *tbx5a* knock-down in neural and visceral LR asymmetry

The analysis of LR asymmetry defects during the development of other structures such as the laterality of the neural structure of the diencephalon and the positioning of the visceral organs of the liver and pancreas with respect to the gut resulted in some striking results.

The expression and involvement of Nodal signalling pathway in the establishment of LR asymmetry in the neural structure of the dorsal diencephalon has been extensively reported. This fact prompted us to test the laterality of *lefty1* expressed in this structure which was shown to be randomized. Multiple mutations in zebrafish have been reported to interfere with LR patterning in the diencephalon. Among the mutated ge-

nes, there are some members of the Nodal signalling pathway (*i.e.* *oep*, *cyc*). Nevertheless, interference with genes involved in the laterality of the dorsal diencephalon results in the majority of the cases with bilateral or absent expression of the asymmetric markers expressed in the left diencephalon in wildtype conditions (e.g. *lefty1*, *cyc*, *pitx2*)[317,369]. These altered expression is probably due to midline ablation and therefore expression results in either absent or bilateral, depending on the gene mutated. In the case of *tbx5a* knock-down, there is a total randomization with cases of left, right, bilateral and lack of expression. Within the Nodal-related genes, *charon* morphants show a total randomized *lefty1* expression in the dorsal diencephalon that coincides with the observed phenotype in *tbx5a* morphants. However, in the case of *charon*, this randomized expression does not occur in the LPM, since it is rare to find *spaw* or *lefty1* expression totally absent[309]. Hence, it is probable that *charon* could not fully explain the phenotype observed after *tbx5a* knock-down.

In the case of visceral laterality, despite the frequency of embryos with a phenotype is lower than in the other two structures where laterality was analysed, the penetrance is significant enough to consider that *tbx5a* knock-down also affects the positioning of the visceral organs. In this case, within the variety of presence and location of the liver and pancreas organs, the most prevalent phenotype is the absence of both structures. Since the positioning of these endodermal organs is also impaired, all three types of laterality analysed are found to be affected after *tbx5a* interference (*i.e.* cardiac, neural and visceral), suggesting that the signalling defects after *tbx5a* knock-down arise much earlier, affecting the establishment of LR asymmetry in the embryo during early stages of embryonic development so that the knock-down of *tbx5a* results in impaired organogenesis of all the analysed structures and organs.

9. Consequences of *tbx5a* knock-down in the DFC lineage

The phenotype detected in the asymmetric event of the jogging during heart morphogenesis demonstrates that targeting the DFCs lineage is sufficient to obtain the LR asymmetry phenotypes. The phenotypes that DFC-targeted morphants exhibited were more severe than in 1-cell stage injected embryos with cases of *cardia bifida* and other defects in fusion. This apparent paradox could be explained by the fact that the same dose of MO is injected in a much-reduced cell population, thus causing a stronger phenotype in the morphant embryos. In addition, *tbx5a* knock-down LR asymmetry defects that arise after only targeting the DFCs lineage support the hypothesis of an early role for *tbx5a* during LR establishment. The fact that LR asymmetry is affected when the DFCs cells are targeted indicate that *tbx5a* is indeed expressed in these cells that will eventually form the KV, which has not been previously reported. To confirm this finding, RT-PCR experiments from early developmental stages embryos were performed.

10. *tbx5a* is expressed during early zebrafish development

An early expression from *tbx5a* at shield and 1SS is coherent with the specific phenotype found when the injection of *tbx5a* MO was done only targeting the DFCs. Hence, the design of the probe is crucial to detect faint expression levels. It is also relevant to highlight the expression around the KV at 10SS for *tbx5a*, which could be important for the transmission of the signalling cues generated in the KV to the surrounding tissue. The analysis of numerous markers within the KV or on its vicinity revealed some interesting changes in the expression patterns and levels of the genes of interest. Remarkably, the characteristic expression of the Nodal inhibitor gene *charon* gets altered after *tbx5a* knock-down, probably leading to a reduction on the solidity of the establishment of LR asymmetry and therefore to the randomization of the left-side mar-

kers in the LPM. Furthermore, *bmp4* levels surrounding the KV result diminished after interfering with *tbx5a* (Figure 5.3), whereas the genes belonging to the Fgf signalling pathway or the any of the rest of the genes analysed remain unaffected. Interestingly, *ntl* and *lefty1* expression in the midline are unaltered which means that signalling cues are not able to leak from one side to the other in *tbx5a* morphants. The preservation of the midline expression of both genes is consistent with the subsequent total randomization of the Nodal-related genes in the LPM, since as previously mentioned, the perturbation of the integrity of this structure would result in either total absence or bilateral expression of these markers.

The Nodal signalling pathway members *spaw*, *pitx2* and *gdf3* did not show significant expression differences at 10SS. In addition, as already mentioned, *pitx2* mutants do not result in LR asymmetry phenotypes in zebrafish. The zebrafish *pitx2*HD mutants, which present indel mutations in the homeodomain - predicted to prevent DNA binding and disrupt both isoforms (*pitx2a* and *pitx2c*) - exhibit eye and tooth defects, characteristic of Axenfeld-Rieger Syndrome, but heart and gut looping remain unaffected[278]. However, it should be considered that it is not rare that in mutants other compensatory mechanisms (*i.e*. genetic compensation) rescue the lack of the disrupted gene resulting in a milder phenotype than in knock-down approaches. Regarding *gdf3* expression, it has been recently published that zygotic contribution of this gene does not result in LR asymmetry defects[370-372]. Despite being expressed in domains of critical importance for LR asymmetry establishment, *i.e*. KV area and LPM, Z*gdf3* mutants exhibit no LR defects. Consequently, zygotic Gdf3 is described as not required for LR patterning in the presence of maternal Gdf3 and therefore, the zygotic contribution only results in an increase of robustness of the system[370-372]. Consequently, even if *pitx2* or *gdf3* were affected they could not explain the LR phenotypes obtained after *tbx5a* knock-down.

11. Bmp signalling is downregulated after *tbx5a* DFC-specific knock-down

The lack of consequences in the expression of the Fgf ligands, which have been related to *tbx5a* in other structures (e.g. *fgf10* and *fgf24* in the pectoral fin) and/ or related to LR asymmetry e.g. *fgf4* and *fgf8*, together with the absence in phenotype in some other promising genes like *prrx1a*, which shows an asymmetric expression in the LPM later in development, prompted to perform some qPCRs. The use of two different reference genes *ef1a* and *hatn10* make the results obtained by qPCR more reliable, especially since *hatn10* gene has been described to be a very solid reference gene. Indeed, the expression stability of *hatn10*, together with two other EREs, *dna15ta1* and *loopern4*, has been found to be better than the common reference genes (e.g. *gapdh* or *ß-actin2*)[348].

qPCR results confirm that Fgf signalling pathway members remain unaltered after *tbx5a* knock-down, whereas many Bmp signalling members show a significant down-regulation. Together with *fgf4*, *fgf8*, *fgf10a* and *fgfr2*, *cx43.4*, *prrx1a* and *spaw* are not found to significantly change their expression levels after *tbx5a* DFC-targeted knock-down. The lack of detection of differences in the transcription levels of the aforementioned genes could be explained by two main reasons. The most straight-forward would be that, regardless many of these genes have been described to be linked to *tbx5* in other developmental stages and tissues, they are not related at this developmental stage. Another explanation could be that regardless these genes could be suffering an up- or downregulation after interfering with *tbx5a* its effect could be masked, since the injection confined to the DFC lineage might only cause a slight variation that cannot be detected as significant when analysing the expression levels in whole embryos. Nevertheless, it was considered that it is more accurate to perform a DFC-targeted injection followed by an RNA extraction of the whole embryos at 10SS, rather than a full injection and dissecting the posterior part of the embryo, since the extracted part might not be totally equal in all embryos and, in addition, since a high number of em-

bryos is required to obtain enough genetic material, between the cut and collection of the dissected embryos some necrotic events could already be triggered, also creating some differences in the conditions in which the embryos are collected. Therefore, despite the technique used for RNA extraction to subsequently determine changes in the expression levels by qPCR could be missing some minor changes, the method was considered the most thorough approach to treat the samples homogenously and avoid differences in the groups compared.

Since the most promising signalling pathway to be acting downstream of *tbx5a* according to both ISH and qPCR results was Bmp, the regulatory regions of the Bmp signalling members assessed here were analysed. Despite all of them contained a putative Tbx5 binding site, the particular case of *bmp4* is the most remarkable since the binding site could be detected in higher vertebrates, including human . In addition, when the *bmp4* regulatory region was further analysed, the putative binding site was found to be within its proximal regulatory region. However, some controversy exists regarding the role for *bmp4* in LR asymmetry. *bmp4* MO experiments identified *bmp4* as presumably responsible for the inhibition of *spaw* in the right LPM at the early segmentation stage and hence of controlling both visceral and cardiac LR asymmetry[210]. The phenotype observed in MZ*bmp4*^{Y180*} mutants suggests that *bmp4* would be limiting the responsiveness of LPM cells to nodal signals, setting a threshold for Nodal signalling pathway activation in the LPM that could not be surpassed by low concentrations of Spaw[272]. Nevertheless, organ laterality is properly established in most of this MZ mutants (89%) and *spaw* expression is initiated and maintained correctly in the majority of these embryos. Therefore, Lenhart and colleagues suggest that *bmp4* is not necessary for *lefty1* expression at the midline and that *bmp4* is not the main ligand required for posterior repression[272]. Alternatively, they suggest that *bmp2b* could be the Bmp ligand responsible for mediating this inhibition, since it is highly expressed in the ventral mesoderm and epidermis posterior to the KV[373]. Interestingly, *bmp2b*

was also found downregulated in our qPCR analysis and a putative binding site for Tbx5 was found in its regulatory region conserved also in higher vertebrates, since it was also found in mouse. In addition, it has been described that *bmp2b* overexpression abolishes *spaw* expression in the LPM[210]. Unfortunately, although some overexpression experiments have been carried out using the *tg(hs:bmp2b)* line, specific approaches that enable spatiotemporal inhibition of this ligand should still be developed, since loss of *bmp2b* causes strong DV patterning defects. *bmp2b* mutants have an important disruption of ventral posterior tissue formation that results in embryo lethality before 10SS[374], impeding the study of further phenotypes during zebrafish development. Yet, despite 1-cell stage MO injection against *bmp2b* or *bmp7* results in profound DV patterning defects, it has been described that MO injection against *bmp2b* or *bmp7* has no effect on *spaw* expression when injected at 512-cell stage, that specifically targets the DFC/KV lineage[210]. In contrast, DFC-targeted injection of *bmp4* MO causes bilateral expression of *spaw*.

Considering all the data mentioned above, a plausible explanation that would reconcile all these observations is that, although *bmp4* could have a relevant role in transmitting LR information to the LPM, the MZ phenotype of *bmp4* mutants could be compensated by other members of the bmp signalling pathway, whose promiscuity has been extensively described[375-376]. Thus, the phenotype would be rescued, showing a milder effect on LR asymmetry establishment. With respect to our qPCR results, it is clear that many Bmp signalling ligands and receptors suffer a significant decrease on their transcriptional levels. Nonetheless, *tbx5a* does not completely abolish Bmp signalling in the tissue surrounding the KV structure. However, the sole fact of a reduction on the expression levels of Bmp cascade could be sufficient to resolve in a decrease on the robustness of Nodal signalling pathway activation, as shown by an altered typical horse-shoe *charon* expression in a significant percentage of *tbx5a* morphants (Figure 5.6 C). Indeed, it is feasible that this reduction in Bmp signalling consequently leads to

a bistable system where any additional subtle signalling change could eventually lead to the activation or repression of Nodal signalling pathway in one or both sides of the embryo (Figure 24 B).

It is important to keep in mind that the midline was not depleted of *lefty1* expression in *tbx5a* morphants, meaning that this barrier has always been present despite the reduction on Bmp signalling. This enforces to think that the reason why we observe that the randomization of the expression of Nodal signalling pathway members is probably due to a decrease on the solidity of the activation of the Nodal signalling pathway and not due to a leakage from signalling cues from left to right or viceversa in the embryo. Regarding the Bmp signalling receptors found downregulated in DFC-targeted morphants, *bmpr1* receptors (*bmpr1aa* and *bmpr1ab)* are known to be required to regulate *lefty1* expression in the midline [378]. Nevertheless, the *bmpr1aa* paralogue, whose transcriptional levels have not been significantly altered in our analysis, has been reported to affect phenotypic severity more robustly than loss of *bmpr1ab*[378]. Expression levels expression of *bmpr1ba* and *bmpr1bb* have also been found downregulated by qPCR in *tbx5a* DFC-targeted morphants. In this case, there is no literature describing an early role for these genes related to LR asymmetry. Finally, despite *bmpr2* receptors (*i.e*. *bmpr2a* and *bmpr2b*) have also been related to LR asymmetry in zebrafish[379], we did not detect significant expression levels. In addition, in all these members of the Bmp signalling pathway a putative binding site for Tbx5 was found, but it was not detected as conserved in higher vertebrates, which diminishes the probability that these putative binding sites are indeed biologically functional and the possibility that these genes are downstream effectors of *tbx5a*.

12. *tbx5a* knock-down results in altered KV parameters

Some of the features of the KV appear to be affected to some extent in *tbx5a* morphants. Despite migration of the DFCs seemed unaffected by *tbx5a* knock-down, the KV was smaller. The fact no defects observed in the expression pattern of ephrins (*efnb2a* and *ephb4b*) and *cx43.4*, analysed by qPCR, which are important for collective migration in a cohesive manner, is consistent with the unaffected *sox17* expression during epiboly, which indicates no significant defects in the migration of the DFCs. The reduction in size of the KV in *tbx5a* morphants could be due to a reduced ability to lumen inflation within the vesicle, which has been previously described to be triggering LR defects since it impedes to reach a directional stable fluid flow[271,381,382]. The variability existing between different strains and within individuals of the same strain in wildtype conditions is also quite remarkable, but, in any case, a threshold of 1300μm^2 should be surpassed to ensure the correct signalling transmission to the KV neighbouring tissue and subsequently to the LPM. On the contrary, *spaw* expression in the LPM results randomized and consequently it results in LR asymmetry defects.

Finally, the functionality of the cilia is thought to be unaffected, since the expression levels of *dnah9* were not altered after DFC-targeted *tbx5a* knockdown, as shown by qPCR, tempting the suggestion that cilia motility is not impaired after *tbx5a* knock-down. As previously mentioned, *dnah9* lies under the regulation of *foxj1a*, a master regulator of cilia motility. Interestingly, *dnah9* expression has been found to be remain unaffected after DFC-targeted *bmp4* MO injection[210]. Nevertheless, to assess whether cilia motility is really affected in the *tbx5a* morphants live imaging experiments of the beating cilia should be performed. Finally, cilia length in the KV has been observed to remain unaltered in *tbx5a* morphants. Nonetheless, the number of cilia present in the KV should also be assessed, since the reduction on cilia number could also lead to the inability to reach a solid directional flow within the KV.

Hence, the mechanism that triggers LR asymmetry defects in the neural, cardiac and visceral structures seems to be driven by a diminished robustness of the directional fluid flow due to a reduction of the KV area followed by an altered expression of charon expression domain around the KV and a reduction on Bmp signalling levels (Figure 24 A). The decrease in the Bmp signalling expression levels could be either a direct consequence of *tbx5a* knock-down, as a downstream effectors of *tbx5a* (indicated by the putative binding sites found in the *bmp4* regulatory region) or an indirect effect, as a consequence of lack of a stable directional flow than can be sensed and transmitted by the KV cilia. These defects would trigger the laterality phenotypes observed later in development in the LPM signalling due to a randomized Nodal signalling pathway activation (Figure 24 B) and during the morphogenetic events that resulted in organs that exhibited a LR phenotype when *tbx5a* was knocked-down (Figure 24 C).

tbx5a does not seem to have a specific role in establishing polarity along LR axis, but nonetheless ensures the robustness of the subsequent critical signalling cues that lead towards a correct signalling in the LPM and proper organ positioning. These observations are also in tune with a recent publication that identifies *Tbx5* in mouse as a buffering factor of the inherent LR asymmetries that secures symmetric limb formation[54].

Further studies are needed to demonstrate the physical interaction of *tbx5a* with the regulatory region of Bmp factors to demonstrate that the action of *tbx5a* transcription factor is directly regulating these genes to ensure LR asymmetric expression. Nevertheless, the aforementioned results point towards this possibility.

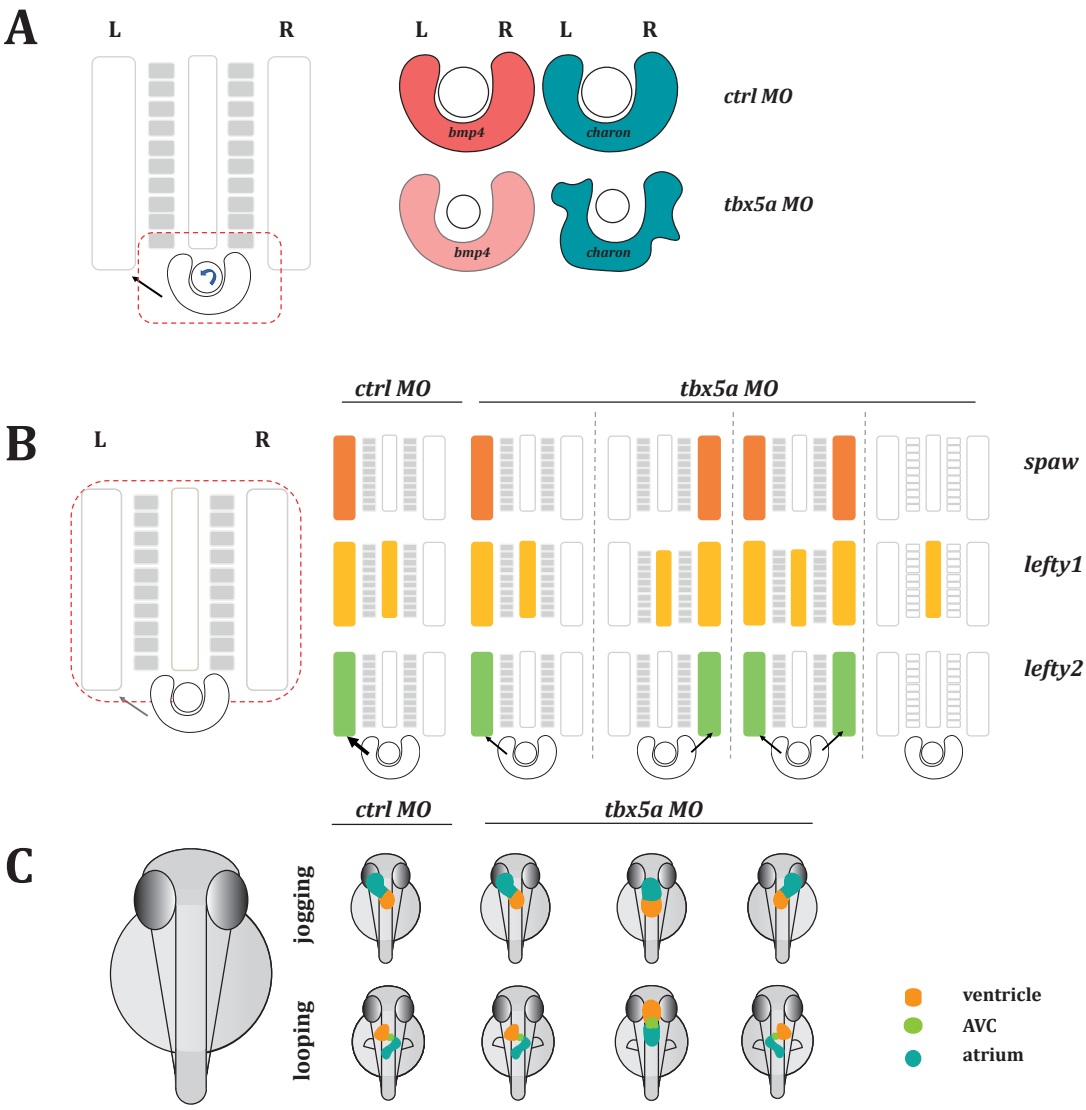

Figure 24 | *General model for tbx5a role in LR asymmetry.* *During the phase in which a directional flow is created in the KV and transmitted to the surrounding tissue (A) tbx5a knock-down results in a reduction on the KV size, a reduction on Bmp signalling around the KV as well as an altered shape of charon expression pattern. All this will result in an inefficient transmission of LR cues to the LPM, and consequently a randomization of the left-side markers spaw, lefty1 and lefty2 (B). Altogether, the cumulative defects in LR patterning results in a randomization of the cardiac asymmetric events of the jogging and lopping (C) and also the laterality of the diencephalon and liver and pancreas are affected.*

13. Final remarks: the different relationship between the *tbx5* paralogues during the development of the retina, pectoral fin and heart

tbx5 paralogues have been demonstrated to be required for the development of different organs in the zebrafish embryo. Nonetheless, their role and relationship on each of the territories where they are expressed varies. It has been shown that in the dorsal retina both paralogues ensure dorsal identity and only when both paralogues are knocked-down a significant reduction on the expression domain of the dorsal marker *efnb2a* in the retina can be observed. In contrast, when only one of the genes is targeted, in the case of *bmp2b* a significant decrease in the expression domain is observed, whereas in the case of *efnb2a* the other paralogue is able to rescue its reduction on its expression. This indicates that for *efnb2a* expression *tbx5* paralogues have redundant roles in the dorsal identity maintenance probably to ensure the subsequent correct retinotectal projections, which are essential to acquire proper visual function (Figure 25). The case of the pectoral fin is quite different, since *tbx5a* function is early required for the initiation of fin bud outgrowth, whereas *tbx5b* is only required later to keep a sustained outgrowth of the structure (Figure 25). In the case of the heart, despite both genes have been shown to result in the same phenotype, indicating that they must be collaborating and acting in the same pathway, *tbx5a* seems to have an earlier role since *tbx5b* morphants do not show defects in the directional migration towards the midline, or at least *tbx5b* shows a more significant role during zebrafish embryonic development in the jogging and looping events, whereas its contribution in earlier stages at the LPM is minor (Figure 25). In any case, the laterality phenotypes in the heart together with the neural and visceral laterality after *tbx5a* knock-down have their origin much earlier in development.

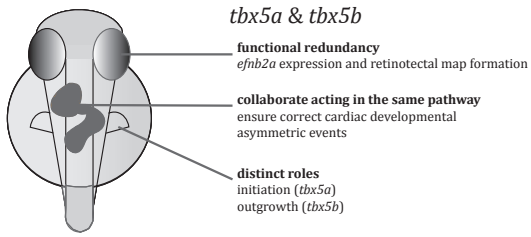

Figure 25 | *tbx5a and tbx5b paralogues maintain different relationships during retina, heart and pectoral fin development.* *Schematic representation of a zebrafish embryo at 48hpf shows the distinct roles and relationships of the tbx5 paralogues during zebrafish development on each tissue where they are co-expressed.*

Conclusions

The main conclusions of this Doctoral Thesis are:

1. The zebrafish *tbx5* genes have essential roles in the different organs where they are expressed (*i.e.* retina, heart and pectoral fin), but the relationship between the two paralogues and their specific requirement differs in every tissue where these genes are expressed.

2. *tbx5* paralogues are required for correct DV patterning of the retina. Knock-down of both paralogues (*tbx5a* and *tbx5b*) cause a significant reduction of dorsal identity markers expression concomitant with an expansion of ventral markers expression domain, especially significant in the ventro-nasal domain of the retina.

2.1. Functional redundancy of *tbx5* paralogues in the retina only results in a significant downregulation of *efnb2a* expression in double morphants. Dorsal identity is never completely abolished, since other members of Tbx2 subfamily, co-expressed in this domain, may impede complete downregulation of dorsal retina markers.

2.2. *tbx5* double morphants have thinner retinotectal projections at 48hpf, probably reflecting the loss of proper DV patterning in the retina.

3. Pectoral fin development has different requirements for each *tbx5* paralogue: *tbx5a* is early required for the initiation of pectoral fin outgrowth, whereas *tbx5b* is required later for the sustained and timely outgrowth of the pectoral fin.

3.1. Lack of *tbx5a* results in a failure of compaction of the mesenchymal tissue and Fgf factors are never activated in the mesenchyme, whilst *tbx5b* morphants show a delay on activation of Fgf signalling in the overlying ectoderm and downregulation of *fgf24* expression in the mesenchyme. Accordingly, *tbx5a* morphants completely lack pectoral fins, whereas *tbx5b* morphants have smaller pectoral fins compared to control siblings.

4. *tbx5* genes act in the same pathway during heart morphogenesis. Both genes cooperate ensuring jogging and looping asymmetric events.

4.1. *tbx5a* and/or *tbx5b* knock-down result in a randomized jogging (left-, mid-, right-jogging) and looping (D-, L-, no-loop) events.
4.2. The *hst* mutation behaves as an hypomorphic allele with regard to cardiac LR asymmetric development.
4.3.*tbx5a* knock-down results in migration and fusion defects of the rostral LPM population towards the midline.

5. The expression of left-sided LPM markers from the Nodal signalling pathway (spaw, lefty1 and lefty2) is randomized (left, right, bilateral, absent expression) after tbx5a knock-down.

5.1. Diencephalic *lefty1* expression is randomized after *tbx5a* knock-down, indicating laterality defects.
5.2. The visceral position of the liver and pancreas is altered after *tbx5a* knock-down.

6. A specific LR phenotype arises from affecting *tbx5a* function in the cellular lineage that gives rise to the KV.

6.1. *tbx5a* MO DFC-targeted injection results in randomized jogging.
6.2. Cardiac jogging defects in DFC-targeted morphants are more severe than 1-cell stage injected embryos.
6.3. *tbx5a* MO yolk-targeted injection does not result in laterality defects.

7. Early expression of *tbx5a* in zebrafish development is required for the correct establishment of LR patterning

7.1.*tbx5a* is expressed at shield and 1S stages, earlier than what had been previously described in zebrafish embryos.

7.2. *bmp4* expression levels and charon characteristic expression pattern around the KV at 10SS are altered after *tbx5a* knock-down.

7.3. Bmp signalling at 10SS is down-regulated after *tbx5a* DFC-targeted injection.

7.4. The genomic regions of *bmpr1aa*, *bmpr1ab*, *bmpr1ba*, *bmpr1bb*, *bmpr2a*, *bmpr2b*, *bmp2b* and *bmp4* contain a predicted binding site for Tbx5. This site is conserved in higher vertebrates for *bmp2b* and *bmp4*.

7.5. *tbx5a* knock-down results in a reduced KV area at 10SS.

References

1. Chapman, D. L. et al. Expression of the T-box family genes, Tbx1-Tbx5, during early mouse development. Dev. Dyn. 206, 379–390 (1996).

2. Papaioannou, V. E. The T-box gene family: emerging roles in development, stem cells and cancer. Development 141, 3819–3833 (2014).

3. Conlon, F. L., Sedgwick, S. G., Weston, K. M. & Smith, J. C. Inhibition of Xbra transcription activation causes defects in mesodermal patterning and reveals autoregulation of Xbra in dorsal mesoderm. Development 122, 2427–2435 (1996).

4. Kispert, A., Koschorz, B. & Herrmann, B. G. The T protein encoded by Brachyury is a tissue-specific transcription factor. EMBO J. 14, 4763–4772 (1995).

5. Agulnik, S. I. et al. Evolution of mouse T-box genes by tandem duplication and cluster dispersion. Genetics 144, 249–254 (1996).

6. Naiche, L. A., Harrelson, Z., Kelly, R. G. & Papaioannou, V. E. T-Box Genes in Vertebrate Development. Annu. Rev. Genet. 39, 219–239 (2005).

7. Wilson, V. & Conlon, F. L. The T-box family. Genome Biol. 3, 3008.1-3008.7 (2002).

8. Sebé-Pedrós, A. et al. Early evolution of the T-box transcription factor family. Proc. Natl. Acad. Sci. U. S. A. 110, 16050–16055 (2013).

9. Merscher, S. et al. TBX1 is responsible for cardiovascular defects in velo-cardio-facial/DiGeorge syndrome. Cell 104, 619–629 (2001).

10. Jerome, L. A. & Papaioannou, V. E. DiGeorge syndrome phenotype in mice mutant for the T-box gene, Tbx1. Nat. Genet. 27, 286–91 (2001).

11. Liu, J. et al. Tbx19, a tissue-selective regulator of POMC gene expression. Proc. Natl. Acad. Sci. U. S. A. 98, 8674–8679 (2001).

12. Lamolet, B. et al. A pituitary cell-restricted T box factor, Tpit, activates POMC transcription in cooperation with Pitx homeoproteins. Cell 104, 849–859 (2001).

13. Chang, F. et al. The role of T-box genes in the tumorigenesis and progression of cancer (Review). Oncol. Lett. 12, 4305–4311 (2016).

14. Bertolessi, M., Linta, L., Seufferlein, T., Kleger, A. & Liebau, S. A Fresh Look on T-Box Factor Action in Early Embryogenesis (T-Box Factors in Early Development). Stem Cells Dev. 24, 1833–1851 (2015).

15. Zhu, T. et al. T-box family of transcription factor-TBX5, insights in development and disease. Am. J. Transl. Res. 9, 442–453 (2017).

16. Conlon, F. L., Fairclough, L., Price, B. M., Casey, E. S. & Smith, J. C. Determinants of T box protein specificity. Development 128, 3749–3758 (2001).

17. Stennard, F. A. et al. Cardiac T-box factor Tbx20 directly interacts with Nkx2-5, GATA4, and GATA5 in regulation of gene expression in the developing heart. Dev. Biol. 262, 206–224 (2003).

18. Carreira, S., Dexter, T. J., Yavuzer, U., Easty, D. J. & Goding, C. R. Brachyury-related transcription factor Tbx2 and repression of the melanocyte-specific TRP-1 promoter. Mol. Cell. Biol. 18, 5099–5108 (1998).

19. Ouimette, J.-F., Jolin, M. L., L'honoré, A., Gifuni, A. & Drouin, J. Divergent transcriptional activities determine limb identity. Nat. Commun. 1, 1–9 (2010).

20. Wattler, S., Russ, a, Evans, M. & Nehls, M. A combined analysis of genomic and primary protein structure defines the phylogenetic relationship of new members if the T-box family. Genomics 48, 24–33 (1998).

21. Abrahams, A., Parker, M. I. & Prince, S. The T-box transcription factor Tbx2: Its role in development and possible implication in cancer. IUBMB Life 62, 92–102 (2010).

22. Goering, L. M. et al. An interacting network of T-box genes directs gene expression and fate in the zebrafish mesoderm. Proc. Natl. Acad. Sci. U. S. A. 100, 9410–5 (2003).

23. Rallis, C. et al. Tbx5 is required for forelimb bud formation and continued outgrowth. Development 130, 2741–2751 (2003).

24. Sakiyama, J.-I., Yamagishi, A. & Kuroiwa, A. Tbx4-Fgf10 system controls lung bud formation during chicken embryonic development. Development 130, 1225–34 (2003).

25. Horton, A. C. et al. Conservation of linkage and evolution of developmental function within the Tbx2/3/4/5 subfamily of T-box genes: Implications for the origin of vertebrate limbs. Dev. Genes Evol. 218, 613–628 (2008).

26. Sheeba, C. J. & Logan, M. P. O. The Roles of T-Box Genes in Vertebrate Limb Development. T-box Genes in Development 122, (Elsevier Inc., 2017).

27. Agulnik, S. I., Bollag, R. J. & Silver, L. M. Conservation of the T-box gene family from Mus musculus to Caenorhabditis elegans. Genomics 25, 214–219 (1995).

28. Holland, P. W. H., Garcia-Fernàndez, J., Williams, N. A. & Sidow, A. Gene duplications and the origins of vertebrate development. Developm 125–133 (1994).

29. Pasquier, J. et al. Gene evolution and gene expression after whole genome duplication in fish: the PhyloFish database. BMC Genomics 17, 368 (2016).

30. Glasauer, S. M. K. & Neuhauss, S. C. F. Whole-genome duplication in teleost fishes and its evolutionary consequences. Mol. Genet. Genomics 289, 1045–1060 (2014).

31. Ahn, D., You, K. H. & Kim, C. H. Evolution of the Tbx6/16 subfamily genes in vertebrates: Insights from zebrafish. Mol. Biol. Evol. 29, 3959–3983 (2012).

32. Bamshad, M. et al. Mutations in human TBX3 alter limb, apocrine and genital development in ulnar-mammary syndrome. Nat. Genet. 16, 311–315 (1997).

33. Bongers, E. M. H. F. et al. Mutations in the human TBX4 gene cause small patella syndrome. Am. J. Hum. Genet. 74, 1239–1248 (2004).

34. Law, D. J., Gebuhr, T., Garvey, N., Agulnik, S. I. & Silver, L. M. Identification, characterization, and localization to chromosome 17q21-22 of the human TBX2 homolog, member of a conserved developmental gene family. Mamm. Genome 6, 793–7 (1995).

35. Linden, H., Williams, R., King, J., Blair, E. & Kini, U. Ulnar mammary syndrome and TBX3 : Expanding the phenotype. Am. J. Med. Genet. Part A 149A, 2809–2812 (2009).

36. Ramirez, R. N. & Kozin, S. H. Ulnar Mammary Syndrome. J. Hand Surg. Am. 39, 803–805 (2014).

37. Rallis, C., Del Buono, J. & Logan, M. P. O. Tbx3 can alter limb position along the rostrocaudal axis of the developing embryo. Development 132, 1961–1970 (2005).

38. Schinzel, A. Ulnar-mammary syndrome. J. Med. Genet. 24, 778–781 (1987).

39. Bamshad, M. et al. Mutations in human TBX3 alter limb, apocrine and genital development in ulnar-mammary syndrome. Nat. Genet. 16, 311–315 (1997).

40. Klopocki, E. et al. Ulnar–mammary syndrome with dysmorphic facies and mental retardation caused by a novel 1.28 Mb deletion encompassing the TBX3 gene. Eur. J. Hum. Genet. 14, 1274–1279 (2006).

41. Naiche, L. A., Arora, R., Kania, A., Lewandoski, M. & Papaioannou, V. E. Identity and fate of Tbx4-expressing cells reveal developmental cell fate decisions in the allantois, limb, and external genitalia. Dev. Dyn. 240, 2290–300 (2011).

42. Naiche, L. A. & Papaioannou, V. E. Tbx4 is not required for hindlimb identity or post-bud hindlimb outgrowth. Development 134, 93–103 (2007).

43. Scott, J. E. & Taor, W. S. The Small Patella Syndrome. J. Bone Jt. Surg. 61–B, 172–175 (1979).

44. Albalat, R., Baquero, M. & Minguillón, C. Identification and characterisation of the developmental expression pattern of tbx5b, a novel tbx5 gene in zebrafish. Gene Expr. Patterns 10, 24–30 (2010).

45. Holt, M. & Oram, S. Familial heart disease with skeletal malformations. Br. Heart J. 22, 236–42 (1960).

46. Hurst, A., Hall, C. M. & Baraitser, M. The Holt-Oram syndrome. J Med Genet 28, 406–410 (1991).

47. Basson, C. T. et al. Mutations in human cause limb and cardiac malformation in Holt-Oram syndrome. Nat. Genet. 15, 30–35 (1997).

48. Yi Li, Q. et al. Holt-Oram syndrome is caused by mutations in TBX5, a member of the Brachyury (T) gene family. Nat. Genet. 15, 21–29 (1997).

49. Mcdermott, D. A. et al. TBX5 genetic testing validates strict clinical criteria for Holt-Oram syndrome. Pediatr. Res. 58, 981–986 (2005).

50. Debeer, P., Race, V., Gewillig, M., Devriendt, K. & Frijns, J. P. Novel TBX5 mutations in patients with Holt-Oram syndrome. Clin Orthop Relat Res 462, 20–26 (2007).

51. Fan, C. et al. Novel TBX5 mutations and molecular mechanism for Holt-Oram syndrome. J. Med. Genet. 40, 1–7 (2003).

52. Gruenauer-Kloevekorn, C. & Froster, U. G. Holt-Oram syndrome: A new mutation in the TBX5 gene in two unrelated families. Ann. Genet. 46, 19–23 (2003).

53. Boogerd, C. J. J. et al. Functional analysis of novel TBX5 T-box mutations associated with Holt-Oram syndrome. Cardiovasc. Res. 88, 130–139 (2010).

54. Sulaiman, F. A. et al. Tbx5 Buffers Inherent Left/Right Asymmetry Ensuring Symmetric Forelimb Formation. PLoS Genet. 12, 1–18 (2016).

55. Brassington, A. M. et al. Expressivity of Holt-Oram syndrome is not predicted by TBX5 genotype. Am. J. Hum. Genet. 73, 74–85 (2003).

56. Isphording, D., Leylek, A. M., Yeung, J., Mischel, A. & Simon, H. G. T-box genes and congenital heart/limb malformations. Clin. Genet. 66, 253–264 (2004).

57. Basson, C. T. et al. Different TBX5 interactions in heart and limb defined by Holt-Oram syndrome mutations. Proc. Natl. Acad. Sci. U. S. A. 96, 2919–24 (1999).

58. Krause, A. et al. Tbx5 and Tbx4 transcription factors interact with a new chicken PDZ-LIM protein in limb and heart development. Dev. Biol. 273, 106–120 (2004).

59. Garg, V. et al. GATA4 mutations cause human congenital heart defects and reveal an interaction with TBX5. Nature 424, 443–447 (2003).

60. Camarata, T. et al. LMP4 regulates Tbx5 protein subcellular localization and activity. J. Cell Biol. 174, 339–348 (2006).

61. Moskowitz, I. P. G. et al. The T-Box transcription factor Tbx5 is required for the patterning and maturation of the murine cardiac conduction system. Development 131, 4107–16 (2004).

62. Bruneau, B. G. et al. A murine model of Holt-Oram syndrome defines roles of the T-Box transcription factor Tbx5 in cardiogenesis and disease. Cell 106, 709–721 (2001).

63. Takabatake, Y., Takabatake, T. & Takeshima, K. Conserved and divergent expression of T-box genes Tbx2-Tbx5 in Xenopus. Mech. Dev. 91, 433–437 (2000).

64. Gibson-Brown, J. J., Agulnik, S. I., Silver, L. M., Niswander, L. & Papaioannou, V. E. Involvement of T-box genes Tbx2-Tbx5 in vertebrate limb specification and development. Development 125, 2499–2509

(1998).

65. McEwen, G. K. et al. Ancient duplicated conserved noncoding elements in vertebrates: A genomic and functional analysis. Genome Res. 16, 451–465 (2006).

66. Goode, D. K., Callaway, H. A., Cerda, G. A., Lewis, K. E. & Elgar, G. Minor change, major difference: divergent functions of highly conserved cis-regulatory elements subsequent to whole genome duplication events. Development 138, 879–884 (2011).

67. Beaster-Jones, L. Cis-regulation and conserved non-coding elements in amphioxus. Brief. Funct. Genomics 11, 118–130 (2012).

68. Kimmel, C. B., Ballard, W. W., Kimmel, S. R., Ullmann, B. & Schilling, T. F. Stages of Embryonic Development of the Zebrafish. Dev. Dyn. 10, 253–310 (1995).

69. Veldman, M. B. & Lin, S. Zebrafish as a Developmental Model Organism for Pediatric Research. Pediatr. Res. 64, 470–476 (2008).

70. Moulton, J. D. Guide for Morpholino Users: Toward Therapeutics. J. Drug Discov. Dev. Deliv. 3, 1023–2 (2016).

71. Stainier, D. Y. R. et al. Guidelines for morpholino use in zebrafish. PLOS Genet. 13, e1007000 (2017).

72. Thi Thu, H. N., Haw Tien, S. F., Loh, S. L., Bok Yan, J. S. & Korzh, V. tbx2a Is Required for Specification of Endodermal Pouches during Development of the Pharyngeal Arches. PLoS One 8, e77171 (2013).

73. Sedletcaia, A. & Evans, T. Heart chamber size in zebrafish is regulated redundantly by duplicated tbx2 genes. Dev. Dyn. 240, 1548–1557 (2011).

74. Ribeiro, I. et al. Tbx2 and Tbx3 Regulate the Dynamics of Cell Proliferation during Heart Remodeling. PLoS One 2, e398 (2007).

75. Drummond, B. E., Li, Y., Marra, A. N., Cheng, C. N. & Wingert, R. A. The tbx2a/b transcription factors direct pronephros segmentation and corpuscle of Stannius formation in zebrafish. Dev. Biol. 421, 52–66 (2017).

76. Choi, T.-Y. et al. Bone morphogenetic protein signaling governs biliary-driven liver regeneration in zebrafish through tbx2b and id2a. Hepatology 66, 1616–1630 (2017).

77. Alvarez-Delfin, K. et al. Tbx2b is required for ultraviolet photoreceptor cell specification during zebrafish retinal development. Proc. Natl. Acad. Sci. 106, 2023–2028 (2009).

78. Snelson, C. D., Burkart, J. T. & Gamse, J. T. Formation of the asymmetric pineal complex in zebrafish requires two independently acting transcription factors. Dev. Dyn. 237, 3538–3544 (2008).

79. Snelson, C. D., Santhakumar, K., Halpern, M. E. & Gamse, J. T. Tbx2b is required for the development of the parapineal organ. Development 135, 1693–1702 (2008).

80. Gross, J. M. & Dowling, J. E. Tbx2b is essential for neuronal differentiation along the dorsal/ventral axis of the zebrafish retina. Proc. Natl. Acad. Sci. U. S. A. 102, 4371–4376 (2005).

81. Dheen, T. et al. Zebrafish tbx-c functions during formation of midline structures. Development 126, 2703–2713 (1999).

82. Don, E. K. et al. Genetic basis of hindlimb loss in a naturally occurring vertebrate model. Biol. Open 5, 359–366 (2016).

83. French, C. R., Stach, T. R., March, L. D., Lehmann, O. J. & Waskiewicz, A. J. Apoptotic and Proliferative Defects Characterize Ocular Development in a Microphthalmic BMP Model. Investig. Opthalmology Vis. Sci. 54, 4636 (2013).

84. Ruvinsky, I., Oates, A. C., Silver, L. M. & Ho, R. K. The evolution of paired appendages in vertebrates: T-box genes in the zebrafish. Dev. Genes Evol. 210, 82–91 (2000).

85. Begemann, G. & Ingham, P. W. Developmental regulation of Tbx5 in zebrafish embryogenesis. Mech. Dev. 90, 299–304 (2000).

86. Ahn, D., Kourakis, M. J., Rohde, L. A., Silver, L. M. & Ho, R. K. T-box gene tbx5 is essential for formation of the pectoral limb bud. Nature 417, 754–758 (2002).

87. Garrity, D. M., Childs, S. & Fishman, M. C. The heartstrings mutation in zebrafish causes heart/fin Tbx5 deficiency syndrome. Development 129, 4635–4645 (2002).

88. Parrie, L. E., Renfrew, E. M., Wal, A. Vander, Mueller, R. L. & Garrity, D. M. Zebrafish tbx5 paralogs demonstrate independent essential requirements in cardiac and pectoral fin development. Dev. Dyn. 242, 485–402 (2013).

89. Fuhrmann, S. Eye Morphogenesis and Patterning of the Optic Vesicle. Curr. Top. Dev. Biol. 93, 61–84 (2010).

90. Sinn, R. & Wittbrodt, J. An eye on eye development. Mech. Dev. 130, 347–358 (2013).

91. Veien, E. S., Rosenthal, J. S., Kruse-Bend, R. C., Chien, C.-B. & Dorsky, R. I. Canonical Wnt signaling is required for the maintenance of dorsal retinal identity. Development 135, 4101–11 (2008).

92. Kwan, K. M. et al. A complex choreography of cell movements shapes the vertebrate eye. Development 139, 359–72 (2012).

93. Stigloher, C. et al. Segregation of telencephalic and eye-field identities inside the zebrafish forebrain territory is controlled by Rx3. Development 133, 2925–2935 (2006).

94. Loosli, F. et al. Loss of eyes in zebrafish caused by mutation of chokh/rx3. EMBO Rep. 4, 894–899 (2003).

95. Weaver, M. & Hogan, B. Powerful ideas driven by simple tools: lessons from experimental embryo-

logy. Nat. Cell Biol. 3, E165–E167 (2001).

96. Brown, K. E. et al. Nlcam modulates midline convergence during anterior neural plate morphogenesis. Dev. Biol. 339, 14–25 (2010).

97. Martinez-Morales, J. R. & Wittbrodt, J. Shaping the vertebrate eye. Curr. Opin. Genet. Dev. 19, 511–517 (2009).

98. Yun, S. et al. Lhx2 links the intrinsic and extrinsic factors that control optic cup formation. Development 136, 3895–3906 (2009).

99. Green, E. S., Stubbs, J. L. & Levine, E. M. Genetic rescue of cell number in a mouse model of microphthalmia: interactions between Chx10 and G1-phase cell cycle regulators. Development 130, 539–52 (2003).

100. Hodgkinson, C. A. et al. Mutations at the mouse microphthalmia locus are associated with defects in a gene encoding a novel basic-helix-loop-helix-zipper protein. Cell 74, 395–404 (1993).

101. Sigulinsky, C. L., Green, E. S., Clark, A. M. & Levine, E. M. Vsx2/Chx10 ensures the correct timing and magnitude of Hedgehog signaling in the mouse retina. Dev. Biol. 317, 560–575 (2008).

102. Lister, J. A., Robertson, C. P., Lepage, T., Johnson, S. L. & Raible, D. W. nacre encodes a zebrafish microphthalmia-related protein that regulates neural-crest-derived pigment cell fate. Development 126, 3757–67 (1999).

103. Lister, J. A., Close, J. & Raible, D. W. Duplicate mitf Genes in Zebrafish: Complementary Expression and Conservation of Melanogenic Potential. Dev. Biol. 237, 333–344 (2001).

104. Ramón Martínez-Morales, J., Rodrigo, I. & Bovolenta, P. Eye development: a view from the retina pigmented epithelium. BioEssays 26, 766–777 (2004).

105. Smith, A. N., Miller, L.-A., Radice, G., Ashery-Padan, R. & Lang, R. A. Stage-dependent modes of Pax6-Sox2 epistasis regulate lens development and eye morphogenesis. Development 136, 2977–2985 (2009).

106. Kamachi, Y., Uchikawa, M., Collignon, J., Lovell-Badge, R. & Kondoh, H. Involvement of Sox1, 2 and 3 in the early and subsequent molecular events of lens induction. Development 125, 2521–32 (1998).

107. Ashery-Padan, R., Marquardt, T., Zhou, X. & Gruss, P. Pax6 activity in the lens primordium is required for lens formation and for correct placement of a single retina in the eye. Genes Dev. 14, 2701–11 (2000).

108. Seo, H.-C., Drivenes, Ø., Ellingsen, S. & Fjose, A. Expression of two zebrafish homologues of the murine Six3 gene demarcates the initial eye primordia. Mech. Dev. 73, 45–57 (1998).

109. Nornes, S. et al. Zebrafish contains two Pax6 genes involved in eye development. Mech. Dev. 77, 185–196 (1998).

110. Kleinjan, D. A. et al. Subfunctionalization of Duplicated Zebrafish pax6 Genes by cis-Regulatory Di-

vergence. PLoS Genet. 4, e29 (2008).

111. Ma, L., Parkhurst, A. & Jeffery, W. R. The role of a lens survival pathway including sox2 and αA-crystallin in the evolution of cavefish eye degeneration. Evodevo 5, 28 (2014).

112. Loosli, F., Winkler, S. & Wittbrodt, J. Six3 overexpression initiates the formation of ectopic retina. Genes Dev. 13, 649–54 (1999).

113. Oliver, G., Loosli, F., Köster, R., Wittbrodt, J. & Gruss, P. Ectopic lens induction in fish in response to the murine homeobox gene Six3. Mech. Dev. 60, 233–9 (1996).

114. French, C. R., Erickson, T., French, D. V., Pilgrim, D. B. & Waskiewicz, A. J. Gdf6a is required for the initiation of dorsal-ventral retinal patterning and lens development. Dev. Biol. 333, 37–47 (2009).

115. Faber, S. C. et al. Fgf receptor signaling plays a role in lens induction. Development 128, 4425–38 (2001).

116. Gotoh, N. et al. Tyrosine phosphorylation sites on FRS2 responsible for Shp2 recruitment are critical for induction of lens and retina. Proc. Natl. Acad. Sci. 101, 17144–17149 (2004).

117. Nakayama, Y. et al. Fgf19 is required for zebrafish lens and retina development. Dev. Biol. 313, 752–766 (2008).

118. Molotkov, A., Molotkova, N. & Duester, G. Retinoic acid guides eye morphogenetic movements via paracrine signaling but is unnecessary for retinal dorsoventral patterning. Development 133, 1901–10 (2006).

119. Behesti, H., Holt, J. K. & Sowden, J. C. The level of BMP4 signaling is critical for the regulation of distinct T-box gene expression domains and growth along the dorso-ventral axis of the optic cup. BMC Dev. Biol. 6, 62 (2006).

120. Wagner, E., McCaffery, P. & Dräger, U. C. Retinoic acid in the formation of the dorsoventral retina and its central projections. Dev. Biol. 222, 460–70 (2000).

121. McCaffery, P., Wagner, E., O'Neil, J., Petkovich, M. & Dräger, U. C. Dorsal and ventral retinal territories defined by retinoic acid synthesis, break-down and nuclear receptor expression. Mech. Dev. 82, 119–130 (1999).

122. Lupo, G. et al. Dorsoventral patterning of the Xenopus eye: a collaboration of Retinoid, Hedgehog and FGF receptor signaling. Development 132, 1737–1748 (2005).

123. Halilagic, A. et al. Retinoids control anterior and dorsal properties in the developing forebrain. Dev. Biol. 303, 362–375 (2007).

124. Matt, N. et al. Retinoic acid-dependent eye morphogenesis is orchestrated by neural crest cells. Development 132, 4789–4800 (2005).

125. Torres, M., Gómez-Pardo, E. & Gruss, P. Pax2 contributes to inner ear patterning and optic nerve trajectory. Development 122, 3381–3391 (1996).

126. Mui, S. H., Hindges, R., O'Leary, D. D. M., Lemke, G. & Bertuzzi, S. The homeodomain protein Vax2 patterns the dorsoventral and nasotemporal axes of the eye. Development 129, 797–804 (2002).

127. Mic, F. A., Molotkov, A., Molotkova, N. & Duester, G. Raldh2 expression in optic vesicle generates a retinoic acid signal needed for invagination of retina during optic cup formation. Dev. Dyn. 231, 270–277 (2004).

128. Veien, E. S., Rosenthal, J. S., Kruse-Bend, R. C., Chien, C.-B. & Dorsky, R. I. Canonical Wnt signaling is required for the maintenance of dorsal retinal identity. Development 135, 4101–4111 (2008).

129. Sakuta, H. et al. Role of bone morphogenic protein 2 in retinal patterning and retinotectal projection. J. Neurosci. 26, 10868–10878 (2006).

130. Plas, D. T. et al. Bone morphogenetic proteins, eye patterning, and retinocollicular map formation in the mouse. J. Neurosci. 28, 7057–67 (2008).

131. Kobayashi, T., Yasuda, K. & Araki, M. Coordinated regulation of dorsal bone morphogenetic protein 4 and ventral Sonic hedgehog signaling specifies the dorso-ventral polarity in the optic vesicle and governs ocular morphogenesis through fibroblast growth factor 8 upregulation. Dev. Growth Differ. 52, 351–363 (2010).

132. Gosse, N. J. & Baier, H. An essential role for Radar (Gdf6a) in inducing dorsal fate in the zebrafish retina. Proc. Natl. Acad. Sci. U. S. A. 106, 2236–41 (2009).

133. Kruse-Bend, R. et al. Extraocular ectoderm triggers dorsal retinal fate during optic vesicle evagination in zebrafish. Dev. Biol. 371, 57–65 (2012).

134. Sowden, J. C., Holt, J. K., Meins, M., Smith, H. K. & Bhattacharya, S. S. Expression of Drosophila omb-related T-box genes in the developing human and mouse neural retina. Invest Ophthalmol Vis Sci 42, 3095–3102 (2001).

135. Behesti, H., Papaioannou, V. E. & Sowden, J. C. Loss of Tbx2 delays optic vesicle invagination leading to small optic cups. Dev. Biol. 333, 360–372 (2009).

136. Erickson, T., French, C. R. & Waskiewicz, A. J. Meis1 specifies positional information in the retina and tectum to organize the zebrafish visual system. Neural Dev. 5, (2010).

137. Horndli, C. S. & Chien, C.-B. Sonic hedgehog is indirectly required for intraretinal axon pathfinding by regulating chemokine expression in the optic stalk. Development 139, 2604–2613 (2012).

138. Hutson, L. D. & Chien, C. B. Wiring the zebrafish: Axon guidance and synaptogenesis. Curr. Opin. Neurobiol. 12, 87–92 (2002).

139. Kita, E. M., Scott, E. K. & Goodhill, G. J. Topographic wiring of the retinotectal connection in zebrafish. Dev. Neurobiol. 75, 542–556 (2015).

140. Koshiba-Takeuchi, K. Tbx5 and the Retinotectum Projection. Science (80-.). 287, 134–137 (2000).

141. Schulte, D., Furukawa, T., Peters, M. A., Kozak, C. A. & Cepko, C. L. Misexpression of the Emx-Related Homeobox Genes cVax and mVax2 Ventralizes the Retina and Perturbs the Retinotectal Map. Neuron 24, 541–553 (1999).

142. McLaughlin, T., Hindges, R. & O'Leary, D. D. M. Regulation of axial patterning of the retina and its topographic mapping in the brain. Curr. Opin. Neurobiol. 13, 57–69 (2003).

143. Duboc, V. & Logan, M. P. O. Regulation of limb bud initiation and limb-type morphology. Dev. Dyn. 240, 1017–1027 (2011).

144. Mercader, N. Early steps of paired fin development in zebrafish compared with tetrapod limb development. Dev. Growth Differ. 49, 421–437 (2007).

145. Gibson-browna, J. J. et al. Evidence of a role for T- □ genes in the evolution of limb morphogenesis and the specification of forelimb / hindlimb identity and the specification of forelimb / hindlimb identity. 56, 93–101 (2014).

146. Lanctôt, C., Moreau, a, Chamberland, M., Tremblay, M. L. & Drouin, J. Hindlimb patterning and mandible development require the Ptx1 gene. Development 126, 1805–1810 (1999).

147. Isaac, A. et al. Tbx genes and limb identity in chick embryo development. Development 125, 1867–1875 (1998).

148. Ohuchi, H. et al. Correlation of wing-leg identity in ectopic FGF-induced chimeric limbs with the differential expression of chick Tbx5 and Tbx4. Development 125, 51–60 (1998).

149. Logan, M., Simon, H. G. & Tabin, C. Differential regulation of T-box and homeobox transcription factors suggests roles in controlling chick limb-type identity. Development 125, 2825–2835 (1998).

150. Ohuchi, H. et al. The mesenchymal factor, FGF10, initiates and maintains the outgrowth of the chick limb bud through interaction with FGF8, an apical ectodermal factor. Development 124, 2235–2244 (1997).

151. Sekine, K. et al. Fgf10 is essential for limb and lung formation. Nat. Genet. 21, 138–41 (1999).

152. Agarwal, P. Tbx5 is essential for forelimb bud initiation following patterning of the limb field in the mouse embryo. Development 130, 623–633 (2003).

153. Naiche, L. A. Loss of Tbx4 blocks hindlimb development and affects vascularization and fusion of the allantois. Development 130, 2681–2693 (2003).

154. Kawakami, Y. et al. Islet1-mediated activation of the -catenin pathway is necessary for hindlimb

initiation in mice. Development 138, 4465–4473 (2011).

155. Logan, M., Tabin, C. Role of Pitx1 Upstream of Tbx4 in Specification of Hindlimb Identity. Science (80-.). 283, 1736–1739 (1999).

156. Coumoul, X. & Deng, C. X. Roles of FGF Receptors in Mammalian Development and Congenital Diseases. Birth Defects Res. Part C - Embryo Today Rev. 69, 286–304 (2003).

157. Boulet, A. M., Moon, A. M., Arenkiel, B. R. & Capecchi, M. R. The roles of Fgf4 and Fgf8 in limb bud initiation and outgrowth. Dev. Biol. 273, 361–372 (2004).

158. Sun, X., Mariani, F. V. & Martin, G. R. Functions of FGF signalling from the apical ectodermal ridge in limb development. Nature 418, 501–508 (2002).

159. Min, H. et al. Fgf-10 is required for both limb and lung development and exhibits striking functional similarity to Drosophila branchless. Genes Dev. 12, 3156–3161 (1998).

160. Lewandoski, M., Sun, X. & Martin, G. R. Fgf8 signalling from the AER is essential for normal limb development. Nat. Genet. 26, 460–463 (2000).

161. Norton, W. H. J. HSPG synthesis by zebrafish Ext2 and Extl3 is required for Fgf10 signalling during limb development. Development 132, 4963–4973 (2005).

162. Ang, H. L., Deltour, L., Hayamizu, T. F., Zgombic-Knight, M. & Duester, G. Retinoic Acid Synthesis in Mouse Embryos during Gastrulation and Craniofacial Development Linked to Class IV Alcohol Dehydrogenase Gene Expression. J. Biol. Chem. 271, 9526–9534 (1996).

163. Grandel, H. et al. Retinoic acid signalling in the zebrafish embryo is necessary during pre-segmentation stages to pattern the anterior-posterior axis of the CNS and to induce a pectoral fin bud. Development 129, 2851–2865 (2002).

164. Stephens, T. D. & McNulty, T. R. Evidence for a metameric pattern in the development of the chick humerus. J. Embryol. Exp. Morphol. 61, 191–205 (1981).

165. Sweeney, R. M. & Watterson, R. L. Rib development in chick embryos analyzed by means of tantalum foil blocks. Am. J. Anat. 126, 127–149 (1969).

166. Nishimoto, S., Wilde, S. M., Wood, S. & Logan, M. P. O. RA Acts in a Coherent Feed-Forward Mechanism with Tbx5 to Control Limb Bud Induction and Initiation. Cell Rep. 12, 879–891 (2015).

167. Begemann, G., Schilling, T. F., Rauch, G. J., Geisler, R. & Ingham, P. W. The zebrafish neckless mutation reveals a requirement for raldh2 in mesodermal signals that pattern the hindbrain. Development 128, 3081–3094 (2001).

168. Niederreither, K., Subbarayan, V., Dolle, P. & Chambon, P. Embryonic retinoic acid synthesis is essential for early mouse post-implantation development. Nat. Genet. 21, 444–448 (1999).

169. Morriss-Kay, G.M.; Sokolova, N. Embryonic development and pattern formation. FASEB J. 10, 961–968 (1996).

170. Stratford, T. H., Kostakopoulou, K. & Maden, M. Hoxb-8 has a role in establishing early anterior-posterior polarity in chick forelimb but not hindlimb. Development 124, 4225–4234 (1997).

171. Riddle, R. D., Johnson, R. L., Laufer, E. & Tabin, C. Sonic hedgehog mediates the polarizing activity of the ZPA. Cell 75, 1401–1416 (1993).

172. Niswander, L. Pattern formation: old models out on a limb. Nat. Rev. Genet. 4, 133–143 (2003).

173. Takeuchi, J. K. Tbx5 and Tbx4 trigger limb initiation through activation of the Wnt/Fgf signaling cascade. Development 130, 2729–2739 (2003).

174. Xu, X. et al. Fibroblast growth factor receptor 2 (FGFR2)-mediated reciprocal regulation loop between FGF8 and FGF10 is essential for limb induction. Development 125, 753–765 (1998).

175. Camarata, T. et al. Pdlim7 is required for maintenance of the mesenchymal/epidermal Fgf signaling feedback loop during zebrafish pectoral fin development. BMC Dev. Biol. 10, 104 (2010).

176. Grandel, H. & Schulte-Merker, S. The development of the paired fins in the zebrafish (Danio rerio). Mech. Dev. 79, 99–120 (1998).

177. Mao, Q., Stinnett, H. K. & Ho, R. K. Asymmetric cell convergence-driven fin bud initiation and pre-pattern requires Tbx5a control of a mesenchymal Fgf signal. Development 142, 4329–4339 (2015).

178. Fischer, S., Draper, B. W. & Neumann, C. J. The zebrafish fgf24 mutant identifies an additional level of Fgf signaling involved in vertebrate forelimb initiation. Development 130, 3515–3524 (2003).

179. Harvey, S. A. & Logan, M. P. O. Sall4 Acts Downstream of Tbx5 and Is Required for Pectoral Fin Outgrowth. Development 133, 1165–1173 (2006).

180. Bakkers, J., Verhoeven, M. C. & Abdelilah-Seyfried, S. Shaping the zebrafish heart: From left-right axis specification to epithelial tissue morphogenesis. Dev. Biol. 330, 213–220 (2009).

181. Stainier, D. Y. Zebrafish genetics and vertebrate heart formation. Nat. Rev. Genet. 2, 39–48 (2001).

182. Tam, P. P., Parameswaran, M., Kinder, S. J. & Weinberger, R. P. The allocation of epiblast cells to the embryonic heart and other mesodermal lineages: the role of ingression and tissue movement during gastrulation. Development 124, 1631–42 (1997).

183. Pérez-Pomares, J. M., González-Rosa, J. M. & Muñoz-Chápuli, R. Building the vertebrate heart - An evolutionary approach to cardiac development. Int. J. Dev. Biol. 53, 1427–1443 (2009).

184. Brand, T. Heart development: Molecular insights into cardiac specification and early morphogenesis. Dev. Biol. 258, 1–19 (2003).

185. Goetz, S. C., Brown, D. D. & Conlon, F. L. TBX5 is required for embryonic cardiac cell cycle progres-

sion. Development 133, 2575–84 (2006).

186. Harvey, R. P. Organogenesis: Patterning the vertebrate heart. Nat. Rev. Genet. 3, 544–556 (2002).

187. Fishman, M. C. & Chien, K. R. Fashioning the vertebrate heart: earliest embryonic decisions. Development 124, 2099–117 (1997).

188. Miquerol, L. & Kelly, R. G. Organogenesis of the vertebrate heart. Wiley Interdiscip. Rev. Dev. Biol. 2, 17–29 (2013).

189. Stephenson, A., Adams, J. W. & Vaccarezza, M. The vertebrate heart : an evolutionary perspective. J. Anat. 10, 1–11 (2017).

190. Bakkers, J. Zebrafish as a model to study cardiac development and human cardiac disease. Cardiovasc. Res. 91, 279–288 (2011).

191. Ye, D., Xie, H., Hu, B. & Lin, F. Endoderm convergence controls subduction of the myocardial precursors during heart-tube formation. Development 142, 2928–40 (2015).

192. Peterson, R. T., Mably, J. D., Chen, J. N. & Fishman, M. C. Convergence of distinct pathways to heart patterning revealed by the small molecule concentramide and the mutation heart-and-soul. Curr. Biol. 11, 1481–1491 (2001).

193. Smith, K. A. et al. Rotation and Asymmetric Development of the Zebrafish Heart Requires Directed Migration of Cardiac Progenitor Cells. Dev. Cell 14, 287–297 (2008).

194. Rohr, S., Bit-Avragim, N. & Abdelilah-Seyfried, S. Heart and soul/PRKCi and nagie oko/Mpp5 regulate myocardial coherence and remodeling during cardiac morphogenesis. Development 133, 107–115 (2006).

195. Rohr, S., Otten, C. & Abdelilah-Seyfried, S. Asymmetric involution of the myocardial field drives heart tube formation in zebrafish. Circ. Res. 102, e12–e19 (2008).

196. Bussmann, J., Bakkers, J. & Schulte-Merker, S. Early endocardial morphogenesis requires Scl/Tal1. PLoS Genet. 3, 1425–1437 (2007).

197. Stainier, D. Y., Weinstein, B. M., Detrich, H. W., Zon, L. I. & Fishman, M. C. Cloche, an early acting zebrafish gene, is required by both the endothelial and hematopoietic lineages. Development 121, 3141–3150 (1995).

198. Holtzman, N. G., Schoenebeck, J. J., Tsai, H.-J. & Yelon, D. Endocardium is necessary for cardiomyocyte movement during heart tube assembly. Development 134, 2379–2386 (2007).

199. Reiter, J. F., Verkade, H. & Stainier, D. Y. R. Bmp2b and Oep Promote Early Myocardial Differentiation through Their Regulation of gata5. Dev. Biol. 234, 330–338 (2001).

200. Hochgreb, T. et al. A caudorostral wave of RALDH2 conveys anteroposterior information to the car-

diac field. Development 130, 5363–5374 (2003).

201. Yelon, D. Cardiac Patterning and Morphogenesis in Zebrafish. Dev Dyn 222, 552–563 (2001).

202. Niederreither, K. et al. Embryonic retinoic acid synthesis is essential for heart morphogenesis in the mouse. Development 128, 1019–1031 (2001).

203. Chen, J. N. et al. Left-right pattern of cardiac BMP4 may drive asymmetry of the heart in zebrafish. Development 124, 4373–4382 (1997).

204. Liu, W. & Foley, A. C. Signaling pathways in early cardiac development. Wiley Interdiscip. Rev. Syst. Biol. Med. 3, 191–205 (2011).

205. Trinh, L. A. & Stainier, D. Y. R. Fibronectin regulates epithelial organization during myocardial migration in zebrafish. Dev. Cell 6, 371–382 (2004).

206. Trinh, L. A., Yelon, D. & Stainier, D. Y. R. Hand2 Regulates Epithelial Formation during Myocardial Differentiation. Curr. Biol. 128, 189–190 (2005).

207. Yan, Y. et al. Conserved requirement for EGF – CFC genes in vertebrate left – right axis formation. Genes Dev. 13, 2527–2537 (1999).

208. Long, S., Ahmad, N., Rebagliati, M. The zebrafish nodal-related gene southpaw is required for visceral and diencephalic left-right asymmetry. Development 130, 2303–2316 (2003).

209. de Campos-Baptista, M. I. M. & 1, 4, Nathalia Glickman Holtzman2, 3, Deborah Yelon2, and A. F. S. Nodal signaling promotes the speed and directional movement of cardiomyocytes in zebrafish. Dev. Dyn. 6, 760–769 (2008).

210. Chocron, S., Verhoeven, M. C., Rentzsch, F., Hammerschmidt, M. & Bakkers, J. Zebrafish Bmp4 regulates left-right asymmetry at two distinct developmental time points. Dev. Biol. 305, 577–588 (2007).

211. Lenhart, K. F., Holtzman, N. G., Williams, J. R. & Burdine, R. D. Integration of Nodal and BMP Signals in the Heart Requires FoxH1 to Create Left-Right Differences in Cell Migration Rates That Direct Cardiac Asymmetry. PLoS Genet. 9, e1003109 (2013).

212. Noel, E. S. et al. A Nodal-independent and tissue-intrinsic mechanism controls heart-looping chirality. Nat. Commun. 4, 2754 (2013).

213. Ocaña, O. H. et al. A right-handed signalling pathway drives heart looping in vertebrates. Nature 549, 86–90 (2017).

214. Wassarman, P. M. et al. T-box Genes in Development and Disease. Current Topics in Developmental Biology 1, (Elsevier Inc., 2017).

215. Hatcher, C. J., Goldstein, M. M., Mah, C. S., Delia, C. S. & Basson, C. T. Identification and localization of TBX5 transcription factor during human cardiac morphogenesis. Dev Dyn 219, 90–95 (2000).

216. van Weerd, J. H. & Christoffels, V. M. The formation and function of the cardiac conduction system. Development 143, 197–210 (2016).

217. Hatcher, C. J. & Basson, C. T. Specification of the cardiac conduction system by transcription factors. Circ. Res. 105, 620–30 (2009).

218. Plageman, T. F. & Yutzey, K. E. T-box genes and heart development: Putting the 'T' in hearT. Developmental Dynamics 232, 11–20 (2005).

219. Hoffmann, A. D. et al. Foxf Genes Integrate Tbx5 and Hedgehog Pathways in the Second Heart Field for Cardiac Septation. PLoS Genet. 10, e1004604 (2014).

220. Waldron, L. et al. The Cardiac TBX5 Interactome Reveals a Chromatin Remodeling Network Essential for Cardiac Septation Article The Cardiac TBX5 Interactome Reveals a Chromatin Remodeling Network Essential for Cardiac Septation. Dev. Cell 36, 262–275 (2016).

221. Arnolds, D. E. et al. TBX5 drives Scn5a expression to regulate cardiac conduction system function. J. Clin. Invest. 122, 2509–2518 (2012).

222. Moskowitz, I. P. G. et al. A Molecular Pathway Including Id2, Tbx5, and Nkx2-5 Required for Cardiac Conduction System Development. Cell 129, 1365–1376 (2007).

223. Mori, A. D. et al. Tbx5-dependent rheostatic control of cardiac gene expression and morphogenesis. Dev. Biol. 297, 566–586 (2006).

224. Hiroi, Y. et al. Tbx5 associates with Nkx2-5 and synergistically promotes cardiomyocyte differentiation. Nat. Genet. 28, 276–80 (2001).

225. Xie, L. et al. Tbx5-Hedgehog Molecular Networks Are Essential in the Second Heart Field for Atrial Septation. Dev. Cell 23, 280–291 (2012).

226. Puskaric, S. et al. Shox2 mediates Tbx5 activity by regulating Bmp4 in the pacemaker region of the developing heart. Hum. Mol. Genet. 19, 4625–4633 (2010).

227. Leigh, M. W. et al. Clinical and Genetic Aspects of Primary Ciliary Dyskinesia / Kartagener Syndrome. Genet. Med. 11, 473–87 (2009).

228. Masiwal, P., Chenthil, K. S., Priyadarsini, B., Gnanaprakasam, J. & Srihari, I. Ivemark Syndrome. J. Assoc. Physicians India 64, 2015–2017 (2016).

229. Fliegauf, M., Benzing, T. & Omran, H. When cilia go bad: cilia defects and ciliopathies. Nat. Rev. Mol. Cell Biol. 8, 880–893 (2007).

230. Catana, A. & Apostu, A. P. The determination factors of left-right asymmetry disorders- a short review. Clujul Med. 90, 139–146 (2017).

231. Sutherland, M. J. & Ware, S. M. Disorders of left-right asymmetry: Heterotaxy and situs inversus. Am.

J. Med. Genet. Part C Semin. Med. Genet. 151, 307–317 (2009).

232. Casey, B. Two rights make a wrong: Human left-right malformations. Hum. Mol. Genet. 7, 1565–1571 (1998).

233. Paulozzi, L. J. & Lary, J. M. Laterality patterns in infants with external birth defects. Teratology 60, 265–271 (1999).

234. Levin, M. Left-right asymmetry in embryonic development: A comprehensive review. Mech. Dev. 122, 3–25 (2005).

235. Smith, A. T. & Sack, G. H. Holt-Oram syndrome. J. Pediatr. 95, 538–543 (1979).

236. Leanage, R., Raebum, J. A. & Young, I. D. Holt-Oram syndrome: a clinical genetic study. J Med Genet 33, 300–307 (1996).

237. Bruneau, B. G. et al. Chamber-specific cardiac expression of Tbx5 and heart defects in Holt-Oram syndrome. Dev. Biol. 211, 100–8 (1999).

238. Levin, M. & Palmer, A. R. Left-right patterning from the inside out: Widespread evidence for intracellular control. BioEssays 29, 271–287 (2007).

239. Adachi, H. et al. Determination of left/right asymmetric expression of nodal by a left side-specific enhancer with sequence similarity to a lefty-2 enhancer. Genes Dev. 13, 1589–1600 (1999).

240. Mercola, M. Left-right asymmetry: nodal points. J. Cell Sci. 116, 3251–3257 (2003).

241. Vandenberg, L; Levin, M. Synthesis of Molecular Models of Embryonic Laterality. Dev. Biol. 379, 1–15 (2014).

242. Brown, N. A. & Wolpert, L. The development of handedness in left/right asymmetry. Development 109, 1–9 (1990).

243. Basu, B. & Brueckner, M. Cilia: Multifunctional Organelles at the Center of Vertebrate Left-Right Asymmetry. Curr. Top. Dev. Biol. 85, 151–174 (2008).

244. Brueckner, M. Cilia propel the embryo in the right direction. Am. J. Med. Genet. 101, 339–344 (2001).

245. Tabin, C. J. The Key to Left-Right Asymmetry. Cell 127, 27–32 (2006).

246. Lobikin, M. et al. Early, nonciliary role for microtubule proteins in left-right patterning is conserved across kingdoms. Proc. Natl. Acad. Sci. 109, 12586–12591 (2012).

247. Oviedo, N. J. & Levin, M. Gap Junctions Provide New Links in Left-Right Patterning. Cell 129, 645–647 (2007).

248. Stephen, L. A. et al. The chicken left right organizer has nonmotile cilia which are lost in a stage-dependent manner in the talpid3 ciliopathy. Genesis 52, 600–613 (2014).

249. Blum, M., Feistel, K., Thumberger, T. & Schweickert, A. The evolution and conservation of left-right patterning mechanisms. Development 141, 1603–1613 (2014).

250. Tanaka, Y., Okada, Y. & Hirokawa, N. FGF-induced vesicular release of Sonic hedgehog and retinoic acid in leftward nodal flow is critical for left–right determination. Nature 435, 172–177 (2005).

251. Oki, S. et al. Sulfated glycosaminoglycans are necessary for Nodal signal transmission from the node to the left lateral plate in the mouse embryo. Development 134, 3893–3904 (2007).

252. Burdine, R. D. & Grimes, D. T. Antagonistic interactions in the zebrafish midline prior to the emergence of asymmetric gene expression are important for left–right patterning. Philos. Trans. R. Soc. B Biol. Sci. 371, 20150402 (2016).

253. Kato, Y. The multiple roles of Notch signaling during left-right patterning. Cell. Mol. Life Sci. 68, 2555–2567 (2011).

254. Shiratori, H. The left-right axis in the mouse: from origin to morphology. Development 133, 2095–2104 (2006).

255. Hirokawa, N., Tanaka, Y., Okada, Y. & Takeda, S. Nodal Flow and the Generation of Left-Right Asymmetry. Cell 125, 33–45 (2006).

256. Yost, H. J. Left-Right Asymmetry: Nodal Cilia Make and Catch a Wave. Curr. Biol. 13, 808–809 (2003).

257. McGrath, J., Somlo, S., Makova, S., Tian, X. & Brueckner, M. Two populations of node monocilia initiate left-right asymmetry in the mouse. Cell 114, 61–73 (2003).

258. McGrath, J. & Brueckner, M. Cilia are at the heart of vertebrate left-right asymmetry. Curr. Opin. Genet. Dev. 13, 385–392 (2003).

259. Tabin, C. J. & Vogan, K. J. A two-cilia model for vertebrate left-right axis specification. Genes Dev. 17, 1–6 (2003).

260. Norris, D. P. Cilia, calcium and the basis of left-right asymmetry. BMC Biol. 10, 102 (2012).

261. Grimes, D. T. & Burdine, R. D. Left-Right Patterning: Breaking Symmetry to Asymmetric Morphogenesis. Trends Genet. 33, 616–628 (2017).

262. Schier, A. F. Nodal morphogens. Cold Spring Harb. Perspect. Biol. 1, 1–21 (2009).

263. Schier, A. F. & Shen, M. Nodal signalling in vertebrate development. Nature 403, 385–389 (1999).

264. Shen, M. M. Nodal signaling : developmental roles and regulation. Development 134, 1023–1034 (2007).

265. Meinhardt, H. & Gierer, A. Pattern formation by local self-activation and lateral inhibition. BioEssays 22, 753–760 (2000).

266. Sakuma, R. et al. Inhibition of Nodal signalling by Lefty mediated through interaction with common receptors and efficient diffusion. Genes to Cells 7, 401–412 (2002).

267. Saijoh, Y. et al. Left-right asymmetric expression of lefty2 and nodal is induced by a signaling pathway that includes the transcription factor FAST2. Mol. Cell 5, 35–47 (2000).

268. Meno, C. et al. Diffusion of Nodal Signaling Activity in the Absence of the Feedback Inhibitor Lefty2. Dev. Cell 1, 127–138 (2001).

269. Chen, C. & Shen, M. M. Two Modes by which Lefty Proteins Inhibit Nodal Signaling. Curr. Biol. 14, 618–24 (2014).

270. Tanaka, C., Sakuma, R., Nakamura, T., Hamada, H. & Saijoh, Y. Long-range action of Nodal requires interaction with GDF1. Genes Dev. 21, 3272–3282 (2007).

271. Amack, J. D., Wang, X. & Yost, H. J. Two T-box genes play independent and cooperative roles to regulate morphogenesis of ciliated Kupffer's vesicle in zebrafish. Dev. Biol. 310, 196–210 (2007).

272. Lenhart, K. F., Lin, S.-Y., Titus, T. A., Postlethwait, J. H. & Burdine, R. D. Two additional midline barriers function with midline lefty1 expression to maintain asymmetric Nodal signaling during left-right axis specification in zebrafish. Development 138, 4405–4410 (2011).

273. Lohr, J. L., Danos, M. C. & Yost, J. H. Left-right asymmetry of a nodal-related gene is regulated by dorsoanterior midline structures during Xenopus development. Development 124, 1465–1472 (1997).

274. Kelly, K. A., Wei, Y. & Mikawa, T. Cell death along the embryo midline regulates left-right sidedness. Dev. Dyn. 224, 238–244 (2002).

275. Saijoh, Y., Oki, S., Ohishi, S. & Hamada, H. Left-right patterning of the mouse lateral plate requires Nodal produced in the node. Dev. Biol. 256, 160–172 (2003).

276. Brennan, J., Norris, D. P. & Robertson, E. J. Nodal activity in the node governs left-right asymmetry. Genes Dev. 16, 2339–2344 (2002).

277. Shiratori, H., Yashiro, K., Shen, M. M. & Hamada, H. Conserved regulation and role of Pitx2 in situs-specific morphogenesis of visceral organs. Development 133, 3015–3025 (2006).

278. Ji, Y., Buel, S. M. & Amack, J. D. Mutations in zebrafish pitx2 model congenital malformations in Axenfeld-Rieger syndrome but do not disrupt left-right placement of visceral organs. Dev. Biol. 416, 69–81 (2016).

279. Fujiwara, T., Dehart, D. B., Sulik, K. K. & Hogan, B. L. M. Distinct requirements for extra-embryonic and embryonic bone morphogenetic protein 4 in the formation of the node and primitive streak and coordination of left-right asymmetry in the mouse. Development 129, 4685–4696 (2002).

280. Yu, X. et al. Cerberus functions as a BMP agonist to synergistically induce Nodal expression during

left-right axis determination in the chick embryo. Dev. Dyn. 237, 3613–3623 (2008).

281. Schlange, T., Arnold, H.-H. & Brand, T. BMP2 is a positive regulator of Nodal signaling during left-right axis formation in the chicken embryo. Development 129, 3421–3429 (2002).

282. Piedra, M. E. & Ros, M. a. BMP signaling positively regulates Nodal expression during left right specification in the chick embryo. Development 129, 3431–40 (2002).

283. Ramsdell, a F. & Yost, H. J. Cardiac looping and the vertebrate left-right axis: antagonism of left-sided Vg1 activity by a right-sided ALK2-dependent BMP pathway. Development 126, 5195–5205 (1999).

284. Zhu, L. et al. Cerberus regulates left-right asymmetry of the embryonic head and heart. Curr. Biol. 9, 931–938 (1999).

285. Yokouchi, Y., Vogan, K. J., Pearse, R. V. & Tabin, C. J. Antagonistic signaling by Caronte, a novel Cerberus-related gene, establishes left-right asymmetric gene expression. Cell 98, 573–583 (1999).

286. Rodriguez-Esteban, C. et al. The T-box genes Tbx4 and Tbx5 regulate limb outgrowth and identity. Nature 398, 814–818 (1999).

287. Kishigami, S. et al. BMP signaling through ACVRI is required for left-right patterning in the early mouse embryo. Dev. Biol. 276, 185–193 (2004).

288. Chang, H., Zwijsen, A., Vogel, H., Huylebroeck, D. & Matzuk, M. M. Smad5 Is Essential for Left–Right Asymmetry in Mice. Dev. Biol. 219, 71–78 (2000).

289. Mine, N., Anderson, R. M. & Klingensmith, J. BMP antagonism is required in both the node and lateral plate mesoderm for mammalian left-right axis establishment. Development 135, 2425–2434 (2008).

290. Raya, Á. & Belmonte, J. C. I. Left–right asymmetry in the vertebrate embryo: from early information to higher-level integration. Nat. Rev. Genet. 7, 283–293 (2006).

291. Zhang, M., Zhang, J., Lin, S.-C. & Meng, A. β-Catenin 1 and β-catenin 2 play similar and distinct roles in left-right asymmetric development of zebrafish embryos. Development 139, 2009–2019 (2012).

292. Lin, X. & Xu, X. Distinct functions of Wnt/beta-catenin signaling in KV development and cardiac asymmetry. Development 136, 207–217 (2009).

293. Kishimoto, N., Cao, Y., Park, A. & Sun, Z. Cystic Kidney Gene seahorse Regulates Cilia-Mediated Processes and Wnt Pathways. Dev. Cell 14, 954–961 (2008).

294. Martin, B. L. & Kimelman, D. Regulation of Canonical Wnt Signaling by Brachyury Is Essential for Posterior Mesoderm Formation. Dev. Cell 15, 121–133 (2008).

295. Hadjantonakis, A. K., Pisano, E. & Papaioannou, V. E. Tbx6 regulates left/right patterning in mouse embryos through effects on nodal cilia and perinodal signaling. PLoS One 3, e2511 (2008).

296. Newbury-Ecob, R., R, L., Raebum, J. & Young, I. Holt-Oram syndrome: a clinical genetic study. J Med

Genet 33, 300–307 (1996).

297. Matsui, T. & Bessho, Y. Left-right asymmetry in zebrafish. Cell. Mol. Life Sci. 69, 3069–3077 (2012).

298. Kupffer, C. Beobachtungen fiber die Entwicklung der Knochenfische. 1, 1–2 (1868).

299. Melby, A. E., Warga, R. M. & Kimmel, C. B. Specification of cell fates at the dorsal margin of the zebrafish gastrula. Development 122, 2225–37 (1996).

300. Cooper, M. S. & D'Amico, L. a. A cluster of noninvoluting endocytic cells at the margin of the zebrafish blastoderm marks the site of embryonic shield formation. Dev. Biol. 180, 184–198 (1996).

301. Oteíza, P., Köppen, M., Concha, M. L. & Heisenberg, C.-P. Origin and shaping of the laterality organ in zebrafish. Development 135, 2807–13 (2008).

302. Wang, G., Manning, M. L. & Amack, J. D. Regional cell shape changes control form and function of Kupffer's vesicle in the zebrafish embryo. Dev. Biol. 370, 52–62 (2012).

303. Wang, G., Yost, H. J. & Amack, J. D. Analysis of Gene Function and Visualization of Cilia-Generated Fluid Flow in Kupffer's Vesicle. J. Vis. Exp. 73, e50038 (2013).

304. Tavares, B. et al. Notch/Her12 signalling modulates, motile/immotile cilia ratio downstream of Foxj1a in zebrafish left-right organizer. Elife 6, e25165 (2017).

305. Gokey, J. J., Ji, Y., Tay, H. G., Litts, B. & Amack, J. D. Kupffer's vesicle size threshold for robust left-right patterning of the zebrafish embryo. Dev. Dyn. 245, 22–33 (2016).

306. Hong, S.-K. & Dawid, I. B. FGF-dependent left-right asymmetry patterning in zebrafish is mediated by Ier2 and Fibp1. Proc. Natl. Acad. Sci. U. S. A. 106, 2230–5 (2009).

307. Shiratori, H. & Hamada, H. The left-right axis in the mouse: from origin to morphology. Development 133, 2095–2104 (2006).

308. Lopes, S. S. et al. Notch signalling regulates left-right asymmetry through ciliary length control. Development 137, 3625–3632 (2010).

309. Hashimoto, H. et al. The Cerberus/Dan-family protein Charon is a negative regulator of Nodal signaling during left-right patterning in zebrafish. Development 131, 1741–53 (2004).

310. Wang, X. & Yost, H. J. Initiation and Propagation of Posterior to Anterior (PA) Waves in Zebrafish Left-Right Development. Dev Dyn 237, 3640–3647 (2008).

311. Cheng, S. K., Olale, F., Brivanlou, A. H. & Schier, A. F. Lefty blocks a subset of TGFβ signals by antagonizing EGF-CFC coreceptors. PLoS Biol. 2, 0215–0226 (2004).

312. Schilling, T. F., Concordet, J. & Ingham, P. W. Regulation of Left – Right Asymmetries in the Zebrafish by Shh and BMP4. Developmental 210, 277–287 (1999).

313. Casey, B. & Hackett, B. P. Left – right axis malformations in man and mouse. Curr. Opin. Genet. Dev. 10, 257–261 (2000).

314. Yoshioka, H. et al. Pitx2 , a Bicoid-Type Homeobox Gene , Is Involved in a Lefty-Signaling Pathway in Determination of Left-Right Asymmetry. Cell 94, 299–305 (1998).

315. Logan, M., Paga, S. M., Smith, D. M., Paganessi, L. & Tabin, C. J. The Transcription Factor Pitx2 Mediates Situs-Specific Morphogenesis in Response to Left-Right Asymmetric Signals. Cell 94, 307–317 (1998).

316. Chin, A. J., Tsang, M. & Weinberg, E. S. Heart and gut chiralities are controlled independently from initial heart position in the developing zebrafish. Dev. Biol. 227, 403–21 (2000).

317. Bisgrove, B. W., Essner, J. J. & Yost, H. J. Multiple pathways in the midline regulate concordant brain, heart and gut left-right asymmetry. Development 127, 3567–79 (2000).

318. Baker, K., Holtzman, N. G. & Burdine, R. D. Direct and indirect roles for Nodal signaling in two axis conversions during asymmetric morphogenesis of the zebrafish heart. Proc. Natl. Acad. Sci. U. S. A. 105, 13924–9 (2008).

319. Männer, J. On rotation, torsion, lateralization, and handedness of the embryonic heart loop: new insights from a simulation model for the heart loop of chick embryos. Anat. Rec. Part A 278, 481–92 (2004).

320. Horne-Badovinac, S. A Cellular Framework for Gut-Looping Morphogenesis in Zebrafish. Science (80-.). 302, 662–665 (2003).

321. Ober, E. A., Field, H. A. & Stainier, D. Y. R. From endoderm formation to liver and pancreas development in zebrafish. Mech. Dev. 120, 5–18 (2003).

322. Field, H. A., Ober, E. A., Roeser, T. & Stainier, D. Y. R. Formation of the digestive system in zebrafish . I . Liver morphogenesis. Dev. Biol. 253, 279–290 (2003).

323. Davis, N. M. et al. The Chirality of Gut Rotation Derives from Left-Right Asymmetric Changes in the Architecture of the Dorsal Mesentery. Dev. Cell 15, 134–145 (2008).

324. Cayuso, J. et al. Epithelial-Mesenchymal Interactions Controlling Article EphrinB1 / EphB3b Coordinate Bidirectional Epithelial-Mesenchymal Interactions Controlling Liver Morphogenesis and Laterality. Dev. Cell 39, 316–328 (2016).

325. Noël, E. S. et al. Organ-specific requirements for Hdac1 in liver and pancreas formation. Dev. Biol. 322, 237–50 (2008).

326. Aizawa, H., Goto, M., Sato, T. & Okamoto, H. Temporally Regulated Asymmetric Neurogenesis Causes Left-Right Difference in the Zebrafish Habenular Structures. Dev. Cell 12, 87–98 (2007).

327. Hüsken, U. & Carl, M. The Wnt/beta-catenin signaling pathway establishes neuroanatomical asymmetries and their laterality. Mech. Dev. 130, 330–335 (2013).

328. Neugebauer, J. M. & Joseph Yost, H. FGF signaling is required for brain left-right asymmetry and brain midline formation. Dev. Biol. 386, 123–134 (2014).

329. Westerfield, M. The zebrafish book. A guide for the laboratory use of zebrafish (Danio rerio). (University of Oregon Press, Eugene.OR 97403 USA, 2007).

330. Fisher, S. et al. Evaluating the biological relevance of putative enhancers using Tol2 transposon-mediated transgenesis in zebrafish. Nat. Protoc. 1, 1297–1305 (2006).

331. Pi-Roig, A., Martin-Blanco, E. & Minguillon, C. Distinct tissue-specific requirements for the zebrafish tbx5 genes during heart, retina and pectoral fin development. Open Biol. 4, (2014).

332. Rothschild, S. C. et al. Tbx5-mediated expression of Ca2+/calmodulin-dependent protein kinase II is necessary for zebrafish cardiac and pectoral fin morphogenesis. Dev. Biol. 330, 175–184 (2009).

333. Yelon, D., Horne, S. A. & Stainier, D. Y. R. Restricted Expression of Cardiac Myosin Genes Reveals Regulated Aspects of Heart Tube Assembly in Zebrafish. Dev. Biol. 214, 23–37 (1999).

334. Powell, R. et al. Wtip is required for proepicardial organ specification and cardiac left/right asymmetry in zebrafish. Mol. Med. Rep. (2016). doi:10.3892/mmr.2016.5550

335. Thisse, C. & Thisse, B. High-resolution in situ hybridization to whole-mount zebrafish embryos. Nat. Protoc. 3, 59–69 (2007).

336. Brend, T. & Holley, S. A. Zebrafish whole mount high-resolution double fluorescent in situ hybridization. J. Vis. Exp. 1–3 (2009). doi:10.3791/1229

337. Holly, V. L., Widen, S. A., Famulski, J. K. & Waskiewicz, A. J. Sfrp1a and Sfrp5 function as positive regulators of Wnt and BMP signaling during early retinal development. Dev. Biol. 388, 192–204 (2014).

338. Amaral, I. P. G. & Johnston, I. A. Experimental selection for body size at age modifies early life-history traits and muscle gene expression in adult zebrafish. J. Exp. Biol. 215, 3895–3904 (2012).

339. Alexander, C., Piloto, S., Le Pabic, P. & Schilling, T. F. Wnt Signaling Interacts with Bmp and Edn1 to Regulate Dorsal-Ventral Patterning and Growth of the Craniofacial Skeleton. PLoS Genet. (2014). doi:10.1371/journal.pgen.1004479

340. Li, C. W. & Ge, W. Spatiotemporal Expression of Bone Morphogenetic Protein Family Ligands and Receptors in the Zebrafish Ovary: A Potential Paracrine-Signaling Mechanism for Oocyte-Follicle Cell Communication. Biol. Reprod. 85, 977–986 (2011).

341. Roy, B., Ferdous, J. & Ali, D. W. NMDA receptors on zebrafish Mauthner cells require CaMKII- for normal development. Dev. Neurobiol. 75, 145–162 (2015).

342. Takamiya, M. et al. Molecular description of eye defects in the zebrafish pax6b mutant, sunrise, reveals a pax6b-dependent genetic network in the developing anterior chamber. PLoS One 10, 1–23 (2015).

343. Leucht, C. & Bally-cuif, L. The Universal ProbeLibrary – a Versatile Tool for Quantitative Expression Analysis in the Zebrafish Gene expression. Biochemica 2, 16–18 (2007).

344. Stulberg, M. J., Lin, A., Zhao, H. & Holley, S. A. Crosstalk between Fgf and Wnt signaling in the zebrafish tailbud. Dev. Biol. 369, 298–307 (2012).

345. Zhao, X. et al. Zebrafish cul4a, but not cul4b, modulates cardiac and forelimb development by upregulating tbx5a expression. Hum. Mol. Genet. 24, 853–864 (2015).

346. Lin, T. Y. et al. Hypoxia-inducible factor 2 alpha is essential for hepatic outgrowth and functions via the regulation of leg1 transcription in the zebrafish embryo. PLoS One 9, (2014).

347. Krol, A. J. et al. Evolutionary plasticity of segmentation clock networks. Development 138, 2783–2792 (2011).

348. Vanhauwaert, S. et al. Expressed repeat elements improve RT-qPCR normalization across a wide range of zebrafish gene expression studies. PLoS One 9, e109091 (2014).

349. Masai, I. N-cadherin mediates retinal lamination, maintenance of forebrain compartments and patterning of retinal neurites. Development 130, 2479–2494 (2003).

350. Yamauchi, H., Miyakawa, N., Miyake, A. & Itoh, N. Fgf4 is required for left–right patterning of visceral organs in zebrafish. Dev. Biol. 332, 177–185 (2009).

351. Thisse, C. & Thisse, B. High Throughput Expression Analysis of ZF-Models Consortium Clones. ZFIN Direct Data Submission. zfin.org 2005 (2005).

352. Zhang, J., Jiang, Z., Liu, X. & Meng, A. Eph/ephrin signaling maintains the boundary of dorsal forerunner cell cluster during morphogenesis of the zebrafish embryonic left-right organizer. Development 143, 2603–2615 (2016).

353. Durbin, L. et al. Eph signaling is required for segmentation and differentiation of the somites. Genes Dev. 12, 3096–3109 (1998).

354. Davis, S. et al. Ligands for EPH-related receptor tyrosine kinases that require membrane attachment or clustering for activity. Science (80-.). 266, 816–819 (1994).

355. Hernández-Vega, A. & Minguillón, C. The Prx1 limb enhancers: Targeted gene expression in developing zebrafish pectoral fins. Dev. Dyn. 240, 1977–1988 (2011).

356. Chatterjee, B. et al. Developmental regulation and expression of the zebrafish connexin43 gene. Dev. Dyn. 233, 890–906 (2005).

357. Bubenshchikova, E. et al. Wtip and Vangl2 are required for mitotic spindle orientation and cloaca morphogenesis. Biol. Open 1, 588–96 (2012).

358. Yu, X., Ng, C. P., Habacher, H. & Roy, S. Foxj1 transcription factors are master regulators of the motile

ciliogenic program. Nat. Genet. 40, 1445–1453 (2008).

359. Greulich, F., Rudat, C. & Kispert, A. Mechanisms of T-box gene function in the developing heart. Cardiovasc. Res. 91, 212–222 (2011).

360. Gyda, M., Wolman, M., Lorent, K. & Granato, M. The Tumor Suppressor Gene Retinoblastoma-1 Is Required for Retinotectal Development and Visual Function in Zebrafish. PLoS Genet. 8, e1003106 (2012).

361. Vance, K. W., Shaw, H. M., Rodriguez, M., Ott, S. & Goding, C. R. The retinoblastoma protein modulates Tbx2 functional specificity. Mol. Biol. Cell 21, 2770–9 (2010).

362. Hasson, P., Del Buono, J. & Logan, M. P. O. Tbx5 is dispensable for forelimb outgrowth. Development 134, 85–92 (2007).

363. Plageman, T. F. & Yutzey, K. E. Microarray Analysis of Tbx5-Induced Genes Expressed in the Developing Heart. Dev Dyn 235, 2868–2880 (2006).

364. Yi Li, Q. et al. Holt-Oram syndrome is caused by mutations in TBX5, a member of the Brachyury (T) gene family. Nat. Genet. 15, 21–29 (1997).

365. Qiao, L. et al. Snail modulates the assembly of fibronectin via α5 integrin for myocardial migration in zebrafish embryos. Sci. Rep. 4, 4470 (2015).

366. Chiavacci, E., Kirchgeorg, L., Felker, A., Burger, A. & Mosimann, C. Early frameshift alleles of zebrafish tbx5a that fail to develop the heartstrings phenotype. bioRxiv 103168 (2017). doi:10.1101/103168

367. Rossi, A. et al. Genetic compensation induced by deleterious mutations but not gene knockdowns. Nature 524, 230–233 (2015).

368. Rikin, A., Rosenfeld, G. E., McCartin, K. & Evans, T. A Reverse Genetic Approach to Test Functional Redundancy During Embryogenesis. J. Vis. Exp. e2020–e2020 (2010). doi:10.3791/2020

369. Concha, M. L., Burdine, R. D., Russell, C., Schier, A. F. & Wilson, S. W. A nodal signaling pathway regulates the laterality of neuroanatomical asymmetries in the zebrafish forebrain. Neuron 28, 399–409 (2000).

370. Bisgrove, B. W., Su, Y.-C. & Yost, H. J. Maternal Gdf3 is an obligatory cofactor in Nodal signaling for embryonic axis formation in zebrafish. Elife 6, e28534 (2017).

371. Montague, T. G. & Schier, A. F. Vg1-Nodal heterodimers are the endogenous inducers of mesendoderm. Elife 6, e28183 (2017).

372. Pelliccia, J. L., Jindal, G. A. & Burdine, R. D. Gdf3 is required for robust Nodal signaling during germ layer formation and left-right patterning. Elife 6, e28635 (2017).

373. Thisse, B., Pflumio, S., F ürthauer, M., Loppin, B., Heyer, V., Degrave, A., Woehl, R., Lux, A., Steffan, T., Charbonnier, X.Q. and Thisse, C. Expression of the zebrafish genome during embryogenesis. zfin.org 15402 (2001).

374. Kishimoto, Y., Lee, K. H., Zon, L., Hammerschmidt, M. & Schulte-Merker, S. The molecular nature of zebrafish swirl: BMP2 function is essential during early dorsoventral patterning. Development 124, 4457–4466 (1997).

375. Mueller, T. D. & Nickel, J. Promiscuity and specificity in BMP receptor activation. FEBS Letters (2012). doi:10.1016/j.febslet.2012.02.043

376. Yadin, D., Knaus, P. & Mueller, T. D. Structural insights into BMP receptors: Specificity, activation and inhibition. Cytokine and Growth Factor Reviews (2016). doi:10.1016/j.cytogfr.2015.11.005

377. Laux, D. W., Febbo, J. A. & Roman, B. L. Dynamic Analysis of BMP-Responsive Smad Activity in Live Zebrafish Embryos. Dev. Dyn. 240, 682–694 (2011).

378. Smith, K. A. et al. Bmp and Nodal independently regulate lefty1 expression to maintain unilateral Nodal activity during left-right axis specification in zebrafish. PLoS Genet. 7, e1002289 (2011).

379. Monteiro, R. et al. Two novel type II receptors mediate BMP signalling and are required to establish left-right asymmetry in zebrafish. Dev. Biol. 315, 55–71 (2008).

380. Roxo-Rosa, M., Jacinto, R., Sampaio, P. & Santos Lopes, S. The zebrafish Kupffer's vesicle as a model system for the molecular mechanisms by which the lack of Polycystin-2 leads to stimulation of CFTR. Biol. Open 4, 1356–1366 (2015).

381. Kim, J., Bae, S.-J., Lee, H. S., Park, J.-H. & Kim, K.-W. Claudin5a is required for proper inflation of Kupffer's vesicle lumen and organ laterality. PLoS One 12, e0182047 (2017).

382. Navis, A., Marjoram, L. & Bagnat, M. Cftr controls lumen expansion and function of Kupffer's vesicle in zebrafish. Development 140, 1703–1712 (2013).

383. Fontenille, L., Rouquier, S., Lutfalla, G. & Giorgi, D. Microtubule-associated protein 9 (Map9/Asap) is required for the early steps of zebrafish development. Cell Cycle 13, 1101–1114 (2014).